Faculty of Science and Engineering
Department of Petroleum Engineering

Evaluation and Selection of an Optimum Material for Coil Tubes in CT Drilling Technology for Hard Rocks in Mineral Exploration

Christopher Kipchumba Lagat

This thesis is presented for the Degree of
Doctor of Philosophy
of
Curtin University

August 2015

Declaration

To the best of my knowledge and belief this thesis contains no material previously published by any other person except where due acknowledgment has been made. This thesis contains no material which has been accepted for the award of any other degree or diploma in any university.

Name: Christopher Kipchumba Lagat

Signature: *Date:18 /08/2015*

Abstract

Research in the development of new drilling technologies for deep mineral exploration is currently being undertaken in Australia. Following an extensive study by Deep Exploration Technologies Cooperative Research Centre (DET CRC) on the available drilling technologies in the market, coiled tube technology has been suggested as a faster and economic drilling method. This is primarily due to its smaller footprint relative to the standard rotary method, ease of unit mobility, less operating personnel, faster rate of penetration, and faster rig up and rig down times. Steel coiled tube material has traditionally been used in the petroleum industry. However, cyclic bending of the steel coiled tubing past its yield strength point leads to progressive weakening of the tube, hence leading to rapid reduction of its service life.

Composite coiled tube (CCT) offers the potential to exceed the performance limitations of steel materials. CCT comprises of high strength fibres embedded in an epoxy matrix. The fibre types which have the highest potential for application in the CCT construction include carbon, glass and Kevlar.

Composite coiled tube can be tailor-made to exhibit unique anisotropic characteristics that optimally address the tensile and compression loads, high strains imposed by bending and internal tube pressures. Composites offer several other benefits compared to steel including low specific gravities, high strength-to-weight and modulus-weight ratios. In addition, they have the potential to offer better fatigue strength than the metallic materials. Hence their choice as a material for coiled tubing.

Structural analysis of composite coiled tube was performed using HyperSizer™ and Abaqus™ software packages. Design calculations were based on 3502 carbon – epoxy composite type AS4, which has a high strength, high strain, standard modulus. Four composite flat sheet samples with different lay-up configurations, i.e. [+70/-70/0/0/+70/-70/0/0], [+70/0/-70/0/-70/0/+70/0], [+90/-90/0/0/+90/-90/0/0], [+90/0/-90/0/-90/0/+90/0], were fabricated and tested under axial loading. The [+70/0/-70/0/-70/0/+70/0] layup displayed highest strength. Experimental results of the composite samples were comparable to simulation predictions. A composite tube was modelled

and fabricated using a fibre layup which exhibited the highest strength in flat sheet samples [+70/0/-70/0/-70/0/+70/0]. The modelled tube was subjected to pure axial load, combined axial/bending and axial/bending/hoop loads. Ply-by-ply fibre failure in tension and compression on the bent tube were predicted by stress-based and strain-based failure models. The tube simulation performance was satisfactory under combined axial, bending and hoop loading. A tube with a [+70/0/-70/0/-70/0/+70/0] fibre configuration was then fabricated using the filament winding method. Fatigue tests as well as tensile tests were undertaken on the tube sample. Similar experimental study was also conducted using commercially available drawn, seam welded steel coiled tubes. The designed composite tube with a fibre orientation of [+70/0/-70/0/-70/0/+70/0] was tested to 1712 bending cycles without failure. Tensile test results also showed that the tube could sustain up to 54 tons of axial load. This is five times the expected axial load on a coiled tube during mineral exploration drilling operations. Experimental results showed that the fatigue life of composite tube is potentially higher than that of steel.

My experimental and simulation study achieved the objective of selecting a composite coiled tube design that can perform satisfactorily in hard rock coiled tube drilling for future mineral exploration projects.

Acknowledgements

I would like to express my gratitude to my supervisors. I thank Dr Reem Roufail, Associate Lecturer at the Department of Petroleum Engineering, Curtin University, for her close supervision and unfailing advice and help throughout my research and writing of this thesis. I am indeed grateful to Professor Brian Evans, Head of Petroleum Engineering department at Curtin University, for his support, thoughtful and creative comments and, more generally, for the care with which he reviewed the research reports. Professor Vamegh Rasouli, was characteristically generous in offering advice and help in my research. Thanks to him for this and his untiring support. I am grateful to Dr Philip Teakle of Teakle Composites Australia Pty for providing composite tube samples and for his general advice on composite materials.

I extend my gratitude to Deep Exploration Technologies Cooperative Research Centre (DET CRC) for the financial support and supply of steel coiled tube samples.

Civil engineering department, Curtin University, and MTS Metallurgical Testing Services graciously allowed me to use their laboratory testing facilities during my research period. In this regard, I am indebted to Dr Ian Chandler, Rob Cutter, John Caroll and Alex Khomoutov.

I am greatly indebted to my colleagues at the Department of Petroleum Engineering, particularly Mohammad Reza, Ben Ameri, Siamak Mishani; for their support during some of my experimental work.

To all friends, whose names I may not have listed, and who have assisted me in one way or another, I feel very much indebted.

Not least, I should thank my wife and my children for their patience and forbearance whilst I have been studying. I hope this end result will be uplifting for my family, friends and colleagues who have supported me all along.

To

My family

Contents

List of Figures

List of Tables

Nomenclature

CT	Coiled tubing
CTU	Coiled tubing unit
BM	Bending machine
A	Area
F	Force
σ	Stress
σ_a	Axial stress (lb/in^2, Pa)
σ_h	Hoop stress (lb/in^2, Pa)
σ_r	Radial stress (lb/in^2, Pa)
τ	Shear stress (lb/in^2, Pa)
E	Young's modulus of elasticity (*msi, GPa*)
X_t	Allowable tension stress of ply in the longitudinal (1) direction (*MPa*)
X_c	Allowable compression stress of ply in the longitudinal (1) direction (*MPa*)
Y_t	Allowable tensile stress of ply in the transverse (2) direction (*MPa*)
Y_c	Allowable compressive stress of ply in the transverse (2) direction (*MPa*)
S, S_{12}	Allowable shear stress of ply (in-plane) (*MPa*)
S_T	Allowable shear stress of ply (transverse) (*MPa*)
σ_{11}	Applied stress of ply in longitudinal (1) direction (*MPa*)
σ_{22}	Applied stress of ply in transverse (2) direction (*MPa*)
τ_{12}	Applied shear stress of ply (*MPa*)
ε	strain
e_{1t}	Tension strain allowable of ply in the longitudinal (1) direction

e_{1c}	Compression strain allowable of ply in the longitudinal (1) direction
e_{2t}	Tension strain allowable of ply in the transverse (2) direction
e_{2c}	Compression strain allowable of ply in the transverse (2) direction
ε_{11}	Applied strain of ply in longitudinal (1) direction
ε_{22}	Applied strain of ply in transverse (2) direction
γ_{12}	Applied shear strain of ply (engineering) pf a ply
μ	Poisson's ratio
MS	Margin of safety
R	Reel bending radius
r	Coiled tubing radius
r_o	Outside radius (coiled tubing)
r_i	Inside radius (coiled tubing)
r_c	Radial clearance (between hole and coiled tubing)
t	Wall thickness of coiled tubing
p_i	Internal pressure
p_o	Outside/external pressure
κ	Fatigue curve constant
σ	Stress range (peak to peak)
m	Fatigue exponent
OD	Outside diameter
ID	Inside diameter
D	Fatigue damage (*in*)
N	Number of cycles to failure
n	Number of cycles that have occurred
HCF	High cycle fatigue
LCF	Low cycle fatigue
σ_{1000}	Stress range at 1,000 cycles to failure
σ_{be}	Stress range at 1,000,000 cycles to failure

σ_u	Ultimate stress of material
C_r	Reliability factor, 0.868 for 95% reliability (2 standard deviations)
C_m	Material type ranging from 0.26 for martensite to 0.55 for ferrite steel
ε_a	Strain amplitude
σ_f'	Fatigue strength coefficient
N_f	Strain reversals
ε'_f	Fatigue ductility coefficient
b	Fatigue strength exponent, usually varying between -0.04 and -0.15 for metals

Chapter 1 Introduction

Australia's mining sector continues to hold the potential to remain the most important Australian export earner for the foreseeable future. The competitive advantage of the mining industry has been based on vast and high quality resources discovered in the 1960s and 1970s. However, many of the deposits that underpin this success are now depleting or experiencing declining grades. The mines are also becoming deeper, more remote and more inaccessible. Research in the development of new drilling technologies for deep mineral exploration is currently being undertaken in Australia. Following an extensive study by Deep Exploration Technologies Cooperative Research Centre (DET-CRC) on the available drilling technologies in the market, coiled tube technology was suggested as a faster and more economic drilling method than the conventional drill rod approach. The steel coiled tubing technology has traditionally been used in the petroleum industry for well servicing operations. Currently, the conventional coiled tubing is milled from High Strength, Low Alloy (HSLA) steel. In spite of advanced developments in the HSLA steel material for coiled tubing applications, there are still limitations in its capability. A review of the literature indicates that the repeated spooling of steel causes fatigue damage thus limiting the tubing life.

Hard rock mineral drilling is not a conventional application for coiled tube rig. Besides, there is no recommended material for coiled tubing for mineral drilling in literature. In order to speed up the drilling process and reduce cost per drilled hole, the concept of a coil tube drilling system needs to have high fatigue strength and low weight. This will increase the number of holes drilled without failure and facilitate ease in transportation and equipment rigging.

This research aims at proposing new coil tubing material to be used in deep hard-rock exploration drilling in the mining industry, with numerical simulations being performed to design models. In order to physically test the designed and manufactured tubing, bending machine was designed and built to carry out experimental validation of the models.

1.1 Coiled tubing

Coiled tubing (CT) is a continuous length of tubular ductile steel or composite material. During operation, it is exposed to multiple mechanical stresses such as tension, compression, creep, fatigue, erosion and corrosion. The main cause of failure of the tube string is the multiple bending events of the tube. Coiled tubing is pulled off a reel by a force from the injector head (event 1), as shown in Figure 1-1. It is then bent at the entrance to the guide arch as it moves forward (event 2). It is straightened at the exit of the guide arch as it travels downwards to the injector head and enters the wellbore (event 3). During the retrieval process, events 4, 5, and 6 occur, which are the reverse events of 3, 2 and 1, respectively (ICoTA, 2005).

Therefore, during the drilling operation of one exploration hole, the coil tube undergoes at least six bending deformation events. A coiled tubing rig utilizes fluid for drilling, which creates an internal force in the form of internal pressure. Hence the bent section of the steel coiled tube is subjected to tri-axial stresses imposed by bending loads and internal pressure. Bending imposes tensile and compressive stresses, while internal pressure causes hoop stresses as illustrated in Figure 1-2. High internal pressure results in 'ballooning' of the tube. Ballooning reduces the average wall thickness of the tubing. Corrosion, as a result of exposure to atmosphere or corrosive fluids, leads to additional reduction in tubing wall thickness. The tubing wall thinning effect could result in tubing burst failure (Sas-Jaworsky & Williams, 1993).

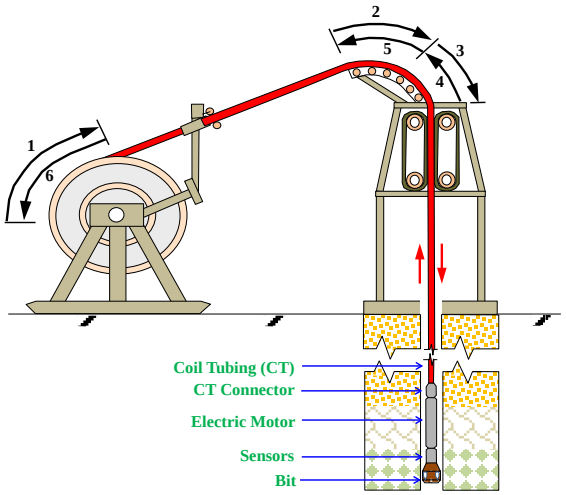

Figure 1-1 Coil tubing bending events, after (Lane, 2005)

The steel coiled tubing is subjected to plastic deformation during cyclic bent events. Plastic deformation induces permanent damage which results in fatigue failure after a certain number of bend cycles (Bridge, 2011).

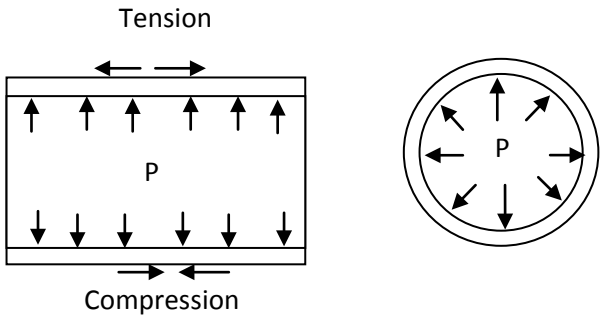

Figure 1-2 Schematic diagram of stress distribution on coil tubing

Numerous attempts have been undertaken to improve the performance ability of coiled tubing. Alternatives explored include the development of High Strength Low Alloy steel (HSLA). High strength, low weight titanium coiled tubing strings are also being explored. Titanium, however, corrodes and etches rapidly when exposed to hydrochloric acid (Sas-Jaworsky & Williams, 1993).

In spite of these improvements, there are still limitations in the capability of the steel coiled tubing and other metallic coiled tubing materials. The metallic materials will still be subjected to repeated spooling and plastic deformation. High strains due to repeated bending with internal pressure will lead to fatigue failure (Feechan, Quigley, & Wideman, 2009).

Composites are a promising alternative to overcome the limitations of coiled tubing made of steel and other metallic materials. Composite tubing materials are resistant to corrosion (S. Fowler, Feechan, & Berning, 1998). Mechanical properties of fibre composite materials can be tailor-made to overcome burst pressures as well as tensile compressive loads. Composite materials are resistant to corrosive fluids (Miracle et al., 2001). However, the composite coiled tubing technology is new in the mining industry, where there is no historical experience or service history in this type of application.

1.2 Research objective

This research is aimed at proposing a new coil tubing material to be used in high speed deep hard rock exploration drilling in the mining industry. The objective was achieved via theoretical and experimental work. The specific objectives were:

- To study fatigue strength of high strength low alloy steel (GT90, HS90 and GT100) and carbon/epoxy composite tubes via experimental work. The tests are undertaken in non-erosive and non-corrosive environment. Hence the effects of erosion and corrosion on steel tubes are not considered.
- To develop an understanding of the effect of fibre orientation on carbon/epoxy composite laminates/tube flexural and axial strengths.
- To create a computer model that simulates coiled tube bending on a reel. The simulation study is undertaken to select a suitable fibre orientation and stacking sequence design for composite coiled tubing material for mineral drilling application and to evaluate the stress distribution of forces across the layers of composite tube.
- To design and fabricate a composite coiled tube sample that would be utilized in mineral exploration drilling.

1.3 Thesis outline

In Chapter 1 of this thesis, coiled tubing is introduced and research objectives are stated. A literature review is presented in Chapter 2. Published literature relating to conventional and composite coiled tubing materials, fatigue strengths and analysis, finite element modelling and simulations are reviewed.

Research tools are presented in Chapter 3. A summary of the finite element modelling software and equipment used are outlined. Lamination theory is presented along with its finite element implementation. Fatigue and tensile testing machines used in the experimental study are presented.

Steel coiled tube experimental results and their analyses are presented in Chapter 4. Fatigue and tensile testing results of steel coiled tube samples are outlined. Composite tube simulation and experimental results are presented in Chapter 5. Analyses of the simulation and experimental results are discussed.

Chapter 6 provides the conclusions of the research. Recommendations for future research are also presented.

Chapter 2 Literature review

Literature review chapter presents the idea of coiled tubing for deep hard drilling application in mineral exploration. Justifications for selecting this technology are discussed. Coiled tubing technology and performance limitations of conventional coiled tubing are reviewed. Several attempts have been made to improve the performance of coiled tubing. Numerous alternatives to conventional carbon steel have been explored in oil and gas industry. These alternatives are reviewed. The suitability of the coiled tubing material in the mining industry is also discussed.

2.1 Mineral exploration drilling

Drilling is one of the most important steps and can be the most expensive all mineral exploration procedures. It locates and defines economic mineralization aspects. A large number of conventional drilling techniques are used in the mining industry. The three commonly used, in order of increasing cost, are auger drilling, rotary percussion drilling and diamond drilling (Majoribanks, 2010). Auger drilling is a method of drilling holes by cutting or gouging with the chiselled tip of a rotating bit. As the drill stem rotates and penetrates the rock, the drill bit produces cuttings that are lifted to the surface by the helical edges or flights of the rotating drill string.

Rotary percussion drilling employs a variety of blades or roller bits mounted on the end of a rotating drilling string. A percussion or hammer action in conjunction with a chisel bit can be used to penetrate hard rock. High pressure air is pumped through the drill sting to the face of the bit lubricates and lift the cuttings to the surface. The cuttings reach the surface along the narrow space between the drill string and the side of the hole.

Reverse circulation (RC) is a type of rotary percussion drilling. Compressed air is pumped down to the drill bit along the annular space between an inner tube and outer drill stem. The cuttings enter the inner tube through a special opening located behind the bit called a crossover sub. The cuttings are carried to the surface through the inside tube. The RC drilling procedure is advantageous in that it prevents the upcoming sample from being contaminated with a material broken from the sides of the hole. Diamond drilling differs from other methods in that a solid core of rock

(generally 27mm to 85mm in diameter), rather than cuttings, are extracted from depth. During drilling, as the drill bit advances, a cylindrical core of rock progressively fills a double-tube core barrel immediately above the drill bit. Core samples are periodically recovered by lowering a cable with an overshot down the drill string, attaching it to the top of the inner tube (inner barrel) of the core barrel, and winching it to the surface. The inner barrel is fitted with a core lifter mechanism to prevent core from dropping out during recovery. While the core sections are being removed from the inner tube and placed in core trays, a replacement inner tube is lowered into the hole so that drilling can recommence. Selecting the right technique is always a trade-off between speed, cost, required sample quality, sample volume, logistics and environmental considerations.

Deep Exploration Technologies Cooperative Research Centre (DET CRC) has carried out a comprehensive review of the available drilling technologies in the market. Following the study, coiled tube drilling technology has been suggested as a faster and cheaper method than conventional pipe drilling.

2.2 Coiled tubing

Coiled tubing (CT) is a continuous length of tubular ductile steel or composite material. It is manufactured in various lengths and spooled onto a reel. Tubing sizes range from 3/4 inch to 4 ½ inches in external diameter. Single reel tubing lengths in excess of 30,000 ft have been commercially manufactured.

Coiled tubing unit (CTU) comprises of four basic units; reel, injector head, control cabin and power pack. The CT is stored in the reel. The surface drive force to run and retrieve the tubing is provided by the injector head. The power pack generates the hydraulic and pneumatic power required to operate the CT unit. The equipment operator monitors and controls the CT operations from the control cabin. The major constituents of the CTU are displayed in Figure 2-1.

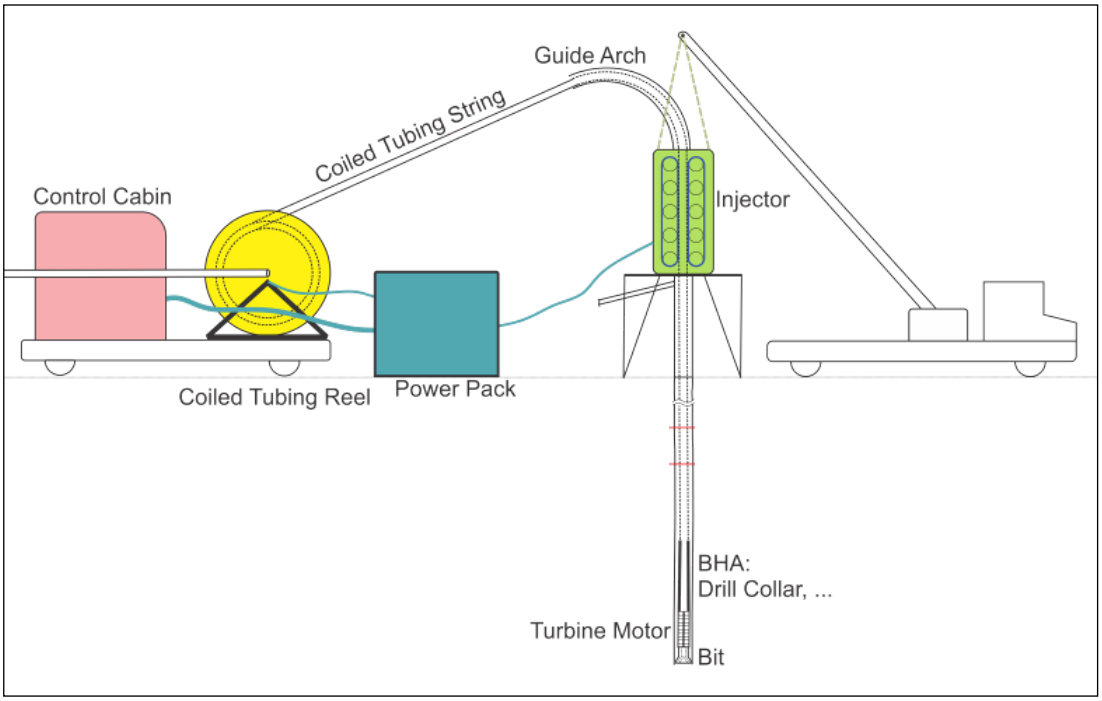

Figure 2-1 Components of a CTU (Kamyab, 2014)

Coiled tubing (CT) has been used historically in the oil and gas industry for well work over services including well unloading, clean-outs, stimulations, well logging, perforations, fishing, setting and retrieving plugs. Although work over applications account for over approximately 75% of CT use, technical advancements have opened new market applications for the CT technology, including drilling (ICoTA, 2005). Coiled tubing (CT) drilling technology offers several advantages (Crouse & Lunan, 2000). The CT rig is a smaller unit compared to a conventional rig, hence minimising mobilization and transportation costs (Perry, 2007). The small size of the rig provides a number of environmental advantages over a conventional rig; smaller access roads are required, smaller equipment yield less air emissions and low noise engines, micro-hole approach requires less drilling fluid and yields fewer cuttings and use of CT rig mitigates the risk of spills due to no drill pipe connections. The no-drill pipe connection system enhances the automation of the drilling process and thus reducing the manpower count on the rig floor. Faster rig up and rig down is another key advantage. Very high rates of penetration have been achieved with CT technology. High drilling as 400ft/hr have been recorded. Improved safety due to less equipment handling from one well site to another is another major advantage. Coiled

tubing technology cost may be considerably lower than conventional drilling (Albright et al., 2005).

2.3 Coiled tubing drilling for mineral exploration

Australia's mining sector continues to hold the potential to remain the most important export earner for the foreseeable future. The competitive advantage of the mining industry has been based on vast and high quality resources discovered in the 1960s and 1970s. However, many of the deposits that underpin this success are now depleting or experiencing declining grades. The mines are also becoming deeper, more remote and more inaccessible (Schodde & Guj, 2012). While the country's resource stocks still look healthy, Australia's position to remain the premier mineral producer is dependent on continued investment in exploration.

New technologies focusing on deeper mining exploration will unlock new search terrains. The untapped deep-seated resources could become commercially accessible if a cheap drilling method were adopted. The CT drilling technology has been suggested as a faster and cheaper method for deep mineral exploration. While there have been several studies on coiled tubing for work over services and other petroleum industry applications, limited studies have been carried out particularly on coiled tubing drilling (ICoTA, 2005). Currently, there is no existing literature of CT string material performance that is suitable for high speed drilling of hard rocks in deep mineral exploration. CT drilling technology is a technology step-change to the mining industry.

The coiled tubing rig for mineral exploration drilling needs to be light in weight for safe and quick transportation to the drilling locations. The main cause of failure of the tubing string is the multiple bending events of the tubing. Coiled tubing material should be able to handle multiple bending events before failing due to fatigue.

The objective of this research is to propose an optimum coiled tubing material to be used in high speed hard rock drilling for mineral exploration. This is discussed in detail in the thesis.

2.4 Performance limitations of steel coiled tubing

The current well-work over services can be performed safely and reliably using the conventional steel tubing. The presently accepted industry standard coiled tubing material is A-606 Type A Modified HSLA steel. The steel CT length is, however, limited by the reel size and its weight (Leising & Newman, 1993). Governments and states have road restrictions. The legal dimension and mass limits in South Australia, for instance, is 2.5m wide, 4.3m high, 19m long and 42.5 tonnes. Transportation of any load outside this limits require a permit ("SA Government Report," 2006). The behaviour of the isotropic material limits its yield strength and tensile load capability. Figure 1-1 shows the bend events the coiled tubing undergoes as it is pulled in and out of the reel. The tubing accumulates damage as a result of the repeated cyclic strains far beyond the elastic limit, and internal fluid pressure. This leads to fatigue failure and consequently a reduction of CT service life (Sas-Jaworsky & Williams, 1993).

Stresses due to pressure are not damaging unless tensile and compressive (bending) stresses are applied (Avakov, Foster, & Smith, 1993). Damage due to cyclic plastic strains is more severe with increasing internal tube pressure. An experimental study by Avakov et al. using 1.25-inch OD and 0.087-inch wall 80 ksi coiled tubing with negligible internal pressure found the tubing life to be 300 trips. However, with 5000 psi internal pressure, the same tubing exhibited life from 50 to 55 cycles. Similar results of pressure influence on the tubing life has been observed by S.M. Tipton, D.A. Newburn, K.R. Newman (Newman, Newburn, & Schlumberger, 1991; Tipton & Newburn, 1996).

2.5 Fatigue damage in steel coiled tubing

Fatigue is the localised damage process of the tubing due to cyclic loading. It consists of three processes (Lee, 2005):

1. Crack initiation
2. Crack propagation
3. Final fracture

During cyclic bending localised plastic deformation occurs in areas of high stress concentration such as a notch, weld, or discontinuities between grain boundaries.

The plastic deformation induces permanent damage in the tubing and crack develops (crack initiation). As the tubing experiences an increasing number of load cycles, the length of the crack increases (crack propagation). After a certain number of load cycles the crack will cause the component to fail (final fracture).

Fatigue damage is defined as the length of crack in a component compared to the crack size that causes complete failure. Hence it has a value of zero (no damage) and one (failure). Cyclic ratio is the number of cycles occurred dived by the number of cycles to failure. Figure 2-2 below shows the relationship between fatigue damage and cyclic ratio. It indicates that if a component experiences cyclic loading with constant amplitude, the crack length grows slowly initially, and then accelerates. The fastest crack occurs nearest to the component failure.

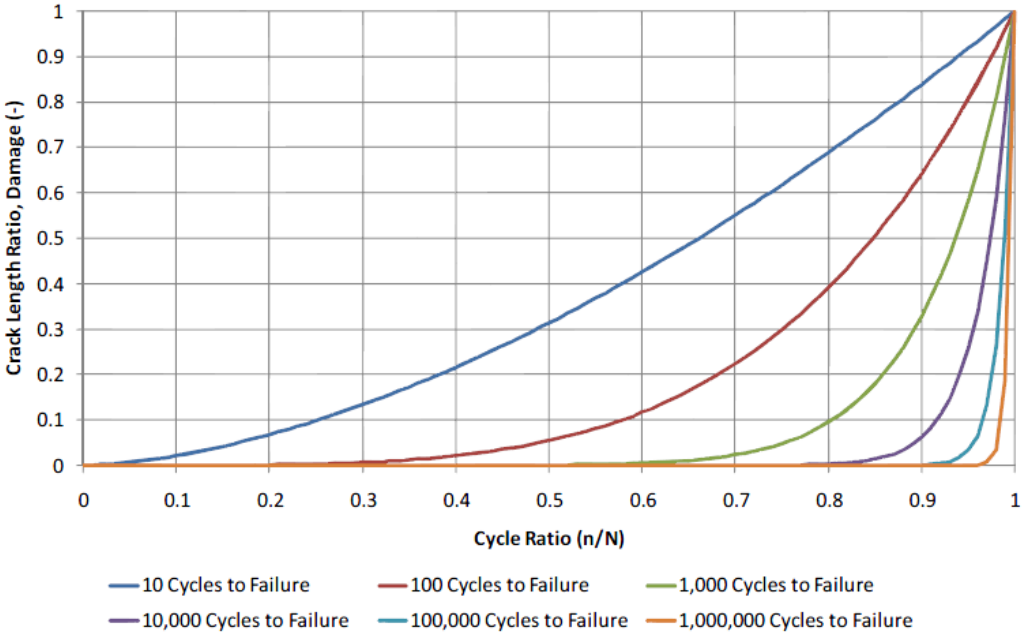

Figure 2-2: Relationship between crack length ratio and cyclic ratio (Bridge, 2011)

Fatigue damage is given by (Lee, 2005):

$$D = \left(\frac{n}{\mathrm{N}}\right)^{\frac{2}{3}\mathrm{N}^{0.4}} \tag{2.1}$$

"D" denotes fatigue damage while n/N is the cyclic ratio. Number of cycles that have occurred is represented by "n" and "N" is the number of cycles to failure. Equation (2.1) depicts a non-linear relationship between fatigue damage and cyclic ration. It is also evident that fatigue damage is dependent on the sequence of the load cycles.

As discussed above, fatigue damage is caused by cycling loading. There are three types of cyclic loads:

- Low cycle – large stress/strain cycles that require less than 10^3 cycles to fail a component.
- High cycle – cycles are generally within the elastic range of the material and require from 10^3 to 10^7 cycles to fail a component.
- Fatigue limit – these are low stress cycles that are considered non-damaging. The street levels are considered to be within the endurance limit of the component.

Steel coiled tubing is generally subjected to cyclic plastic loading, which is considered as low cycle fatigue. Plastic cyclic loading causes crack initiation. Further cyclic bending or loading propagates the crack. Elastic cyclic loading is considered to be high cycle fatigue. Elastic cyclic loading causes crack propagation in an existing crack. If a crack does not exist, the cyclic loading is considered to cause little fatigue damage.

Failure in coiled tubing can be defined in two ways, as a crack initiation or as fracture (Vargo, 2002). In crack initiation, failure occurs at the onset of a crack on CT. At fracture, the crack has propagated the wall of a CT, and the CT cannot hold pressure.

2.6 Coiled tubing stresses

The stresses acting on CT are generally caused by internal fluid pressure and axial force. The axial force puts the CT in either tension or compression. The three principal stresses acting on tubing segment are axial stress (σ_a), radial stress (σ_r) and tangential stress or hoop stress (σ_h) are shown in Figure 2-3.

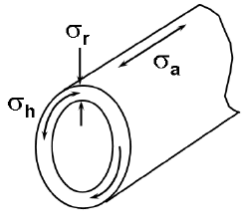

Figure 2-3: Stresses acting on a CT segment (Lane, 2005)

Axial stress

This is caused by axial force (tension or compression) applied to the CT. Hence:

$$\text{Axial stress, } \sigma_a = \frac{F_a}{A} \tag{2.2}$$

F_a is axial force.

A is the cross sectional area of the tubing, given by:

$$A = \pi(r_o^{\,2} - r_i^{\,2}) \tag{2.3}$$

Axial stress is positive for tension and negative for compression.

The CT buckles if the compressive force exceeds the helical buckling load, thereby creating an additional axial bending stress in the CT. The CT buckles into a helix as soon as the axial force becomes compressive. Equation (2.4) below calculates the bending stress on CT:

$$\sigma_a = \frac{F_a R r_o}{2I} \tag{2.4}$$

The compressive stress due to axial load is constant around the CT section. However, the bending stress is tensile on one side and compressive on the other side (Bridge, 2011). The maximum axial stress occurs on the side where the bending stress is compressive. The total maximum compressive stress can be expressed as:

$$\sigma_a = F_a\left[\frac{1}{A} + \frac{R r_o}{2I}\right] \tag{2.5}$$

σ_a is the sum of axial stress due to the axial load and bending stress.

Radial Stress

This is caused by pressure differential across the wall of the segment. According to Lame's equation, the radial stress at any given point in the CT is the stress due to internal and external pressures (Lane, 2005):

$$\sigma_r = \frac{(p_o - p_i) r_o^{\,2} r_o^{\,2}}{r^2\left(r_o^{\,2} - r_i^{\,2}\right)} + \frac{r_i^{\,2} p_i - r_i^{\,2} p_o}{\left(r_o^{\,2} - r_i^{\,2}\right)} \tag{2.6}$$

The subscripts “i” and “o” denotes the ID and OD radial locations.
Radial location for the ID:

$$r_i = \frac{OD - 2t}{2} \tag{2.7}$$

Radial location for the OD:

$$r_o = \frac{OD}{2} \tag{2.8}$$

At r_o, $\sigma_r = -P_o$ and at r_i, $\sigma_r = P_i$

Hoop Stress:

Lame’s equation indicates that the hoop stress at any given location in the CT wall is the stress around the circumference of the CT due to internal and external pressures. Yielding stress occurs first at the inner surface. Hence hoop and radial stresses at the inner surface are normally used in the calculations.

Hoop stress at any radial location, r, in the CT wall segment is given by:

$$\sigma_h = \frac{r_i^2 p_i - r_o^2 p_o}{\left(r_o^2 - r_i^2\right)} - \frac{\left(p_o - p_i\right) r_i^2 r_o^2}{r^2\left(r_o^2 - r_i^2\right)} \tag{2.9}$$

r is the radial location in the CT wall between r_i and r_o at which the stress is being calculated. Thus the maximum stress will always occur at either the inner or outer surface.

2.6.1 Failure stress criterion

The suitability of a CT string is assessed by determining the effects of stress inside the wall of each segment in the tubing string. The stresses should never exceed a given percentage, usually 80%, of the tubing yield stress. The Von Mises overall stress failure criteria is used to calculate the total equivalent stress in each segment of the coiled tube due to a combination of three principle stresses (axial stress, radial stress, and hoop stress) and the shear stress caused by torque. The limiting yield

stress for CT is calculated by the setting the Von Mises stress to the yield stress of the material with appropriate safety margin. The Von Mises stress ignores the following conditions prevalent with CT (CTES, 2005):

i. Residual stresses
ii. Work softening
iii. Not elastic, perfectly plastic behaviour
iv. Tension and compression yield stresses are different
v. Yield stress changes with strain cycling
vi. Ovality

In spite of these shortcomings, the Von Mises stress failure criterion is still a good method for calculating the mechanical limits for steel CT, due to its conservative results.

2.7 Predicting life of tubing

Predicting the number of cycles to failure for a load cycle can be determined using either stress or strain. Stress is typically used for elastic cyclic loading and strain is used for plastic load cycles.

Stress-based fatigue damage

Where stress ranges are in the elastic region, the fatigue damage may be calculated using S-N curve. This is a plot of alternating stress amplitude (σ) versus the number of cycles to failure (N). A typical S-N curve is shown in Figure 2-4 below. The S-N curve equation is given by:

$$N = \kappa\sigma^{-m} \tag{2.10}$$

Where κ, σ and m are fatigue curve constant, stress range (peak to peak) and fatigue exponent, respectively.

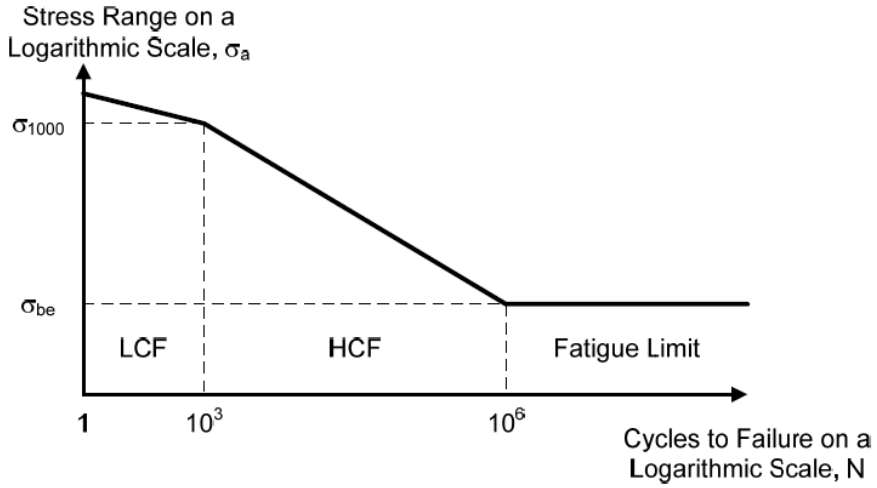

Figure 2-4: Example of S-N curve, after (Lee, 2005)

Equation (2.11) and (2.12) below (Lee, 2005) estimates stress level that correspond to 10^3 and 10^6 cycles to failure, respectively. The S-N curves, are, however, generally derived from experimental data. Fatigue constant and exponent are published in design codes such as DNV-RP-C2003 (Bridge, 2011).

$$\sigma_{1000} = 0.9Cr\sigma_u \tag{2.11}$$

$$\sigma_{be} = C_M Cr\sigma_u \tag{2.12}$$

Where:

σ_{1000} = Stress range at 1,000 cycles to failure

σ_{be} = Stress range at 1,000,000 cycles to failure

σ_u = Ultimate stress of material

C_r = reliability factor, 0.868 for 95% reliability (2 standard deviations)

C_m = material type ranging from 0.26 for martensite to 0.55 for steel

Strain-based fatigue damage

Coiled tubing life may be estimated using the strain-life-method. Here, the number of reversals to failure is determined for strain amplitudes. One load cycle is equivalent to two load reversals. Strain is used because the amplitude of the load reversals is

above the elastic limit of the material. The strain-life fatigue is estimated using the Morrow (1965) equation (2.13), presented in (Lee, 2005):

$$\varepsilon_a = \frac{\sigma_f'}{E}(2N_f)^b + \varepsilon'_f(2N_f)^c \qquad (2.13)$$

Where:

ε_a = strain amplitude

σ_f' = fatigue strength coefficient

N_f = strain reversals

ε'_f = fatigue ductility coefficient

b =fatigue strength exponent, usually varying between -0.04 and -0.15 for metals

There exist several methods used to combine the fatigue life from different load cycles, including:

- Miner's linear damage rule
- Double linear damage rule
- Power law damage rule.

Briefly, Miner's rule, as indicated in equation (2.14) below, assumes that fatigue damage is linearly proportional to the cyclic ratio. Hence for a given load, each cycle causes the same amount of damage. The rule provides reasonable correlation with fatigue test data for elastic cyclic loading (Lee, 2005). It is the most widely used of all the damage methods and is considered the industry standard method. Its drawback is that it is non-conservative and may over-estimate the number of cycles to failure.

$$D_T = \sum \frac{n_i}{N_i} \qquad (2.14)$$

The Power Law Damage Rule, developed by Manson and Hansford, is also derived from damage and cyclic ratio relationship. The rule can be used to calculate fatigue life of two or more load steps. If, for instance, a two load step sequence is assumed, the number of cycles from the first load step can be recorded and damage

calculated for this load step. Similarly, the cyclic ratio for the second load step can be determined.

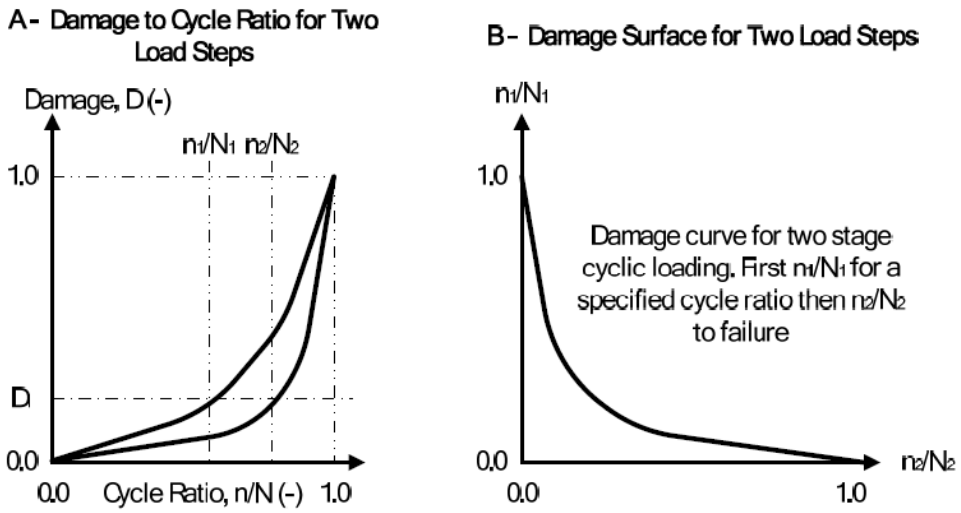

Figure 2-5: Power law damage rule, after (Lee, 2005).

The two cyclic ratio for the two load steps can be added together as shown in Figure 2-5 above. Fatigue damage, D_i, for the initial cyclic ratio for the first and second load steps is given by:

$$D_i = \left(\frac{n_i}{N_1}\right)^{\frac{2}{3}N_1^{0.4}} = \left(\frac{n_i}{N_2}\right)^{\frac{2}{3}N_2^{0.4}} \tag{2.15}$$

Re-arranging Equation (2.15) above, gives the fatigue damage for the first and second load steps as:

$$D_i = \frac{n_i}{N_1} = \left(\frac{n_2}{N_2}\right)^{\left(\frac{N_2}{N_1}\right)^{0.4}} \tag{2.16}$$

2.8 Coiled tubing materials

2.8.1 Steel

Conventional coiled tubing used in oil and gas industry is milled from modified A-606 High Strength Low Alloy (HSLA) steel. The yield strengths of CT steels commonly range from 55,000 psi to 120,000psi (ICoTA, 2005). The CT can be manufactured with diameter ranging from 1.0 inch to 6.625 inches and wall thickness of 0.08 inch to 0.03 inch. It is manufactured in a tube mill from a flat sheet strip, typically 3,000 ft length, which is rolled, formed, and welded by high frequency induction without the addition of filler metal. The desired length of coiled tubing can be achieved by welding length of flat strip together prior to forming the tube in the mill. The tubing is reeled on a spool as it is milled. Then it is hydraulically tested and nitrogen purged before being shipped for use (Yang, 1999).

The behaviour of the isotropic metal limits the life of the tube. During operation, the CT is bend over the reel and the gooseneck and more than 97% of its cross sectional area is subjected to plastic deformation. Hence, strain-life methods are commonly used to predict steel CT life. Cyclic bending causes CT fatigue. As fatigue accumulates, the yield strength of the CT diminishes gradually. Eventually the CT fails.

Steel CT is nearly perfectly round after manufacture. However, its ovality increases with increasing cyclic bending. Ovality significantly decreases the collapse failure pressure. Yang et al. (199) cycled a 2 inch OD, wall thickness 0.109 inch CT with 3,000 psi internal pressure on a bending machine with 72-inch bending radius. The yield strength of the steel CT was 80 ksi. The yield strength was reduced to 65 ksi after 83 cycles. Analytical computations indicated that the initial collapse resistance of the CT was 8164 psi. This reduced to 6618 psi after bending (Yang, 1999). Figure 2-6 below shows the effect of yield strength on the collapse pressure of CT.

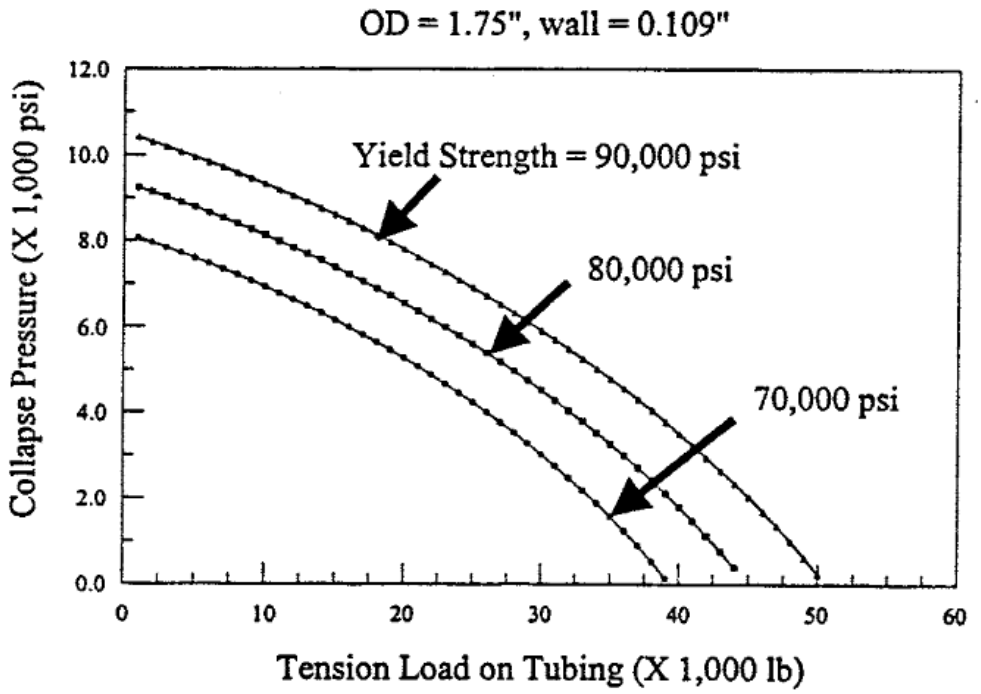

Figure 2-6: Yield strength effect on collapse pressure of CT, after (Yang, 1999)

At higher internal pressure (greater than 3,000 psi), CT fatigue is accompanied by diametrical growth (or ballooning). Ballooning can cause incompatibilities with deployment equipment which could cause severe mechanical damage to the CT. The crack initiation site is usually located at the maximum ballooning position (Urayama et al., 2000). Sour environments such as hydrogen sulphide gas, acid jobs have been known to contribute significantly in deterioration of fatigue life of CT (A. R. Crabtree & Gavin, 2005). Research to provide higher strength materials and special corrosion resistant alloys continues. However, in spite of these improvements, there are still limitations in the capability of the steel coiled tubing. The repeated spooling of steel causes fatigue damage which forces steel CT to be retired after a relatively few number of trips into a well (A Crabtree, Skrzypek, & Wilde, 1997). Additionally, its weight poses high handling risk to personnel. Down-time in transportation and retrieving broken tubing sections results in high economic cost (Feechan et al., 2009).

2.8.2 Polymer composites

Polymer composite is an emerging alternative material for manufacturing coiled tubes. The development of composite coiled tubing begun in the late 1980's and

early 1990's (McClatchie, Reynolds, Walsh, & Lundberg, 1999). The polymer composites consist of fibres, which are the principal load-carrying members, embedded in a matrix with distinct interfaces between them, as shown in Figure 2-7. The matrix retains the fibres in the desired position and orientation. The overall properties of a composite structure depend on the properties of individual components (fibres, matrix and the interfacial region connecting them)

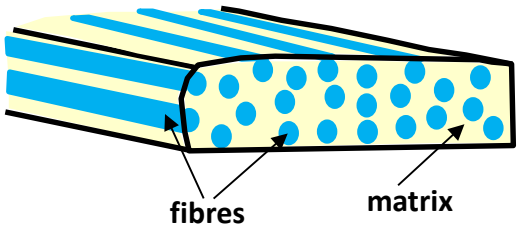

Figure 2-7: Polymer composite

Matrix components of composites

Matrix component of a fibre reinforced composite can either be a thermoset or a thermoplastic resin. The mechanical properties of a thermost resin change when it is heated above a certain themperature, the glass transition temperature. When the resin is heated above this glass transition temperature, its moleculat structure transforms to a softer plymer structure. The softer plymer has lower mechanical properties. When cooled, if not deformed, it regains its mechanical properties. Thermoplastics melt with heat, thus reversing the curing process. They, however, do not loose their mechanical properties. Table 2-1, shows the various types of thermosetting resins and their field of application. The most commonly used thermosetting resins in the composite industry are polysters and epoxy.

Polyesters are mostly used with E-glass and offer a combination of low cost, processing versatilty and resasonaly good performance unmtached by other resins (Miracle et al., 2001). Polyster has low adhesive properties and high shrinkage of up to 8%. Elongation at failure range from 5 to 12%. Polyster decomposes in temperature range of 60^{o}C to 205^{o}C (Mallick, 1993). Polyseter resins are classified into the following groups, based on their structure: (1) ortho resins, (2) isoresins, (3) bisphenol-A fumurates, (4) and chlorendics resins. Ortho resins are also known as general purpose resins. They are based on phthalic anhydrite (PA), maleic anhydrite

(MA) or fumaric acid and glycols. PA is less costly but has less chemical resistanceand lowers thermal resistance of laminates.

Isoresins are prepared using isophthalic acid, MA/fumaric acid and glycol. These resins are more more costlt than ortho resins. They have higher viscosities and thus require higher proportion of of reactive diluent (styrene). High styrene presnce improves water and alkai resistnace to the cured resins. Compared to ortho resins, isoresins have higher chemical, mechanical and thermal properties.

Bisphenol-A fumurates are synthesied by reacting ethoxy-based bisphenol-A with fumaric acid. These resins have improved thermal performance, a higher degree of hardness and rigidity. Chlorendic resins are prepared using chlorine/bromine-containing anhydrites or phenols to enhance their flame retardancy. To make a self-flame extinguishing polyster, the bromine content must be atleast 12% (Malik, CHOUDHARY, & Varma, 2000).

Epoxy resins contain at least two epoxide groups, sometimes refferred to as glycidyl or oxirane group, which cure through the reaction of the epoxided groups with a suitable curing agent. The performance of the resin is highly dependent on the formulation, including base resins, curatives and modifiers (Miracle et al., 2001). Blending different grades of epoxy resins, use of addditives, plasticizers or fillers is done to achieve desired processing and/or final mechanical properties, or to reduce cost.

Common types of epoxy resins include (1) bisphenol A, (2) bisphenol F, (3) novolac, glycidylamine, and (4) aliphatic resins. Bisphenol A epoxy resin is formed from reacting epichlorohydrin with bishenol A to form diglycidyl ethers of bisphenol A. Bisphenol F epoxy resins have lower viscosity and a higher mean epoxy content per gram, which (once cured) gives them increased chemical resistance. Novolac epoxy resin displays high temperature and chemical resistance, but low flexibility. Aliphatic epoxy resins have low viscosity at room temperature (10-200 mPa.s) and are often used as reactive diluents. They are employed to modify (reduce) the viscosity of other epoxy resins. Glycidylamine epoxy resins have higher temperature resistance and higher mechanical properties making them prefered choice in structural applications such as aerospace industry (Ratna, 2009).

Table 2-1: Thermoset resins and their applications, after (Ratna, 2009)

Resin	Precursor	Application
Unsturated polysester	Phenol and formaldehyde	Fibre composites, surface coatings
Epoxy	Epichlorohydrin and bisphenols	Fibre composites, engineering adhesives, paints
Vinyl ester	Epoxy resin and acryclic or methacrylic acid	Fibre composites
Polyurethane (PU)	Diisocyanate and hdroxyl-functionalised oligomer	Adhesives, foams, acid resistant cements
Furan	Furfuryl alcohol	Fibre composites, refractory materials processing, grinding wheels
Polyimide	Diamines and dianhydrite	Fibre composites for high temperature applications, cotaing
Cyanate ester	Cynogen halide and alcohol or phenol	Fibre composites for aircrafts, rockets, missiles
Bilmamcimide	Bismalcic and amine	Fibre composites for aircrafts, rockets, missiles

Vinyl ester resins are produced by the reaction (esterification) between an epoxy resin and unsaturated monocarborlic acid. Thus, these resins comprise a base of polyster resin strengthened with epoxy molecules in the backborne chain. Vinyl ester resin can be “thinned” by reaction with chemical such as styrene. “Thinning” improves workability but reduces strength (Malik et al., 2000). The properties of vynyl esters are midway between polysters and epoxy. Vinyl ester shrinks less than polyseter on curing. Crossbonding is superior than of other polyseter resins, Hence delamination is not a major issue. Glass transition temperature range from 93^{o}C to 135^{o}C. Strain at failure is within 3.5% to 5.5% (Mallick, 1993). Vinyl esters have fewer open sites in the molecular chain, making them more resistant to hydrolisis.

Some properties of commonly used resins (at 23^{o}C) are shown in Figure 2-8 to Figure 2-11.

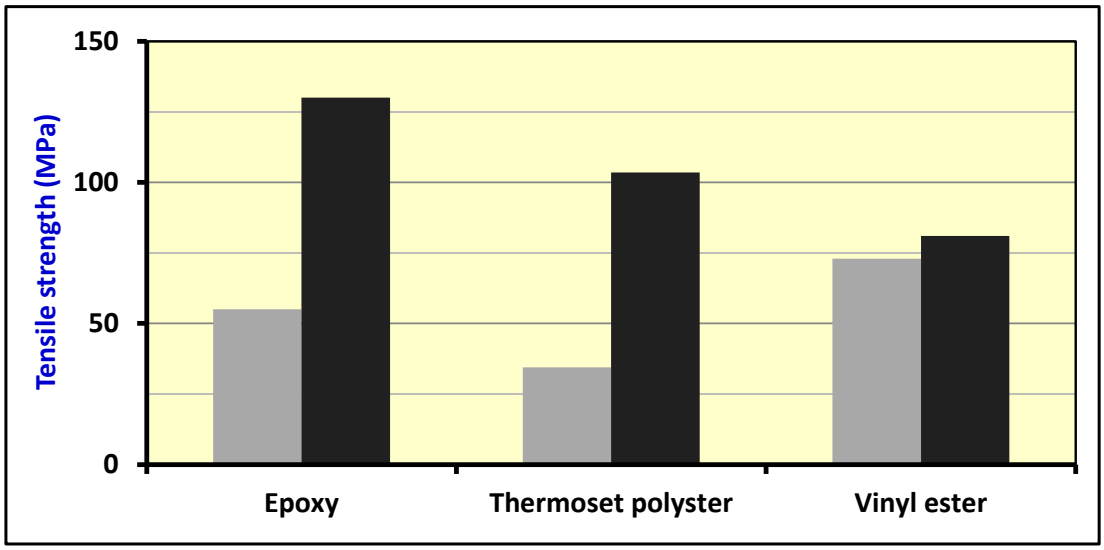

Figure 2-8: Tensile strength (MPa) of commonly used resins, after (Mallick, 1993). Grey bar represents minimum strength and black maximum strength.

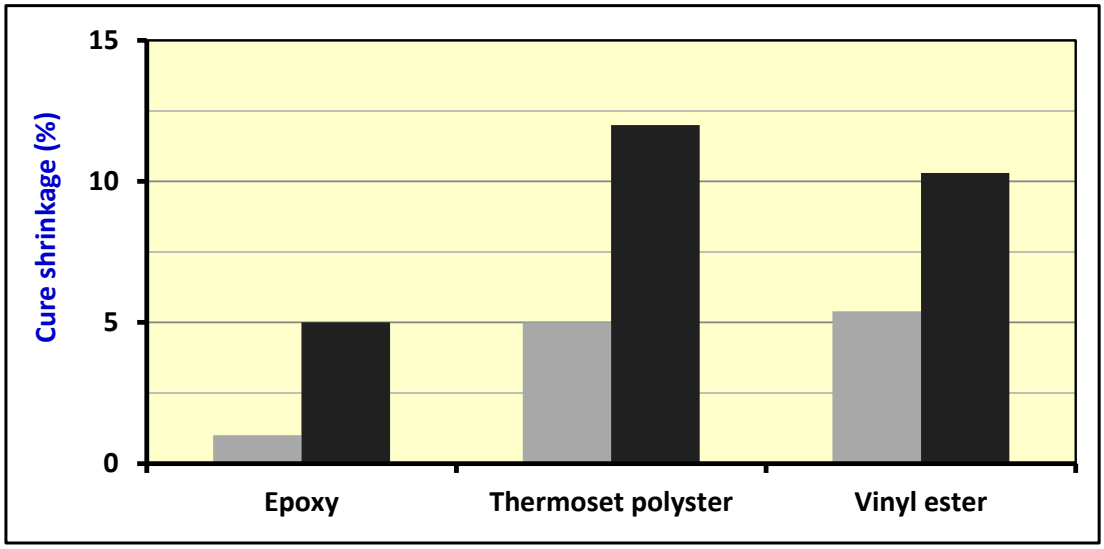

Figure 2-9: Cure shrinkage of commonly used resins, after (Mallick, 1993). Grey bar represents minimum strength and black maximum strength.

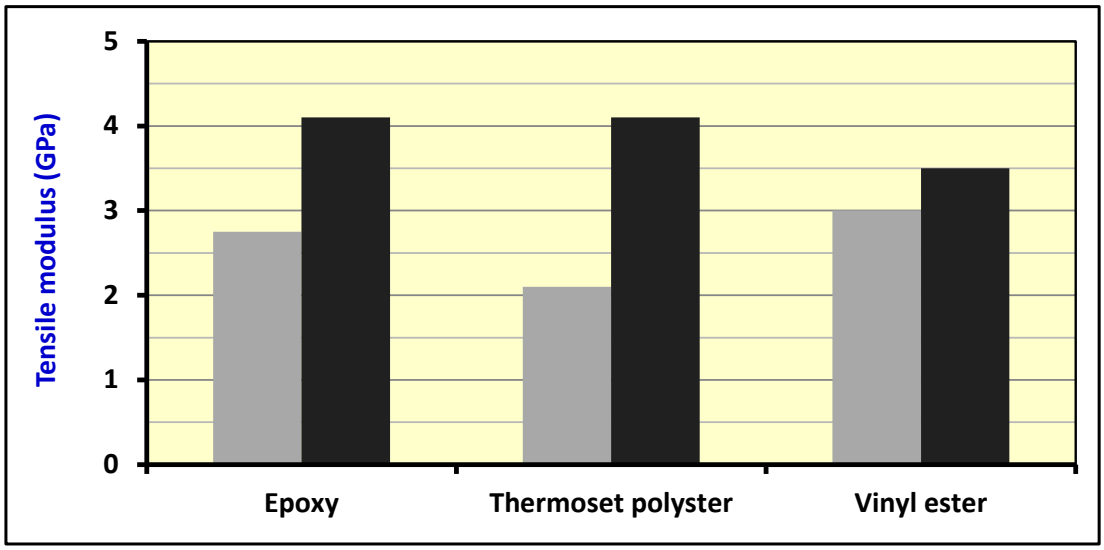

Figure 2-10: Tensile modulus of commonly used resins, After (Mallick, 1993). Grey bar represents minimum strength and black maximum strength.

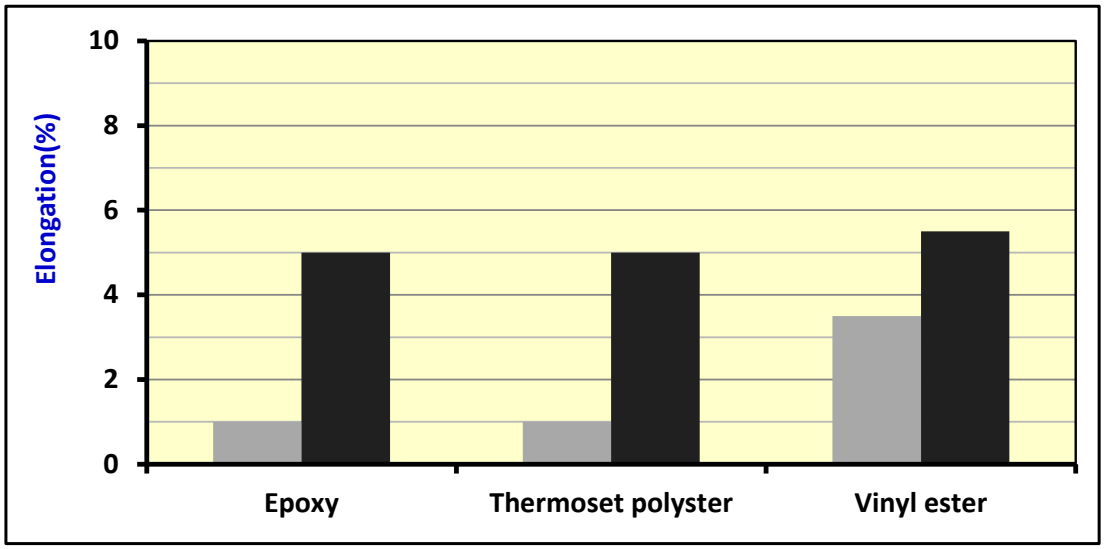

Figure 2-11: Elongation of commonly used resins, After (Mallick, 1993). Grey bar represents minimum strength and black maximum strength.

The failure strain of a resin system should nearly equal to the fibre strain to prevent matrix failure before fibre failure.

The primary charcteristic that determines the sutability of of a polymeric composite is the glass transition temperature, T_g. Glass transition temperature is the temperatute below which a polymer exists in the glassy state where only vibrational motion is present. Above this tempearture, individual molecules are able to move relative to each other. Elerstomer modifiers in resin formulation toughen thermostting matrices. This signifcantly improves impact and fracture strengths of

the cured polymer. The improvement is, however, at the expense of the Tg's of the cured resin.

Fibre components of composites

Reinforcing fibres provide high strength and stiffness to the matrix material so as to satisfy design requirements or repalce an existing part at an equal strength, stifnnsess and lower weight. Generally, the stiffness and strength of a composite material increases with increase in fibre volumetric ratio. After a ratio of 65%, however, the strength will start to decrease. This mainly due to the fact that the matrix cannot hold the fibres together properly (Hancox & Mayer, 1994).

The four commonly used fibres in the industry are E-glass, S-glass, aramid and carbon. Fibre glass have good electrical, fire resistance and strain at fialure. E-glass is the cheapest of all the four fibres. S-glass is more expensive than E-glass and has higher strength and stiffness than E-glass (Hancox & Mayer, 1994).

Kevlar (Dupont), Techora (Teijin) or Twaron (Akzo Nobel) are trade name names, which are mostly used for aramid. It has high impact resistance, which makes it suitable for ballistic applications. Other advantages include high fire resistance, high thermal insulation and low cost. However, aramid have low compressive and flexural strength (Hancox & Mayer, 1994). Carbon fibres refer to fibres which are atleast 92 wt.% carbon in composition (AR Crabtree & Skrzypek, 1998). There are numerous grades of carbon fibres available in the market.

Table 2-2 below compares mechanical properties of of two high performance grades of carbon fibres with other fibres. It can be seen that high strength carbon fibres exhibit highest strength while high modulus carbon fibres exhibit highest modulus of elasticity. The specific modulus of carbon fibre (modulus/density ratio) is equally exceptionally high. Kevlar and polyethelene fibres have loer density than carbon fibre, but their melting point is quite low. The melting pouint of Kevlar is 500 oC and that of polythelene 147 oC, compared to 3700 oC and 1725oC for carbon fibre and glass fibre, respectively (A. R. Crabtree & Gavin, 2005). Commercially available carbon fibres are divided into three groups, the general purpose (GP), high performance, (HP) and activated carbon fibres (ACF). The GP carbon fibres have low tensile strength, low modulus and less costly. High performance carbon fibres are more costly and have high tensile strength and high modulus strength. Activated

carbon fibres have large number of open micropores that act as adsorption sites. Commercail carbon fibres are fabriacted by using pitch or polyacrylonitrile (PAN) as the precursor.Carbon fibres based on pitch attain higher modulus than those based on PAN. This is because pitch is more graphitizable than PAN. High molus is, however, associated with lower elongation. On the other hand, fibres based on PAN exhibit higher tensile strength and greater elongation than those based on pitch.

Table 2-3 shows tensile propeties of various PAN-based high performance carbon fibres available in the market.

Table 2-2: Properties of various fibres, after (A. R. Crabtree & Gavin, 2005)

Material	**Density (g/cm3)**	**Tensile Strength (GPa)**	**Modulus of elasticity (GPa)**	**Strain (%)**	**Specific modulus (10^6 m)**	**Specific strength (10^4 m)**
E-glass	2.55	3.4	72.4	4.7	2.9	14
S-glass	2.50	4.5	86.9	5.2	3.56	18
Carbon (high strength)	1.50	5.7	280	2.0	18.8	19
Carbon (high modulus)	1.5	1.9	530	0.36	36.3	13
Kevlar	1.44	4.5	120	3.8	8.81	25.7
Boron	2.36	3.4	380	0.89	16.4	12
Polyethylene	0.97	2.59	120	2.2	12.4	27.4

Figure 2-12 shows the prices and tensile strengths of glass fibres, carbon fibres and aramid fibres. The greater the tensile strength, the higher the price. Carbon fibres provide higher tensile strength and are more expensive than glass and aramid fibres. Prices differ significantly among the different grades of carbon fibres.

The properties of the composite fibres depend upon their composition, stucture, synthesis and processing. An important index for engineering materials is their performance-to-cost ratio.

Table 2-3: Tensile properties of some available commercial carbon fibres, after (A Crabtree et al., 1997)

Type	Fibre Designation	Tensile Strength (GPa)	Modulus of elasticity (GPa)	Strain at failure (%)	Manufacturer
PAN	T-300	3530	230	1.5	Toray
	T-400H	4410	250	1.8	Toray
	T-800H	5590	294	1.9	Toray
	T-1000	7060	294	2.4	Toray
	MR 50	5490	294	1.9	Mitsubishi Rayon
	MRE 50	5490	323	1.7	Mitsubishi Rayon
	HMS-40	3430	392	0.87	Toho Rayon
	HMS-40X	4700	392	1.2	Toho Rayon
	HMS-60X	3820	588	0.65	Toho Rayon
	AS-1	3105	228	1.32	Hercules
	AS-2	2760	228	1.2	Hercules
	AS-4	3795	235	1.53	Hercules
	AS-6	4140	242	1.65	Hercules
	IM-6	4382	276	1.5	Hercules
	HMS4	2484	338	0.70	Hercules
	HMU	2760	380	0.70	Hercules

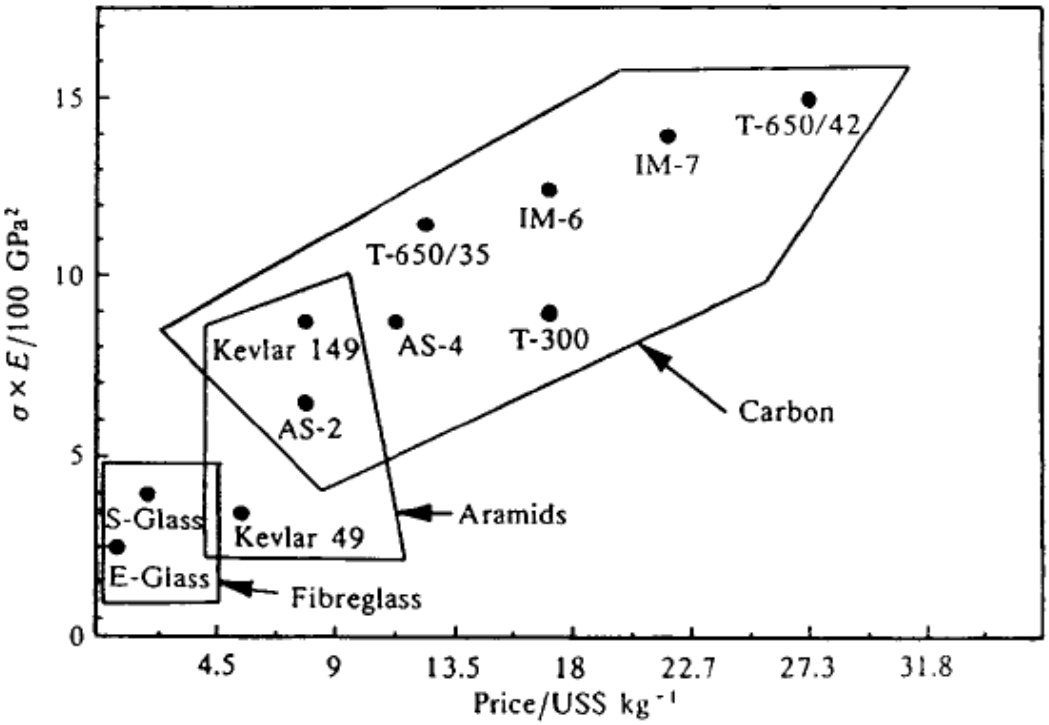

Figure 2-12: Product of tensile strength (σ) and tensile modulus (E) versus price of various composite fibres, after (Chung, 2012)

Clearly, the selection of the composite coiled tubing constituent materials is a critical step in the design process.

2.8.3 Composite coiled tubing

The development of composite coiled tubing (CCT) begun in the late 1980's and early 1990's (McClachie, 1999). The CCT comprise of a thermoplastic extrusion, on which the reinforcement is wound in a continuous process. The reinforcement consist of multiple, counter-wound, fibre layers, usually carbon or glass, or a hybrid of both, in a polymer matrix. The liner (resin) is chemically bonded to the structural reinforcement. The pipe then is cured in a tunnel oven and finished pipe wound into spools.

Composite coiled tubing drilling technology has been suggested as a faster and cheaper method for deep mineral exploration drilling. The composite CT offer several benefits compared to steel, including, excellent cyclic fatigue resistance-exceeds steel by one or twice orders of magnitude (H. Fowler, 1997b), significantly

lighter than steel with similar OD, resistant to corrosive fluids or gases such as carbon di oxide, hydrogen sulphide and hydrochloric acid, improved flow characteristics with smoother inner lining/surface. Figure 2-13 compares the specific strength of various composite tube materials with steel.

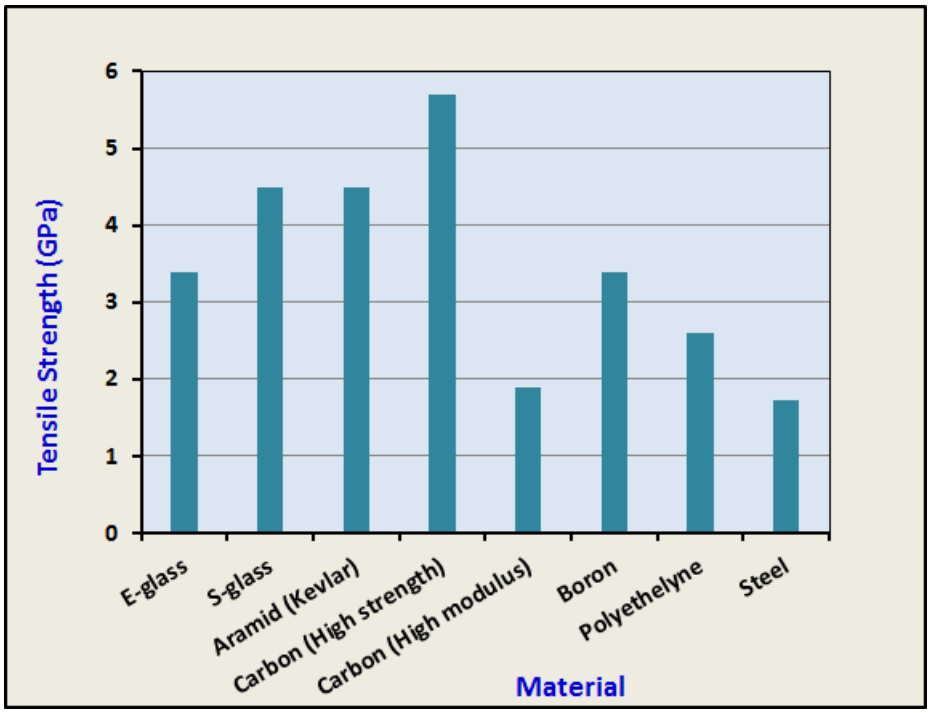

Figure 2-13: Specific strength of various composite materials and steel, after (Chung, 2012)

Figure 2-14 compares the weight of different composite materials with steel. Tests show less frictional loss – up to 25% lower in composite tube than calculated pressure loss for steel tubing with same ID (H. Fowler, 1997b). Composites have low thermal expansion.

Composites offer the potential to overcome the limitations of steel coiled tubing. However, the composite coiled tubing technology is new in the mining industry. There is no historical experience or service history in this type of application.

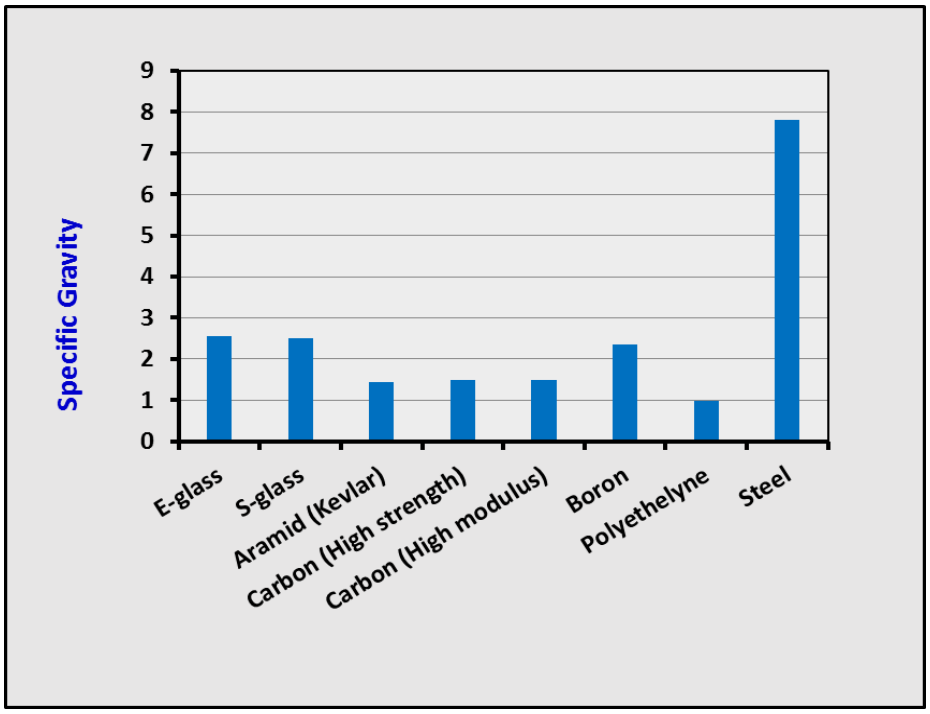

Figure 2-14: Specific weight of various composite fibres and steel, after (Chung, 2012)

2.8.4 Cost of composite vs steel coiled tubing

The cost of composite coiled tubes is generally higher that the steel coiled tube, in the order of three to five times. However, this is balanced with the expectation that the composite coiled tubing may last up to 10 times longer (H. Fowler, 1997a). Composite coiled tubing is also economically justifiable based on its light weight (typically about 1/3 the weight of steel) and its excellent corrosion resistance. Mechanical properties of composite coiled tube can also be custom-made and electrical conductors or optical fibres can be embedded in the tubing wall during manufacture.

2.9 Selection of Optimum Material

Performance index was utilized his study to select the optimum material for the coiled tube drilling string. In the initial stages of material selection, all the requirements of the application and the equivalent material property that would satisfy such requirements are listed. Possible candidate materials with the required properties are chosen. The performance requirements can be categorised as rigid and soft. Rigid requirements entail those that no compromise is allowed.

Soft requirements are usually ignored in the selection process (Farag, 1997). Ashby (1997) developed initial materials selection procedures/charts based on performance indices of two rigid property requirements. A mathematical model to assist in the initial selection procedure was compiled by Dargie, Parmeshwar, & Wilson (1982) Initial selection using rigid parameters is considered an elimination process rather than selection. Hence, initial selection would lead to multiple possible candidate materials. Further quantitative evaluation of soft properties would result in the selection of a better choice material.

Performance index method is a practical quantitative method that can be used to evaluate the soft properties. The selection process is carried out in three main steps. Initially, the material properties required to perform the job is prioritised using the digital logic method and weighting factor. This is followed by evaluation of candidate materials and their properties relative to each other. The final step relates the required priorities to the properties of candidate materials as indicated in Figure 2-15.

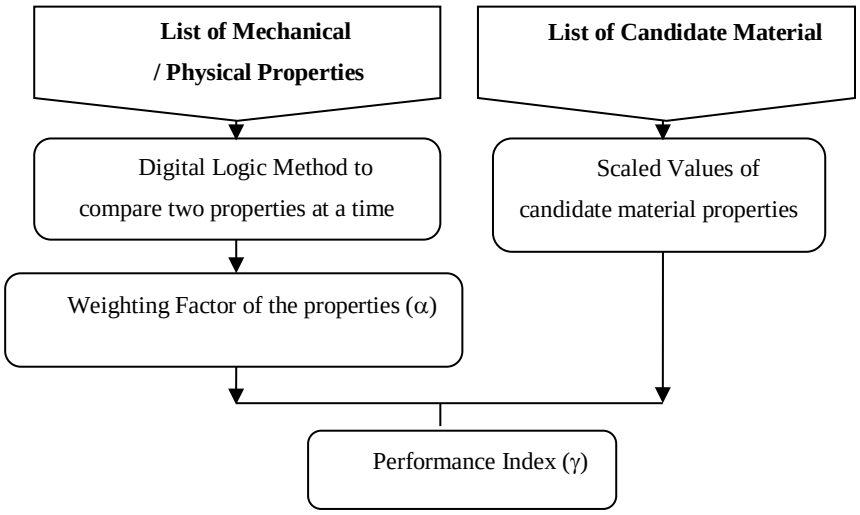

Figure 2-15: Material Selection Flow Chart, after (Farag, 1997)

In the coiled tube material selection, the rigid properties to be considered would be ductility and weight. Coiled tube material need to be ductile in order to bend around the reel and light for ease of mobility and safety. The suggested materials for coiled tube applications would exclude high strength brittle material such as high carbon steels and ceramics. Roufail & Rasouli (2012) carried out a

material selection analysis on a variety of candidate material for coiled tube rig using performance index method, based material unit weight, bend-ability, load carrying capacity, specific stiffness, fracture toughness and corrosion resistance. Two types of high strength-low-alloy steel, GT90 and GT100, including 6061 aluminium alloy, high strength carbon fibre and E-glass fibre composite materials were evaluated. Their study indicated that composite material had the higher performance indices, with glass fibre returning the highest score at 56% (Roufail & Rasouli, 2012).

2.10 Laminate Analysis

Composite laminate analysis and the theory behind laminate analysis are presented hereunder.

2.10.1 Laminate analysis

Composite materials are inherently more complicated in their structures than the single-phase materials such as most metals. For isotropic materials such as metals, the relationship between stress and strain is independent of the direction of the applied force. As such, only one elastic constant (Young's modulus) is required to describe the stress-strain relationship for uniaxially applied force. The stress/strain relationship is written:

$$\sigma = E\varepsilon \tag{2.17}$$

Where:

E, ε = Young's moduli and strain, respectively.

Composites are orthotropic; their mechanical response is dependent on the directional of applied force. Consequently, the stiffness of orthotropic plate must be described by two values, one along the longitudinal direction of fibres, E_1, and one transverse to the direction of fibres, E_2. Therefore, for an orthotropic material, the direction must be specified. For instance, the stress in 1 and 2 direction is denoted by:

$$\sigma_1 = E_1\varepsilon_1 \text{ or } \sigma_2 = E_2\varepsilon_2 \tag{2.18}$$

Figure 2-16 below depicts the differences between an isotropic and orthotropic plate material

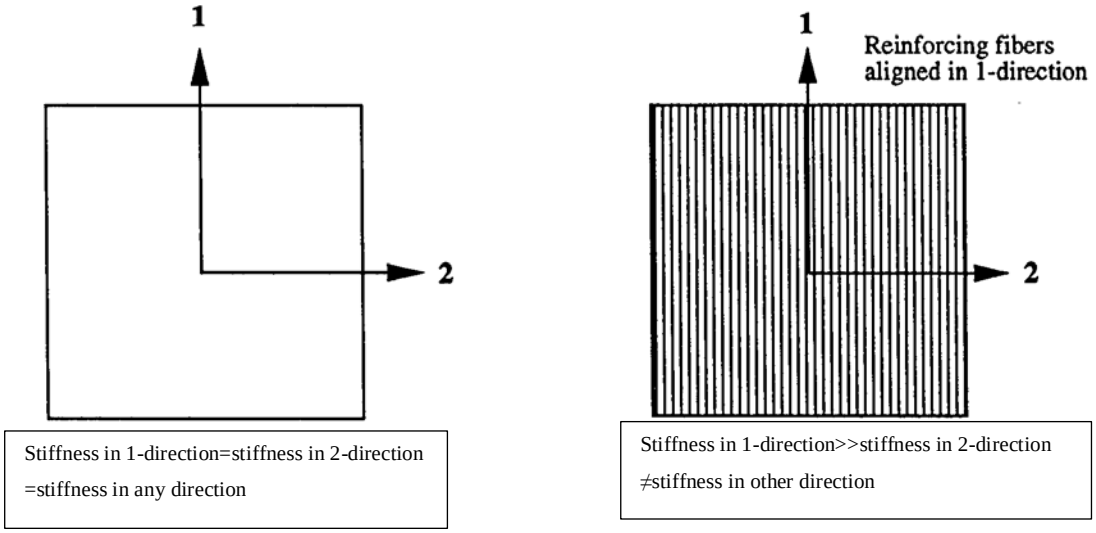

Figure 2-16: Difference between an Isotropic and orthotropic plate (Nettles, 1994)

A plate is considered orthotropic if the applied load is parallel or perpendicular to the fibres.

2.10.2 Classical Lamination theory

To analyse the mechanical response of a laminate, the behaviour of each individual ply must be predicted (Staab, 1999). The theory of laminate analysis, referred to as Classical Laminate Plate Theory, is based on the development of the engineering and physical properties of a ply based on the fibre angle to the principal loading direction. As stated above, plates will experience stresses in more than one direction within the plane. Poisson's ratio becomes important (Nestles, 1994):

$$\upsilon_{12} = -\frac{\varepsilon_2}{\varepsilon_1} \qquad \text{or} \qquad \upsilon_{21} = -\frac{\varepsilon_1}{\varepsilon_2} \tag{2.19}$$

For loading along fibres for loading perpendicular to the fibres

Where:

υ_{12} = Poisson's ratio in 1 direction

υ_{21} = Poisson's ratio in 2 direction

ε_1 = strain in 1 direction

ε_2 = strain in 2 direction

The strain components are now stretched due to applied force, minus the contraction of Poisson's effect due to another force perpendicular to this applied force. Hence (Nestles, 1994):

$$\varepsilon_1 = \frac{\sigma_1}{E_1} - \upsilon_{21}\varepsilon_2 \text{ and } \varepsilon_2 = \frac{\sigma_2}{E_2} - \upsilon_{12}\varepsilon_1 \tag{2.20}$$

Using equation (2.20):

$$\varepsilon_1 = \frac{\sigma_1}{E_1} - \upsilon_{21}\frac{\sigma_2}{E_2} \text{ and } \varepsilon_2 = \frac{\sigma_2}{E_2} - \upsilon_{12}\frac{\sigma_1}{E_1} \tag{2.21}$$

Shear forces can also be present. Shear stress and shear strain are related by shear modulus:

$$\tau_{12} = \gamma_{12}G_{12} \tag{2.22}$$

Where:

τ_{12} = shear stress in 1-2 plane

γ_{12} = shear strain

G_{12} = shear modulus

But since,

$$\upsilon_{21}E_1 = \upsilon_{12}E_2 \tag{2.23}$$

Equations (2.21) and (2.22), the stress-strain-law for an orthotropic material under plane stress conditions, as shown by Tsai, 1966, can be written in the following form(Nestles, 1994):

$$\begin{bmatrix} \varepsilon_1 \\ \varepsilon_2 \\ \varepsilon_{12} \end{bmatrix} = \begin{bmatrix} S_{11} & S_{12} & 0 \\ S_{12} & S_{22} & 0 \\ 0 & 0 & S_{66} \end{bmatrix} \begin{bmatrix} \sigma_1 \\ \sigma_2 \\ \tau_{12} \end{bmatrix} \tag{2.24}$$

Where:

$$S_{11} = 1/E_1\,,\ S_{22} = 1/E_2\,,\ S_{12} = -\upsilon_{12}/E_1 = -\upsilon_{21}/E_2 \text{ and } S_{66} = 1/G_{12} \tag{2.25}$$

The above matrix is called the compliance matrix. The stress, as a function of strain, can be found by inverting the compliance matrix. The inverted compliance matrix, called the stiffness matrix, is written as:

$$\begin{bmatrix} \sigma_1 \\ \sigma_2 \\ \sigma_{12} \end{bmatrix} = \begin{bmatrix} Q_{11} & Q_{12} & 0 \\ Q_{12} & Q_{22} & 0 \\ 0 & 0 & Q_{66} \end{bmatrix} \begin{bmatrix} \varepsilon_1 \\ \varepsilon_2 \\ \varepsilon_{12} \end{bmatrix} \tag{2.26}$$

Where:

$$Q_{11} = \frac{E_1}{1-\upsilon_{12}\upsilon_{21}},\ Q_{22} = \frac{E_2}{1-\upsilon_{12}\upsilon_{21}},\ Q_{12} = \frac{\upsilon_{21}E_1}{1-\upsilon_{12}\upsilon_{21}},\ Q_{66} = G_{12} \tag{2.27}$$

If the unidirectional lamina is loaded at some angle other than 0^o, the stresses and strains must be transformed into coordinates that coincide with principal material directions. Figure 2-17 below shows a free body diagram.

The stresses in 1 and 2 directions, in a transformation matrix form, are represented as:

$$\begin{bmatrix}\sigma_1\\ \rho_2\\ \tau_{12}\end{bmatrix}=\begin{bmatrix}\cos^2\theta & \sin^2\theta & \sin\theta\cos\theta\\ \sin^2\theta & \cos^2\theta & -\sin\theta\cos\theta\\ -\sin\theta\cos\theta & \sin\theta\cos\theta & \left(\cos^2-\sin^2\theta\right)\end{bmatrix}\begin{bmatrix}\sigma_x\\ \sigma_y\\ \tau_{xy}\end{bmatrix} \qquad (2.28)$$

The same matrix can be used to transform the strains. To transform from the 1-2 coordinate system to the x-y coordinate system, the inverse of Equation (2.28) is used.

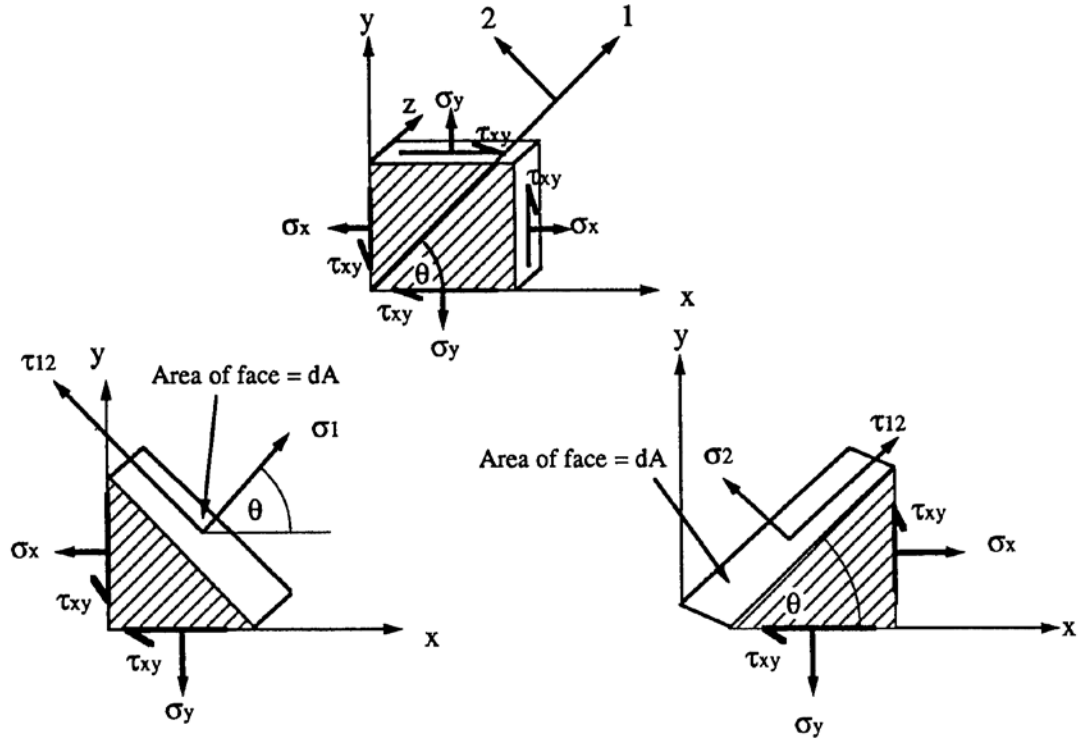

Figure 2-17: Orthotropic lamina (Nettles, 1994)

2.10.3 Constitutive equations of a laminate

Stress in each ply varies through the thickness of a laminate. Thus it is convenient to define stresses in terms of equivalent forces acting at the middle surface. The units of stress resultant are force per length.

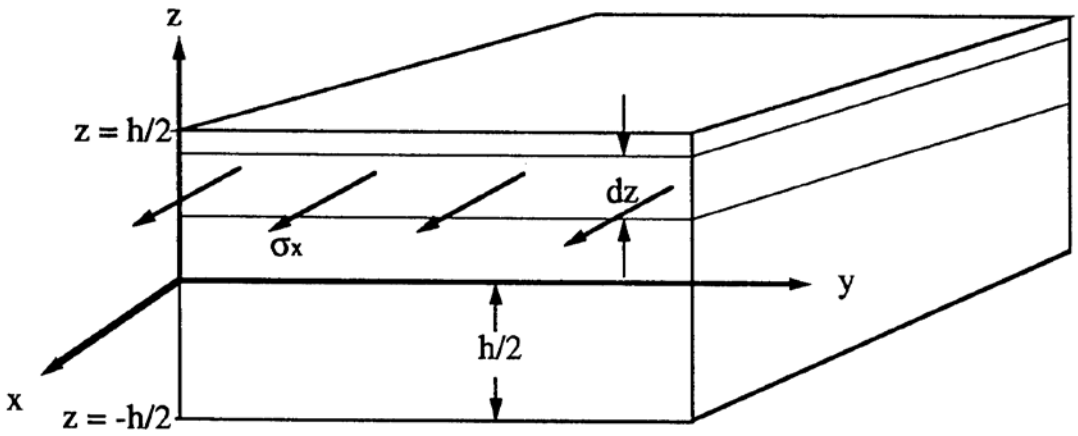

Figure 2-18: Stress resultant definition

$$\text{Total force in x-direction} = \sum \sigma_x (dz)(y)$$

$$\text{But as } dz \rightarrow 0,\ \sum \sigma_x (dz)(y) = y\int_{-h/2}^{h/2} \sigma_x dz \qquad (2.29)$$

$$N_x = \int_{-h/2}^{h/2} \sigma_x dz$$

Similarly, the stress in y-direction and shear stress can be deduced. Hence the three stresses (Nestles, 1994):

$$N_x = \int_{-h/2}^{h/2} \sigma_x dz$$

$$N_y = \int_{-h/2}^{h/2} \sigma_y dz \qquad (2.30$$

$$N_{xy} = \int_{-h/2}^{h/2} \sigma_{xy} dz$$

The stresses acting on the edge produces a moment about the mid-plane. The moment arm is at a distance z from the mid plane. It can also be deduced that the moment resultants can be written as:

$$M_x = \int_{-h/2}^{h/2} \sigma_x z dz$$

$$M_y = \int_{-h/2}^{h/2} \sigma_y z dz \qquad (2.31)$$

$$M_{xy} = \int_{-h/2}^{h/2} \sigma_{xy} z dz$$

The units are torque per unit length.

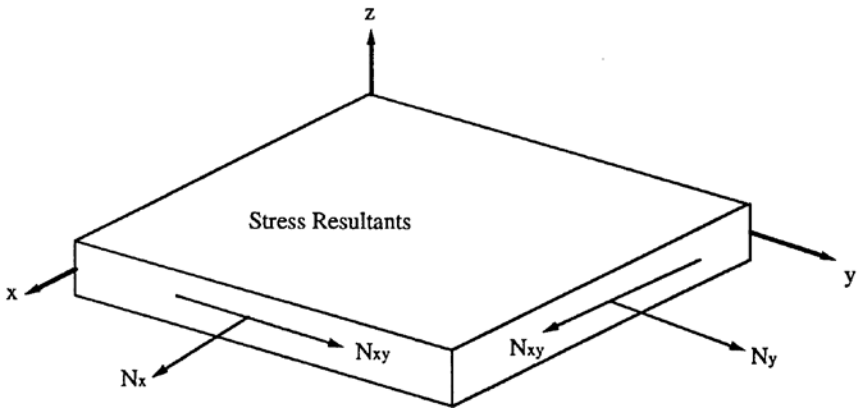

Figure 2-19: Direction of resultant stresses

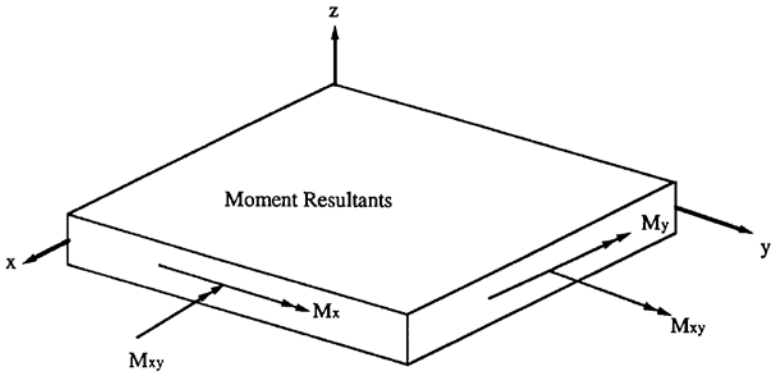

Figure 2-20: Direction of resultant moments

In a matrix form, the constitutive equations can be written as:

$$\begin{bmatrix} N_x \\ N_y \\ N_{xy} \end{bmatrix} = \begin{bmatrix} A_{11} & A_{12} & A_{16} \\ A_{12} & A_{22} & A_{26} \\ A_{16} & A_{26} & A_{66} \end{bmatrix} \begin{bmatrix} \varepsilon_x \\ \varepsilon_y \\ \varepsilon_{xy} \end{bmatrix} \qquad (2.32)$$

Where:

N = load per unit width

A = in-plane stiffness

ε = strain

The in-plane stiffness matrix relates the in-plane strains (axial, transverse and shear) of the laminate to the load per unit width.

Equation (2.33) indicates the flexural behaviour of a laminate. It relates the radii of curvatures to the D matrix to obtain the unit moment.

$$\begin{bmatrix} M_x \\ M_y \\ M_{xy} \end{bmatrix} = \begin{bmatrix} D_{11} & D_{12} & D_{16} \\ D_{12} & D_{22} & D_{26} \\ D_{16} & D_{26} & D_{66} \end{bmatrix} \begin{bmatrix} \kappa_x \\ \kappa_y \\ \kappa_{xy} \end{bmatrix} \tag{2.33}$$

Where:

M = edge moment per unit width

D = flexural stiffness

κ = radii of curvature

The flexure couple stiffness relates the radii of curvatures with unit loads or in-plane strains with unit moments as shown in equation (2.34).

$$\begin{bmatrix} N_x \\ N_y \\ N_{xy} \end{bmatrix} = \begin{bmatrix} B_{11} & B_{12} & B_{16} \\ B_{21} & B_{22} & B_{26} \\ B_{16} & B_{26} & B_{66} \end{bmatrix} \begin{bmatrix} \kappa_x \\ \kappa_y \\ \kappa_{xy} \end{bmatrix} \tag{2.34}$$

Where:

B = flexural coupling stiffness

The constitutive equations can also be written as:

$$\begin{bmatrix} N_x \\ N_y \\ N_{xy} \\ M_x \\ M_y \\ M_{xy} \end{bmatrix} = \begin{bmatrix} A_{11} & A_{12} & A_{16} & B_{11} & B_{12} & B_{16} \\ A_{12} & A_{22} & A_{26} & B_{21} & B_{22} & B_{26} \\ A_{16} & A_{26} & A_{66} & B_{16} & B_{26} & B_{66} \\ B_{11} & B_{12} & B_{16} & D_{11} & D_{12} & D_{16} \\ B_{12} & B_{22} & B_{26} & D_{12} & D_{22} & D_{26} \\ B_{16} & B_{26} & B_{66} & D_{16} & D_{26} & D_{66} \end{bmatrix} \begin{bmatrix} \varepsilon_x \\ \varepsilon_y \\ \varepsilon_{xy} \\ \kappa_x \\ \kappa_y \\ \kappa_{xy} \end{bmatrix} \quad (2.35)$$

The equations depict the in-plane/flexural behaviour of a laminate for a given deformation. In reduced form, Equation (2.35) becomes:

$$\begin{bmatrix} N \\ M \end{bmatrix} = \begin{bmatrix} A & B \\ B & D \end{bmatrix} \begin{bmatrix} \varepsilon^o \\ k \end{bmatrix} \quad (2.36)$$

If the laminate is symmetric and its engineering properties are known, it is possible to determine the in-plane engineering constants of the laminate from the A_{ij} matrix. For symmetric laminates, all the elements of B_{ij} matrix are zero. However, if the stacking sequence of the laminate is unsymmetrical, the computation of the in-plane engineering constants is more complicated as the calculations will involve the use of A_{ij}, B_{ij} and D_{ij} matrices. In a symmetric laminate the plies of the laminate are a mirror image about the geometrical plane.

2.11 Experimental works

During service, the coiled tube is exposed to six bend events for each drilled hole. The main cause of failure of the coiled tube string is the multiple bending events (Sas-Jaworsky & Williams, 1993). Therefore, understanding the coiled tubing life is a major concern. Fatigue testing of steel coiled tubes was initially carried by several CT manufacturing companies using different approaches. There was no standard approach making it difficult to compare the results. A method and testing apparatus for coiled tubing has been developed by Newman and Brown (1993), in an attempt to simplify and standardise fatigue testing. The fatigue test fixture specifications include (Feechan et al., 2009):

i. The CT test sample should be at least 5 ft length. A 2 ft “test section” in the centre of the 5 ft sample must be bent around a fixed radius of curvature and then straightened again to complete one cycle.
ii. It must be possible to change the radius of bending for various tests. This is by changing the bending form around which the CT is being bent.
iii. Bending must occur at a constant speed; one cycle should take about 30 seconds.
iv. The clamps at each end of the test specimen must be positioned in such a way as to allow 6 inch on each side of the test section to remain straight during testing.
v. No axial load may be applied to the CT by the bending machine.
vi. Internal pressure must be maintained in the CT sample with 5% of a set value throughout the test.
vii. Cooling fluid should be sprayed continuously on the outside of the CT to prevent the specimen heating during cyclic bending.
viii. The force required to bend the CT, pressure inside CT and number of cycles since beginning of the test must be monitored.
ix. Size, weight and cost of the bending machine should be kept as low as possible.

Figure 2-21 is a bending machine schematic showing the principle of operation outlined above.

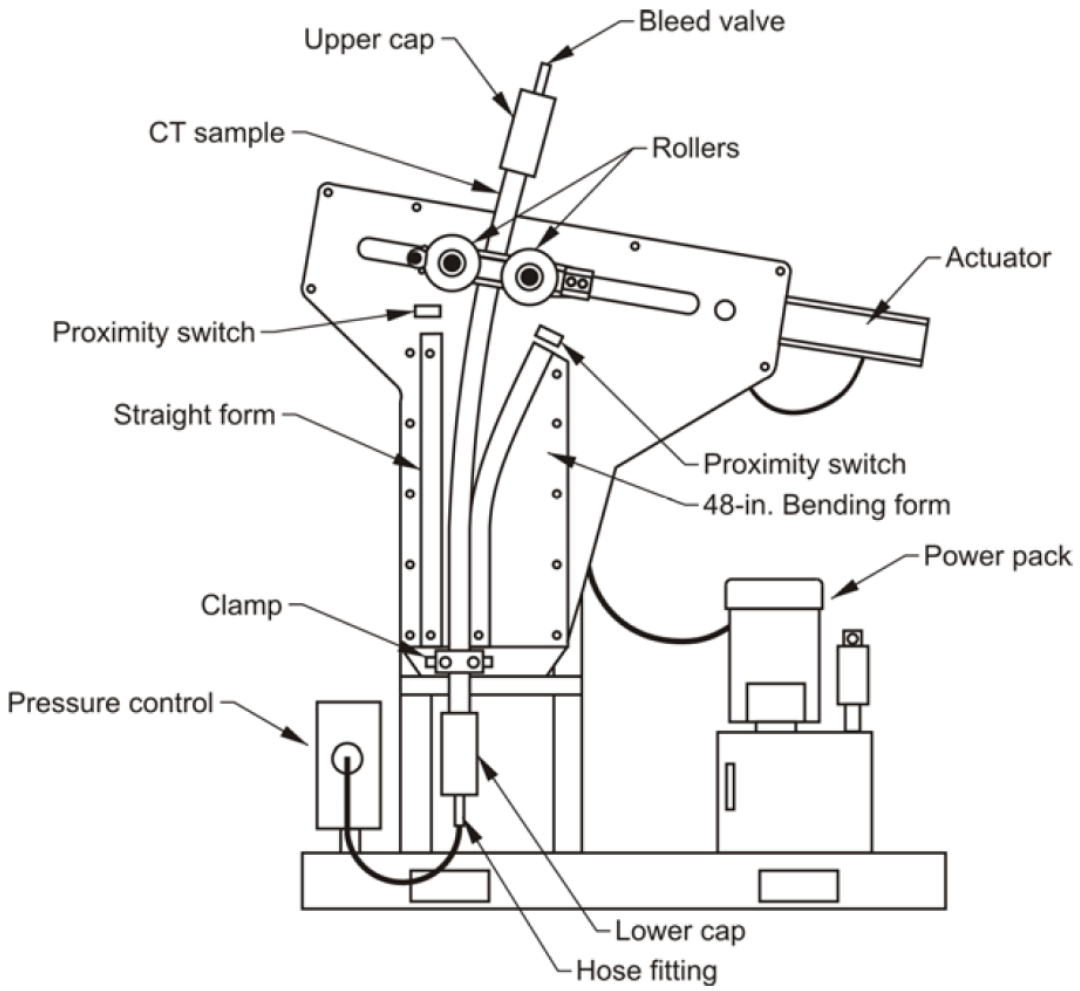

Figure 2-21: Sketch of fatigue bending machine, after (McClatchie et al., 1999)

A new bending machine was developed as part of this research work for evaluation of coiled tubing fatigue life for applications in mineral exploration drilling. Details of this new bending machine are outlined in section 3.4.

2.12 Conclusion

This chapter discusses coiled tubing drilling technology has a technology step-change to the mining industry. Coiled tubing drilling technology was suggested for use in deep mineral exploration drilling in Australia. CT drilling is a fast and reliable method and hence the number of drilled holes per day could be increased significantly. A review of existing literature on conventional steel coiled tubing applications in oil and gas industry is presented. While there have been several attempts to evaluate the performance of coiled tubes in the oil and gas industry, limited or no attempts have been made to assess coiled tubing performance in deep

hard rock mineral exploration drilling. Moreover, there is no existing literature of CT material that is suitable for high speed drilling of hard rocks for deep mineral exploration. A review of alternative CT material (composites) is discussed in this chapter. The composite coiled tubing appear to offer several benefits compared to steel, including light weight (typically about 1/3 the weight of steel), high strength-weight and modulus-weight ratios, corrosion resistance, 'smart tubing' with wound-in conductors and custom mechanical properties. Therefore, this study aims at proposing a suitable coiled tubing material that meets the challenges of deep mining exploration drilling. The research objective will be achieved through numerical and experimental study.

Chapter 3 Research Tools

3.1 Introduction

To meet the objectives of the proposed research program, simulation studies were undertaken using Hypersiszer and Abaqus software. Structural analysis using Hypersizer software was performed in order to investigate the effect of fibre orientation and number of fibre layers in an 8-layer composite flat laminate subjected to axial and flexural loads. A second model was developed using Abaqus software to test the mechanical properties of the 8-layer carbon/epoxy composite flat laminates. A third model consisted of an eight-layer carbon/epoxy tube. It was also constructed using Abaqus software to simulate applied loads and forces distribution across the body of a composite coiled tube.

Experimental study was carried out to evaluate the performance of commercially available steel coiled tubes under cyclic bending. Mechanical properties of the steel tubes were tested using a universal testing machine (UTM) after cyclic bending. Experimental study was also undertaken to test the mechanical properties of fabricated flat laminate composite sheets. Further experimental work was carried out to evaluate fatigue life and axial strength of designed composited coil tube. The flat laminate composite sheet samples were designed and fabricated at Curtin University, Petroleum Engineering Department. The composite tube sample was designed at Curtin University, Petroleum Engineering Department, and fabricated at Teakle Composites facility in Brisbane, Australia.

3.2 Computer modelling software

Composite laminate analysis and the theory behind laminate analysis are presented hereunder.

3.2.1 Hypersizer

Modelling of composite flat sheet laminates was undertaken using HyperSizer^{TM}, computer-based software developed by NASA to analyse, design and optimize laminate composite structural systems. The Hypersizer software analysis methods are

based on aerospace structural methods for strength, stability and stiffness that generates adequately size members and reliable structural integrity (Glenn, 2004). It includes methods for doing laminate-based as well as ply-based analyses.

Hypersizer optimises structures by generating a finite domain of candidate materials for the component. The pool of candidate material are sorted by weight and then analysed sequentially to find the lightest candidate material that passes all margin of safety checks. Hypersizer takes each candidate material design and generates stiffness using constitutive equation. With this stiffness, Hypersizer applies the loads (N_x, N_y, M_x) to obtain the strains. This process is done by applying classical lamination theory.

Governing equations

Hypersizer uses a closed-form classical laminate plate theory. The in-plane stiffness and flexural stiffness determines the overall behaviour of a structural laminate. The in-plane stiffness matrix relates the in-plane strains (axial, transvers and shear) of the laminate as shown in Equation (2.32). The flexural behaviour relates to the matrix (D), as shown in Equation (2.33).

The A, B and D matrices are computed ply-by-ply using the equations below (Research, 2011).

$$A = \sum \bar{Q}_k (z_{k-1} - z_k), B = -\frac{1}{2}\sum \bar{Q}_k \left[(z_{k-1})^2 - (z_k)^2\right], D = -\frac{1}{3}\sum \bar{Q}_k \left[(z_{k-1})^3 - (z_k)^3\right] \quad (3.1)$$

The expressions used to derive the reduced stiffness matrix $\bar{Q}_k$ are listed Equations (3.2) and (3.3) below (Research, 2011):

$$\begin{aligned}
\bar{Q}_{11} &= Q_{11}\cos^4\theta + 2(Q_{12} + 2Q_{66})\sin^2\theta\cos^2\theta + Q_{22}\sin^4\theta \\
\bar{Q}_{12} &= (Q_{11} + Q_{22} - 4Q_{66})\cos^2\theta\sin^2\theta + Q_{12}(\sin^4\theta + \cos^4\theta) \\
\bar{Q}_{22} &= Q_{11}\sin^4\theta + 2(Q_{12} + 2Q_{66})\sin^2\theta\cos^2\theta + Q_{22}\cos^4\theta \\
\bar{Q}_{16} &= (Q_{11} + Q_{12} - 2Q_{66})\sin\theta\cos^3\theta + (Q_{12} + Q_{22} - 2Q_{66})\sin^3\theta\cos\theta \\
\bar{Q}_{26} &= (Q_{11} + Q_{12} - 2Q_{66})\sin^3\theta\cos\theta + (Q_{12} + Q_{22} - 2Q_{66})\sin\theta\cos^3\theta \\
\bar{Q}_{66} &= (Q_{11} + Q_{22} - 2Q_{12} - 2Q_{66})\sin^2\theta\cos^2\theta + Q_{66}(\sin^4\theta + \cos^4\theta)
\end{aligned} \quad (3.2)$$

$$Q_{11} = \frac{E_1}{1-\upsilon_{12}\upsilon_{21}}$$

$$Q_{22} = \frac{E_2}{1-\upsilon_{12}\upsilon_{21}}$$

$$Q_{12} = \frac{\upsilon_{21}E_1}{1-\upsilon_{12}\upsilon_{21}} \qquad (3.3)$$

$$Q_{66} = G_{12}$$

$$\upsilon_{12} = E_2\upsilon_{12}/E_1 \qquad (3.4)$$

Hypersizer employs Max stress and max strain, quadratic and physics failure theories. The quadratic failure criteria including Tsai-Hill and Tsai-Wu failure theories are three-dimensional failure criteria that take into account the stress interactions that occur in composite materials under multi-axial stresses (Research_Corporation, 2012). Tsai-Hill failure theory was applied in this analysis.

Tsai-Hill criterion is based on an anisotropic extension of the Von Mises yield criterion proposed by Hill and applied to ply level failure (Corporation, 2012). The exact form of the Tsai Hill equation depends on the relative strength of the ply in the 1 and 2 direction and the directions of the stresses in each ply. The general form of the interaction equation is shown in Equations (3.5) and (3.6)

$$\text{If X} \geq \text{Y: } \frac{\sigma^2_{11}}{X^2} - \frac{\sigma_{11}\sigma_{22}}{X^2} + \frac{\sigma^2_{22}}{Y^2} + \frac{\sigma^2_{12}}{S^2} \geq 1.0 \qquad (3.5)$$

$$\text{If X < Y: } \frac{\sigma^2_{11}}{X^2} - \frac{\sigma_{11}\sigma_{22}}{Y^2} + \frac{\sigma^2_{22}}{Y^2} + \frac{\sigma^2_{12}}{S^2} \geq 1.0 \qquad (3.6)$$

X and Y is allowable stress of the ply in the longitudinal (1) and transverse (2) directions, respectively. Allowable shear stress of ply (transverse) is denoted by S. The X and Y terms depend on the stress in the 1 and 2 directions:

$$X = \begin{cases} X_t if\ \sigma_{11} \geq 0 \\ X_t\ f\ \sigma_{11} < 0 \end{cases} \tag{3.7}$$

$$Y = \begin{cases} X_t if\ \sigma_{22} \geq 0 \\ X_t\ f\ \sigma_{22} < 0 \end{cases} \tag{3.8}$$

Applied stresses on a ply in the longitudinal (1) and transverse (2) directions are represented by σ_{11} and $\sigma_{22,}$ respectively. τ_{12} denotes shear stress of a ply. X_t and X_c terms are allowable tension and compression stress of a ply in the longitudinal directions, respectively. Similarly, Y_t and Y_c are allowable tension and compression stress in the transverse directions, respectively.

The above interaction equation is rewritten as a margin of safety (MS) and performed for each ply laminate:

$$\text{If } X \geq Y \quad MS = \frac{1}{\sqrt{\frac{\sigma^2_{11}}{X^2} - \frac{\sigma_{11}\sigma_{22}}{X^2} + \frac{\sigma^2_{22}}{Y^2} + \frac{\tau^2_{12}}{S^2}}} - 1 \tag{3.9}$$

$$\text{If } X < Y: MS = \frac{1}{\sqrt{\frac{\sigma^2_{11}}{X^2} - \frac{\sigma_{11}\sigma_{22}}{Y^2} + \frac{\sigma^2_{22}}{Y^2} + \frac{\tau^2_{12}}{S^2}}} - 1 \tag{3.10}$$

In a multi-axial stress field, all three in-plane stress components affect the ply failure. The normal stress failure envelope represented by the Tsai Hill criterion as shown in Figure 3-1.

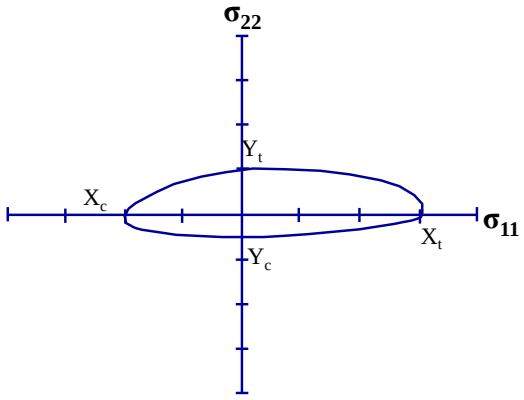

Figure 3-1: Tsai-Hill failure envelope with different compression/tension allowables (After Collier Research Corp.)

Fibre orientation and principal material axes with reference to coordinate axes are shown in Figure 3-2.

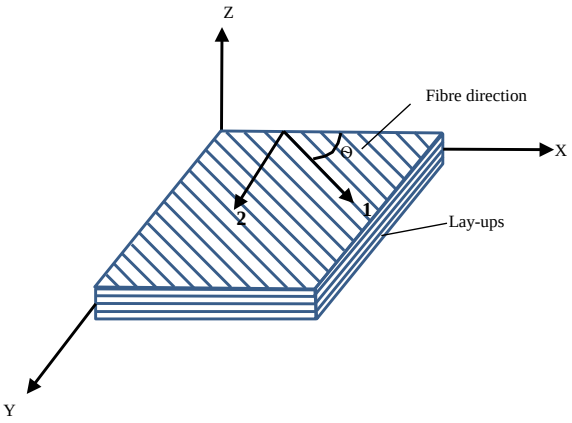

Figure 3-2: Fibre orientation and principal material axes with reference to coordinate axes

The Hashin failure criteria was originally proposed by Hashin in 1973 and revised in 1980 (Research, 2012). The 1980 version is included in Hypersizer. Fibre and matrix failure modes are identified in this criterion. For fibre failure (Research, 2012):

For fibre failure (Research, 2012):

$$\text{If } \sigma_{11} > 0: \; MS = \frac{1}{\left(\frac{\sigma_{11}}{X_T}\right)^2 + \left(\frac{\sigma_{12}}{X_S}\right)^2} - 1 \tag{3.11}$$

$$\text{If } \sigma_{11} < 0: MS = \left|\frac{X_c}{\sigma_{11}}\right| - 1 \tag{3.12}$$

For matrix failure:

$$\text{If } \sigma_{22} > 0: MS = \frac{1}{\left(\frac{\sigma_{22}}{Y_T}\right)^2 + \left(\frac{\sigma_{12}}{X_S}\right)^2} - 1 \tag{3.13}$$

$$\text{If } \sigma_{22} < 0\text{: } MS = \frac{1}{\left(\frac{\sigma_{22}}{2S_T}\right)^2 + \left[\left(\frac{Y_c}{2S_T}\right)^2 - 1\right]\frac{\sigma_{22}}{Y_c} + \left(\frac{\sigma_{12}}{S}\right)^2} - 1 \tag{3.14}$$

Under uniaxial loading conditions, the Tsai Hill Criterion simplifies to the Maximum stress criterion. The Maximum stress criterion governing equations shown below:

$$\text{If } \sigma_{11} > 0\text{: } MS = \frac{X_t}{\sigma_{11}} - 1 \tag{3.15}$$

$$\text{If } \sigma_{11} < 0\text{: } MS = \frac{X_c}{-\sigma_{11}} - 1 \tag{3.16}$$

$$\text{If } \sigma_{22} > 0\text{: } MS = \frac{Y_t}{\sigma_{22}} - 1 \tag{3.17}$$

$$\text{If } \sigma_{22} < 0\text{: } MS = \frac{Y_c}{-\sigma_{11}} - 1 \tag{3.18}$$

$$\text{If } \tau_{12} \neq 0\text{: } MS = \frac{S}{|\tau_{12}|} - 1 \tag{3.19}$$

The maximum stress criterion indicates failure when stress in any of the ply exceeds its uniaxial strength. The maximum stress failure envelope is shown in Figure 3-3.

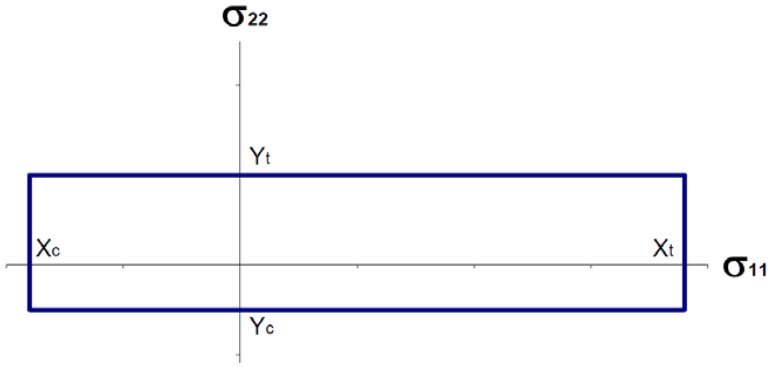

Figure 3-3: Maximum stress failure envelope

3.2.2 Abaqus software

Composite tube was modelled using Abaqus software. Simulation tensile test of composite flat laminate sheet was also modelled using this software. Abaqus is general-purpose finite element software providing powerful analysis features in an interactive and visual environment. The geometry definition of each part is parametric and feature based; it allows quick modifications. Parts can be created in numerous ways and they are then assembled together to create the analysis model. Section and material properties can be defined and assigned to regions of the parts. The program offers a range of analysis procedures, such as: static and dynamic stress analysis, eigenvalue buckling analysis and post buckling analysis.

There are also possibilities to take nonlinear behaviour into consideration, including geometric, material and contact nonlinearity. The loading can be created combining concentrated, distributed and pressure loads and body forces. Abaqus contains advanced algorithms for automatic meshing regions and the density of the mesh can be controlled by applying mesh seeds globally and locally. The software program also includes an extensive element library, including element families such as:

- Solid elements
- Shell elements
- Beam elements
- Rigid elements

Abaqus provides a suite of post processing features in order to enable efficient interpretation of results (Abaqus, 2014).

Abaqus offers modelling of models that enables the prediction of onset of failure for elastic-brittle materials with anisotropic behaviour. Thus the model is primarily intended for use with composite materials since they typically exhibit such behaviour. A composite material can fail in two basic failure modes:

- Failure of individual layers (plies) in tension, compression or shear
- Delamination between plies

Ply failure is associated with membrane and bending stresses. It is dependent on the loading and orientation of the fibres. Delamination is associated with the presence of shear stresses. Delamination failure mode can be important in laminates under fatigue loading. The in-plane (ply) failure mode depends on the direction and sign of

stresses and strains relative to the direction of fibres. Hence, first failure does not necessarily occur in one of the extreme layers. Thus all layers need to be monitored for failure.

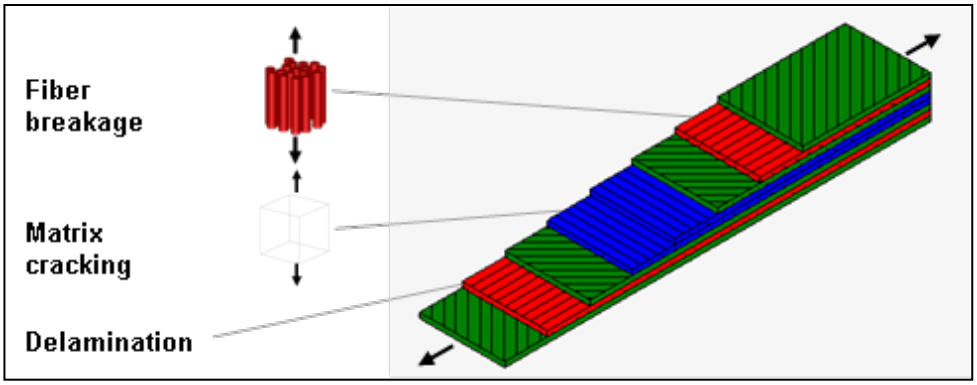

Figure 3-4: Fibre breakage, matrix cracking and delamination failure modes in composites

The ply failure usually occurs due to any or all of the following failure modes:

- Fibre tension or compression
- Matrix tension or compression

Ply failure modes can occur sequentially and are likely to interact. It is a common practice in composite analysis to determine only the first point of failure. Abaqus software has several such "initial failure envelopes". The software offers five standard plane stress orthotropic failure measures.

The stress-based failure option defines tensile and compressive stress limits in 1 and 2 directions and shear strength in 1-2 plane. The strain-based failure option defines tensile and compressive strain limits in 1 and 2 directions and shear strength in 1-2 plane.

Governing equations

The stress-based failure theories include Maximum stress, Tsail Hill, Tsai-Wu and Azzi-Tsai-Hill. Strain-based failure includes Maximum Strain failure theory.

Maximum stress theory is the simplest stress-based failure model. It measures the stress in each ply component against the corresponding stress limit. It is defined:

If $\sigma_{11} > 0$, set $X = X_t$, otherwise set $X = X_c$

If $\sigma_{22} > 0$, set $Y = Y_t$, otherwise set $Y = Y_c$

It requires that:

$$I_F = \left(\frac{\sigma_{11}}{X}, \frac{\sigma_{22}}{Y} \left| \frac{\sigma_{12}}{S} \right| \right) < 1.0 \tag{3.20}$$

The accuracy of this theory is limited since it provides no interaction between stress components in different directions.

Tsai-Hill theory was proposed by Tsai in 1968 as an extension of Hill's anisotropic plasticity model. The model is widely used as a simply failure criterion for composite lamina.

If $\sigma_{11} > 0$, set $X = X_t$, otherwise set $X = X_c$

If $\sigma_{22} > 0$, set $Y = Y_t$, otherwise set

Tsai-Hill criterion requires that:

$$I_F = \left(\frac{\sigma^2{}_{11}}{X^2} - \frac{\sigma_{11}\sigma_{22}}{X^2} + \frac{\sigma^2{}_{22}}{Y^2} + \frac{\sigma^2{}_{12}}{S^2} \right) < 1.0 \tag{3.21}$$

F_F is the failure criterion.

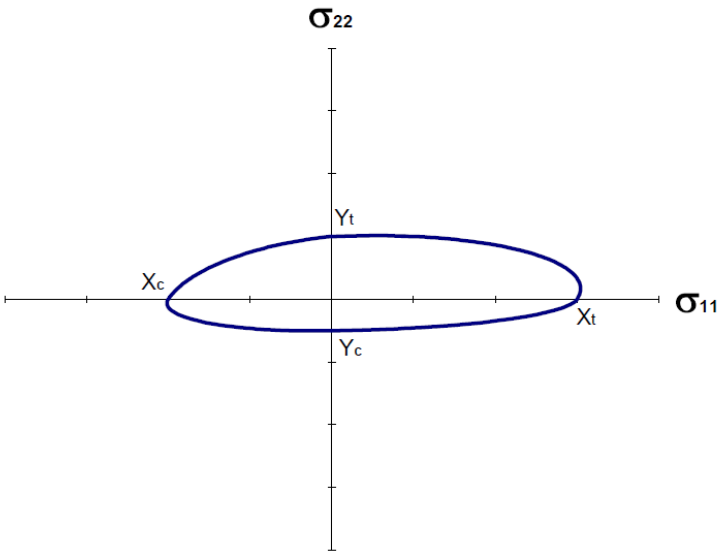

Figure 3-5: Tsai-Hill versus Maximum stress failure envelope

This is a piecewise continuous failure surface; at any given value of shear stress, σ_{12}, four separate elliptical arcs are present (σ_{11} σ_{22}) in space.

Tsau-Wu failure criterion provides for smooth form of Tsai Hill criterion. It uses an additional coefficient (F_{12}). The failure criterion is defined as:

$$I_F = F_1\sigma_{11} + F_2\sigma_{22} + F_1\sigma_{11} + F_{11}\sigma^2{}_{11} + F_{22}\sigma^2{}_{22} + F_{66}\sigma^2{}_{12} + 2F_{12}\sigma_{11}\sigma_{22} < 1.0 \tag{3.22}$$

The Tsai-Wu coefficients are defined as:

$$F_1 = \frac{1}{X_t} + \frac{1}{X_c},\ F_2 = \frac{1}{Y_t} + \frac{1}{Y_c} \tag{3.23}$$

$$F_{11} = \frac{1}{X_t X_c}, F_{22} = \frac{1}{Y_t Y_c},\ F_{66} = \frac{1}{S^2} \tag{3.24}$$

If σ_{biax} is given, then:

$$F_{12} = \frac{1}{2\sigma_{biax}{}^2}\left[1 - \left(\frac{1}{X_t} + \frac{1}{X_c} + \frac{1}{Y_t} + \frac{1}{Y_c}\right)\sigma_{biax} + \left(\frac{1}{X_t X_c} + \frac{1}{Y_t Y_c}\right)\sigma^2{}_{biax}\right] \tag{3.25}$$

Otherwise,

$$F_{12} = f^* \sqrt{F_{11}F_{22}} \tag{3.26}$$

Where:

$-1.0 \leq f^* \leq 1.0$, default value is 0 (zero)

Azzi-Tsai-Hill failure theory is similar to Tsai-Hill theory except that the absolute value of cross product is taken:

$$I_F = \left(\frac{\sigma^2{}_{11}}{X^2} - \frac{|\sigma_{11}\sigma_{22}|}{X^2} + \frac{\sigma^2{}_{22}}{Y^2} + \frac{\sigma^2{}_{12}}{S^2}\right) < 1.0 \tag{3.27}$$

Maximum strain failure theory is a simple model that defines failures from the largest strain component relative to corresponding strain limit.

If $\varepsilon_{11} > 0$, set $X_\varepsilon = X_{\varepsilon t}$, otherwise set $X_\varepsilon = X_{\varepsilon c}$

If $\varepsilon_{22} > 0$, set $Y_\varepsilon = Y_{\varepsilon t}$, otherwise set $Y_\varepsilon = Y_{\varepsilon c}$

The Maximum strain failure criterion requires that:

$$I_F = \max\left(\frac{\varepsilon_{11}}{X_\varepsilon}, \frac{\varepsilon_{22}}{Y_\varepsilon}\left|\frac{\gamma_{12}}{S_\varepsilon}\right|\right) < 1.0 \tag{3.28}$$

Experimental data has shown, however, that this model is generally not accurate as the maximum stress failure theory (Abaqus, 2014)

Stiffness of composite

For a unidirectional lamina, it is assumed that the fibres are parallel and that the fibres and matrix are bonded without any slippage between the interfaces. Hence the fibre and matrix experience the same strain. This isostrain phenomenon, first observed by Voight (1910), is represented as:

$$\varepsilon_c = \varepsilon_f = \varepsilon_m \tag{3.29}$$

$$p_c = p_f + p_m \tag{3.30}$$

If an axial load is applied in the longitudinal direction, it will be shared by the fibre and the matrix, in accordance with the rule of mixture:

$$\sigma_c A_c = \sigma_f A_f + \sigma_m A_m \tag{3.31}$$

Equation (3.31) can be simplified to:

$$E_c = E_f V_f + E_m(1 - V_f) = E_{11} \tag{3.32}$$

E_{11} is the elastic moduli of the laminate in the longitudinal direction.

The Halpin/Tsai model was used. The model applies simple and generalised semi-empirical equations to approximate the modulus of the composite laminate and

considers the geometry of the fibres. The equations are reliable if the fibre volume fraction volume does not equal to 1. The Halpin/Tsai model equations for computing the longitudinal modulus, transverse modulus and shear modulus are listed below:

$$E_{11} = E_m(1 + \varsigma_{11}\eta_{11}V_f)/(1 - \eta_{11}V_f) \tag{3.33}$$

$$E_{22} = E_m(1 + \varsigma_{11}\eta_{22}V_f)/(1 - \eta_{22}V_f) \tag{3.34}$$

$$G_{12} = E_m(1 + \varsigma_{12}\eta_{12}V_f)/(1 - \eta_{12}V_f) \tag{3.35}$$

$$\varsigma_{11} = 2(lt) + 40(V_f)^{10} \tag{3.36}$$

$$\varsigma_{22} = 2(wt) + 40(V_f)^{10} \tag{3.37}$$

$$\varsigma_{12} = (wt)^{1.73} + 40(V_f)^{10} \tag{3.38}$$

$$\eta_{11} = \frac{\left(\frac{E_f}{E_m} - 1\right)}{\left(\frac{E_f}{E_m} + \varsigma_{11}\right)} \tag{3.39}$$

$$\eta_{22} = \frac{\left(\frac{E_f}{E_m} - 1\right)}{\left(\frac{E_f}{E_m} + \varsigma_{22}\right)} \tag{3.40}$$

$$\eta_{12} = \frac{\left(\frac{G_f}{G_m} - 1\right)}{\left(\frac{G_f}{G_m} + \varsigma_{12}\right)} \tag{3.41}$$

ς is a measure of reinforcement which dependant on fibre geometry, packing geometry and loading condition.

3.3 Equipment

3.3.1 Bending machine

During service, the coiled tube is exposed to multiple bend events for each drilled hole. The main cause of failure of the coiled tube string is the multiple bending events (Sas-Jaworsky & Williams, 1993). Therefore, understanding the coiled tubing life is a major concern. Fatigue testing of steel coiled tubes was initially carried by several CT manufacturing companies using different approaches. There was no standard approach making it difficult to compare the results. A method and testing apparatus for coiled tubing has been developed by Newman and Brown (1993), in an attempt to simplify and standardise fatigue testing.

A similar fatigue testing machine has been designed and fabricated at Curtin University, Petroleum Engineering department (CRC, 2014) to evaluate the flexural strength of steel and composite coiled tubes. Figure 3-6 shows a schematic diagram of the machine and test arrangement. Side view of the bending machine is shown in Figure 3-7. The base of the bending machine and the pressure fittings for pressuring coiled tube are shown in

Figure 3-8. The machine is driven by a 4 kW electric pump with hydraulic flow of 12.5 litres per minute. Maximum pressure of the pump's power pack is 17 MPa (2,465 psi). The electric pump drives the hydraulic piston, which pulls the coiled tube test sample over a bend form. The hydraulic cylinder load capacity is approximately 32 ton-force. A load cell is fitted to measure the amount of bending and flattening force resisted by the coiled tube. The direction of force is changed by shuttle valve once the hydraulic piston reaches the extreme end of each bending and flattening event. The bending machine uses bend forms of varying radii from 40-inch to 84-inch for testing. Bending forms of 40 inch and 55 inch radii are shown in Figure 3-9. A counter is fitted in the fixture and records the number of bend events. The specimen is attached vertically between a lower base and the upper arm which is attached to the piston rod. Lock nuts and acetyl sleeves are used to

ensure that the test sample was held in place rigidly at the lower support. At the upper support, the test sample is held by steel rollers attached to hydraulic piston. As the hydraulic piston is displaced linearly in forward and backward motion the coiled tube sample is accordingly subjected to cycles of bending and flattening about the vertical position. Coiled tube specimens of up to 60mm OD can be tested using this machine.

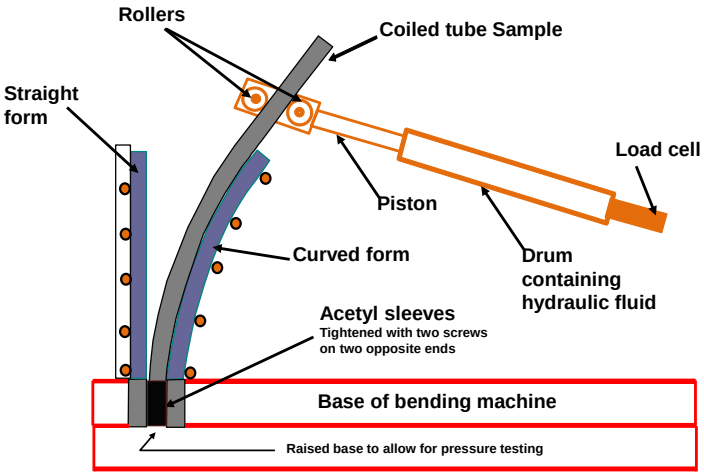

Figure 3-6 Schematic diagram of designed bending machine

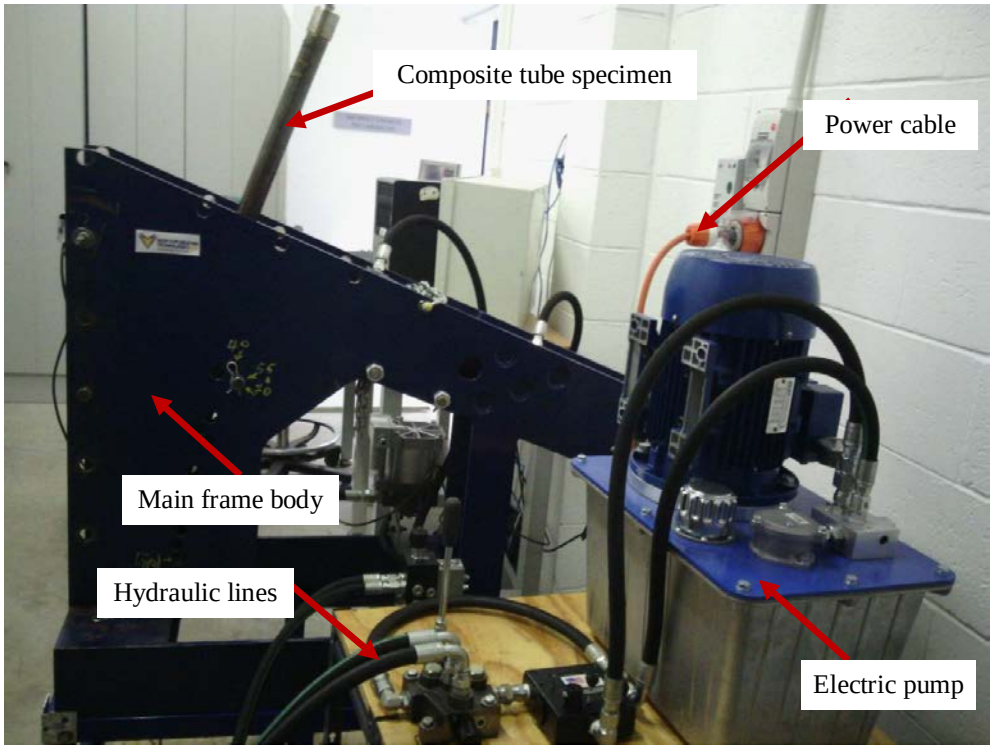

Figure 3-7 Side view of Commissioned Bending machine

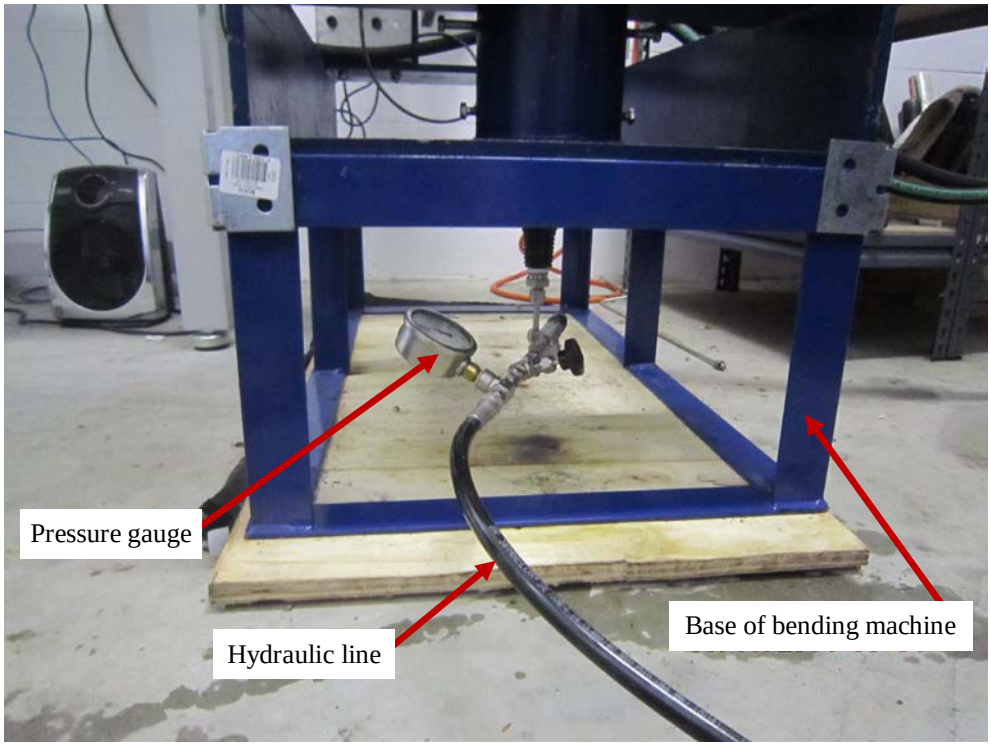

Figure 3-8: Base of bending machine and pressure fittings.

Figure 3-9 40 inch (1016mm)n radius steel bending form

A data acquisition box is shown in Figure 3-10. It captures and saves bending loads from the load cell and the number of bend cycles from the counter. The display of typical information during bending test is shown in Figure 3-11.

.

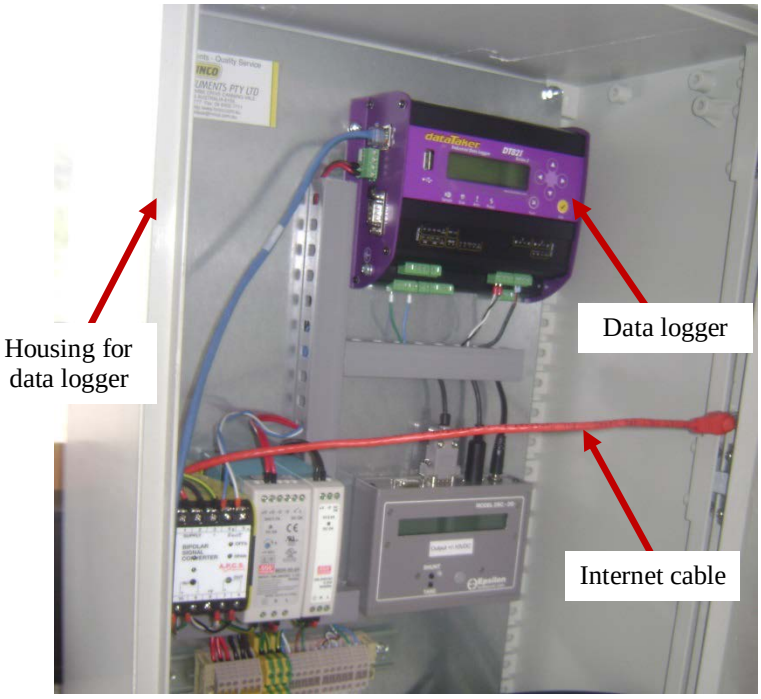

Figure 3-10 Bending machine data logger

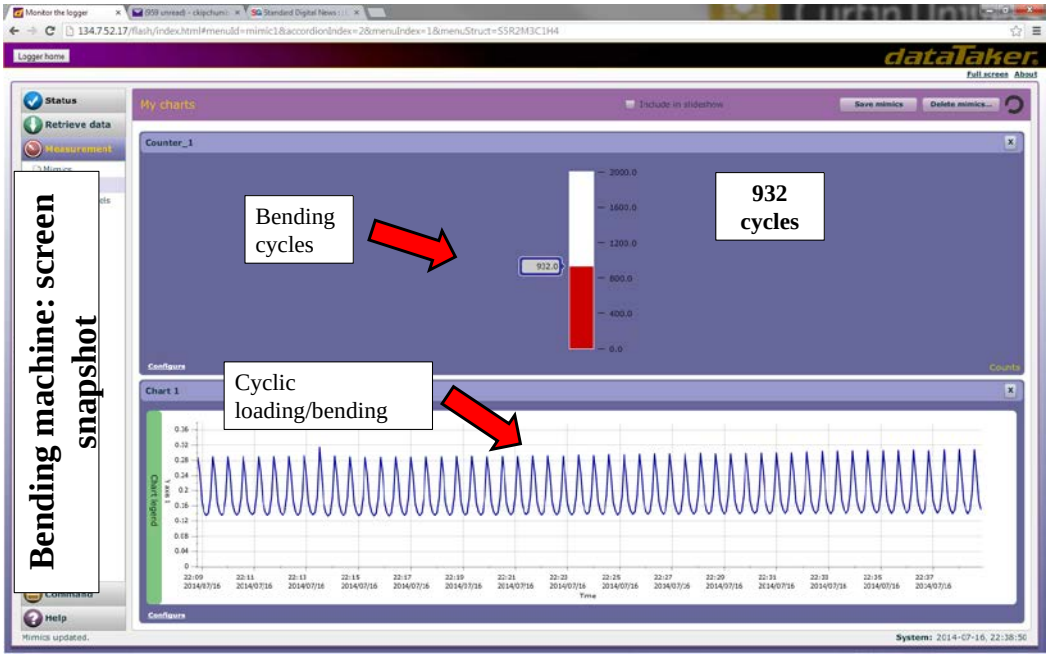

Figure 3-11 Typical display output of bending machine

Bending machine experimental procedures

Experimental set up using the bending machine is outlined in the following steps:

i. Personal protective equipment is required while working with the machine. These include steel capped footwear, safety glasses, and hand gloves.
ii. The equipment must be in 'OFF 'position before commencing any work on it.
iii. Loosen the sleeves-holding block by unscrewing it.
iv. Carefully remove the desired steel pins so as to allow for installation/removal of curved steel plates & straight steel and wooden plates. This will also ensure the smooth levelling of sleeve/pipe-holding block unit.
v. Install the curved steel plates. Ensure that the pins are correctly slotted for a 40" and 50"/70" curved plates.
vi. Install the lower sleeves, followed by the wooden and straight steel plates, which will straighten the pipe during test operations (for steel tubes).
vii. Insert steel pins to hold the steel/wooden plates. Ensure the plates are securely held in place.
viii. Install the pipe. Tighten the lower sleeves until the pipe is firmly gripped.
ix. Install the upper sleeves.
x. Insert steel pin to hold the piston/sleeve block.
xi. Tighten the sleeve block until the pie is firmly held.
xii. Check again to ensure the pipe is firmly held. Ensure there is no obstruction on the path of piston movement.
xiii. In case testing pipe under pressure, fill the tube with water. Test the tube before installing on bending machine to ensure there is no leakage on connections.
xiv. Install the tube and apply desired pressure using the manual hydraulic pump.
xv. Install the safety screen. Ensure no one is standing the "fire line" or the side directly opposite the pipe being bend.

xvi. Carefully run tests and collect required data.

xvii. Switch off the bending machine once the test is complete.

xviii. Uninstall the tube and correctly dispose of waste water/oil in the tube.

3.3.2 Universal testing machine (UTM)

A universal testing machine (UTM) is used to test the tensile and compressive strength of materials. The machine consists of five main parts:

- Main frame
- Load cell
- Movable crosshead
- Load cell and
- Output devise (Digital indicator)
- Drive system

The 613 model of Servo Hydraulic test machine was used in this test. The load capacity was 1000 kN with crosshead speed of 2 in/min (50 mm/min). Mechanical wedge action grips were selected for the test. They are easy to use, are self-tightening and self-aligning. Wedge gripping force increases as the pull load increases.

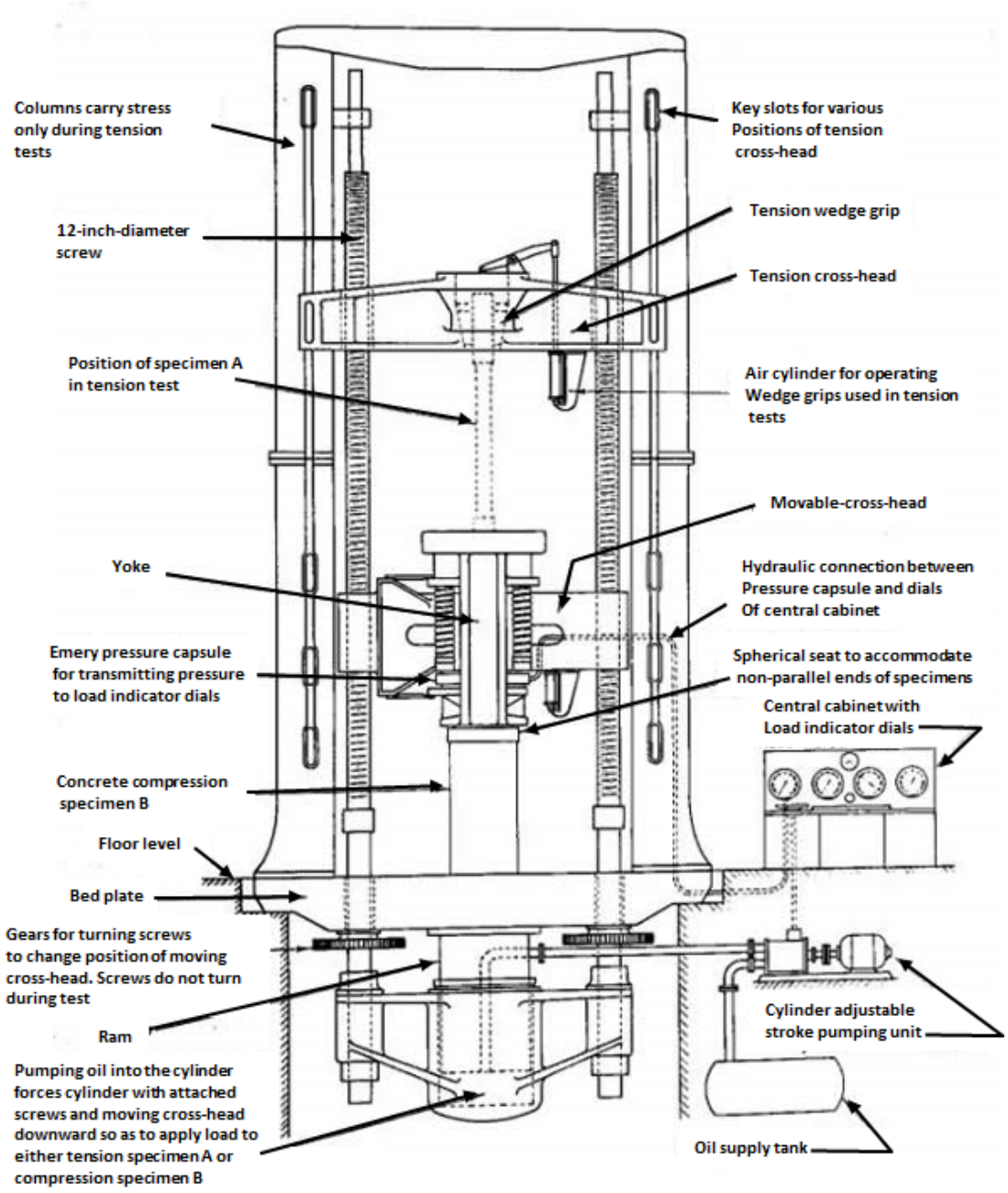

Figure 3-12 Schematic diagram of Universal testing machine (Mechanictips, 2011)

UTM machine experimental procedures

Material sample, with known dimensions is placed between the two grips which clamp the material on the upper and the lower end. The load is then applied on the gripped material at the upper end while the lower end is fixed. The load is increased at a constant rate while at the same time measuring the change in length (displacement) of the sample. A graph of load versus displacement is obtained from this test.

3.4 Conclusion

In order to design a suitable coiled tube for use in mineral exploration drilling and to understand the stress distribution on the tube under operation, a computer simulation will be undertaken. Hypersizer and Abaqus computer software tools to be utilized in this study were introduced in this section.

The experimental part of the research involved designing and building a fatigue bending fixture. The fixture is to be used in imposing bending fatigue events that a typical coil tube is exposed to during operation. The bending machine presented in this chapter complements the work carried out by other researchers in the area of coiled tubing.

Chapter 4 Steel Coiled tube Analysis

4.1 Introduction

The present accepted oil and gas industry standard for coiled tube material is high strength low alloy (HSLA) steel. During CT operations, as mentioned in Chapter 2 of this thesis, the steel coiled tube is plastically deformed. Plastic deformation imparts fatigue on the CT. Fatigue continues to accumulate over the life of the CT until fatigue cracks develop, resulting in failure of the tube.

An experimental study was carried out to evaluate the performance of commercially available HSLA steel coiled tubes under cyclic bending and the tube fatigue life

4.2 Steel CT experimental study

Low cycle fatigue experiments were conducted using commercially available drawn, seam welded steel coiled tubes. The steel coiled tubes were provided by DET-CRC, which obtained them from Global Tubing Company in the USA. The tubes were of two grades, GT90 and GT100, with a range of wall thicknesses.

Four HSLA steel coiled tube samples were used in this study. Mechanical properties and dimensions of the coiled tubes are shown in
Table 4-1.

Table 4-1: Mechanical properties of steel coiled tubes (tubing, 2012)

Tube No.	Material	Yield Strength MPa (Ksi)	OD mm (in)	Wall thickness mm (in)
A	HSLA GT100	689-792 (110-115)	50 (2)	5.69 (0.224)
B	HSLA GT100	689-792(110-115)	50(2)	4.45(0.175)
C	HSLA GT90	621-723(90-105)	50(2)	5.69(0.224)
D	HSLA GT90	621-723(90-105)	50(2)	4.45(0.175)

Steel coiled tube samples are shown is in Figure 4-1. The test samples were of 1200mm lengths. The tubes were each subjected to 70, 150 and 300 bending cycles, cumulatively, with no internal pressure. The bent samples were thereafter evaluated for their possible mechanical deterioration via tensile testing. Two tensile samples

were cut out of each tube. One sample was cut away from the bent section. The other sample contained the bent section within its gauge length. The initial dimensions of the tubes were measured prior each tension test. Testing was carried out at ambient temperature.

Figure 4-1: Steel coiled tube samples (Courtesy of DET-CRC)

Further experimental study was carried out using four HSLA steel coiled tubes. The tubes had similar outside diameter and wall thickness of 44.45mm (1.75 inches) and 3.4mm (0.134 inches), respectively. The tube samples were cut off from coiled tube rig at DET-CRC's Brukunga drill site in Adelaide. The tubes were pressurised with water fluid and subjected to bending tests on a 2800mm (110 inches) diameter bending form. Tube 1 was tested without internal pressure. Tube 2, 3 and 4 were tested with internal pressure of 600 psi, 2200 psi and 3200 psi, respectively.

4.3 Fabrication of steel coiled tubes

All steel coiled tubes begin as large coils of low-alloy carbon-steel sheet. The coils can be up to 1400mm (55 inches) wide and weigh up to 24 tons. The length of sheet depends on the thickness of the sheet. This could range from 300m for 6.35mm thick sheet and 1100m for 2.21mm thickness (Lane, 2005). The initial step in the

fabrication process is to slice flat strips from the coil of sheet using a slitting machine as shown in Figure 4-2. This operation is usually performed by a specialised company which ships the CT mill for further processing as indicated in Figure 4-3. The sheet's thickness sets the CT wall thickness and the OD of the finished CT is determined by the strip's width. In some instances, the gauge thickness of the sheet is tapered over a portion of its length, as shown in Figure 4-4. Tapered CT strings are produced using strips of different thicknesses or strips with continually changing thickness.

The CT strips with similar properties are spliced together using bias welds to form a single continuous strip with desired length of CT string. The CT mill forms the flat strip into a continuous tube and welds the edges together with a continuous longitudinal seam. The mill removes the external bead with a scarfing tool to provide a smooth OD. The weld seam is then normalized using highly localized induction heating. The weld seam is then allowed to cool prior to water cooling. Depending upon the mill setup, full tube eddy current or weld seam ultrasonic inspection may also be performed. The tubing is then passed through sizing rollers that reduce the tube OD slightly to maintain the specified manufacturing diameter tolerances. A full body stress relief treatment is then performed to impart the desired mechanical properties to the steel. The mill flushes any loose material from the finished CT string prior to winding on reel for shipping.

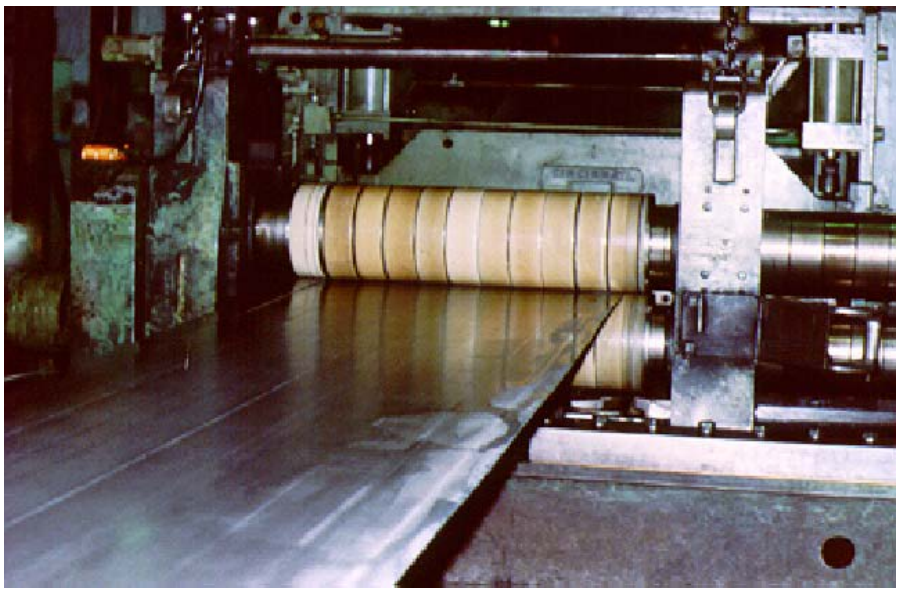

Figure 4-2: Slicing of steel sheet to strips (Lane, 2005)

Figure 4-3: Rolls of steel strips for further processing (Lane, 2005)

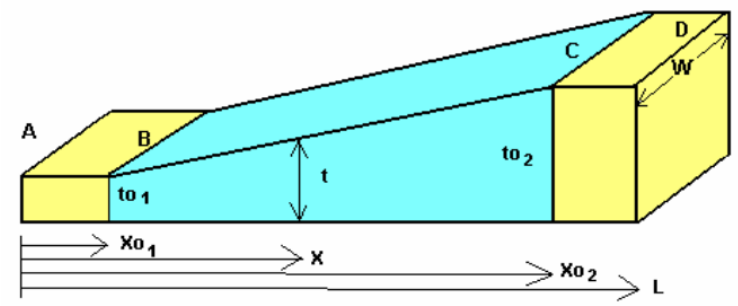

Figure 4-4: Tapered thickness (Lane, 2005)

4.4 Sensitivity analysis for grade and thickness vs fatigue weakening of steel coiled tubes

Bending imposes tensile and compressive stresses on the pipe. In fatigue analysis, it is a convention to consider tensile stresses positive and compressive stresses negative (Yung-Li Lee, 2005). Fatigue data are generated from constant-amplitude loading tests. Figure 4-5 shows a section of the load-time history for tube A. The peak is considered the transition point where the positive sloped-segment turns into a negative-sloped segment. The valley is the point where a negative-sloped section turns to a positive slope. Distance between two peaks or two valleys are considered one cycle.

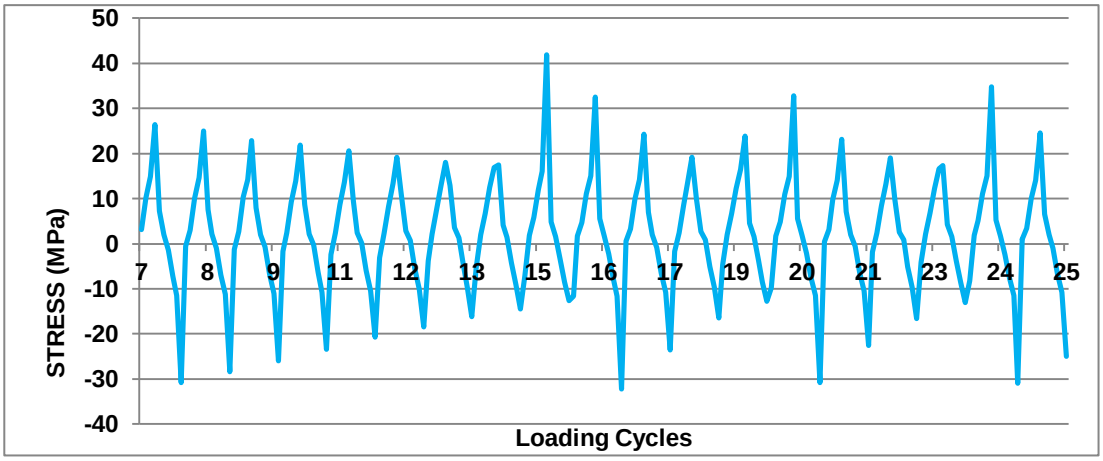

Figure 4-5: Load-time history

The fatigue testing was conducted using fully reversed loading. This indicated that the loading was alternating about a zero mean stress. The mean stress (S_{mean}) shown in Figure 4-6 is defined as

$$S_{mean} = \frac{S_{max} + S_{min}}{2} \tag{4.1}$$

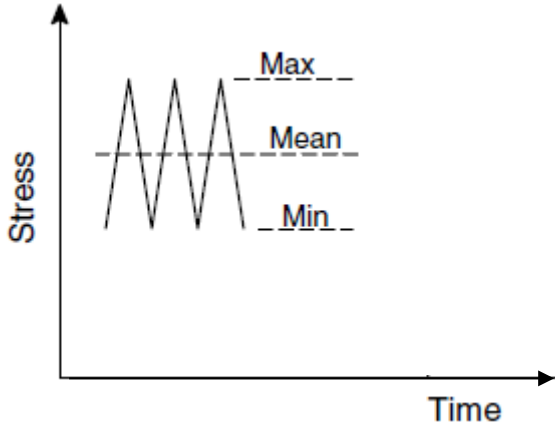

Figure 4-6: Schematic illustrating cyclic loading parameters

During fatigue testing, the specimen is subjected to alternating loads. The applied loads are defined by a constant stress range, S_r, or alternating stress, S_a. The stress

range is the algebraic difference between the maximum stress (S_{max}) and minimum stress (S_{min}) in a cycle (Yung-Li Lee, 2005).

$$S_r = S_{\max} - S_{\min} \tag{4.2}$$

$$S_a = \frac{S_r}{2} = \frac{S_{\max} - S_{\min}}{2} \tag{4.3}$$

Figure 4-7 illustrates the constant stress amplitude response of tube A. The alternating stress is computed using Equation (4.3) (ASM, 2008). The apparent trend line inserted in the graph represents slope or the rate of stress weakening of the tube.

Cyclic bending of coiled tube produces plastic strains (A. Crabtree, Skrzypek, H, and Wilde, G., 1997). The values of maximum alternating stresses, shown in Figure 4-7, decrease with the increase in the number of cycles. Cyclic hardening leads to increasing stress levels, while cyclic softening results in decreasing stress levels with increasing cycles (ASM, 2008) . The observed peaks, therefore, could be attributed to strain hardening of the material.

Figure 4-8 shows the mean stress, which is the algebraic average of the maximum and minimum stress in the cycle (ASM, 2008), as per Eq.(1). For a complete reversed bend, Sm = 0, an increase in mean stress causes a reduction in tube fatigue life (ASM, 2008). The alternating and mean stresses for the all of the tested coiled tube samples in this study are presented in Appendix A. The results indicated that the higher strength, thin-walled coiled tube (sample B) weakens at a lower rate, compared to similar thick-walled tube (sample A), as shown in Figure 4-9.

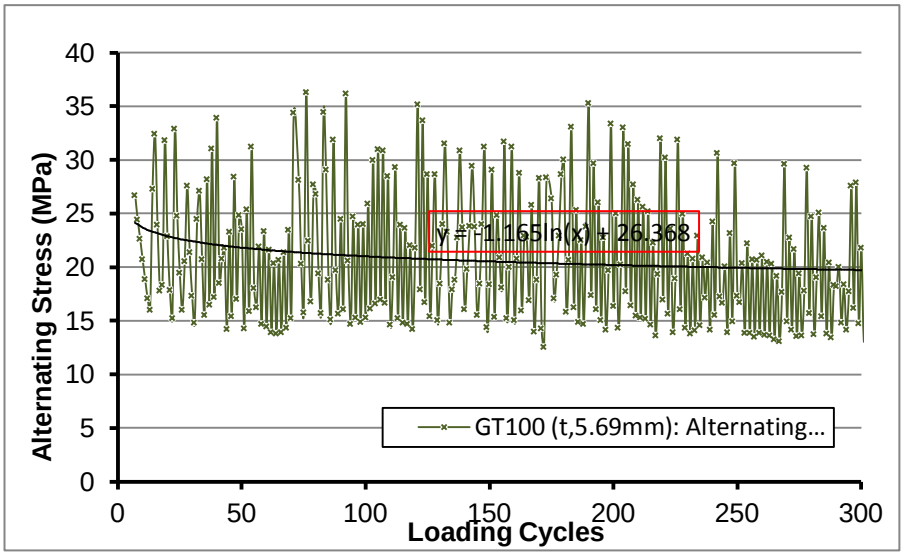

Figure 4-7: Alternating stress of tube A, after (Lagat, Roufail, Rasouli, Evans, & Soe, 2014)

Thin-walled coiled tube with lower strength (sample D) had the highest rate of weakening.

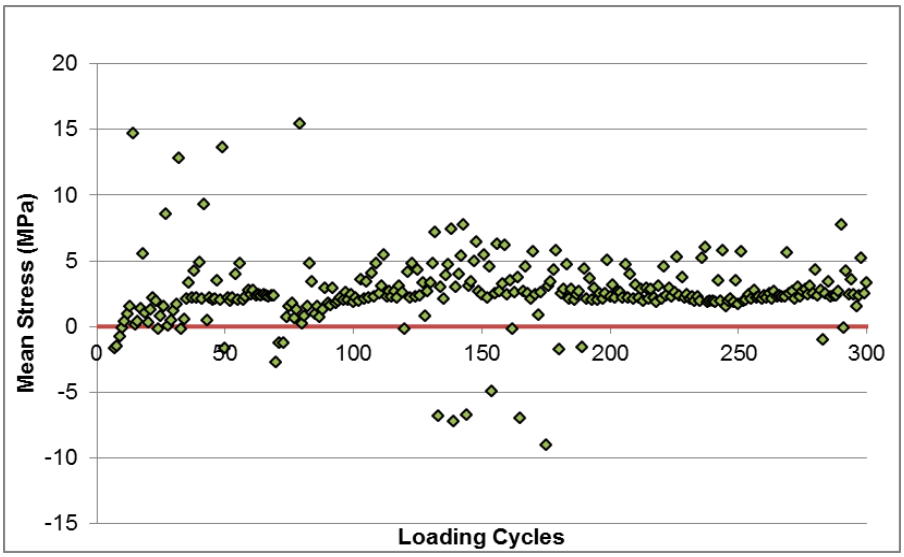

Figure 4-8: Mean stress of tube A, after (Lagat et al., 2014)

Figure 4-9 gives a comparison of rate of stress weakening for the four tube specimens. It was obtained by plotting the slopes from Figure 4-7, Appendix 6-1, Appendix 6-2 and Appendix 6-3 in Appendix 1 for each of the four tubes. Highest slope represents highest rate of stress-weakening.

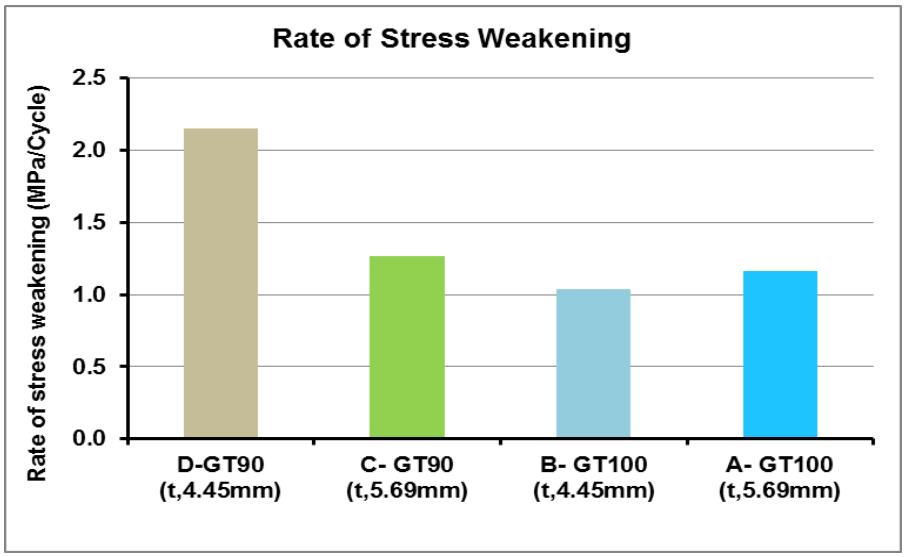

Figure 4-9: Rate of stress weakening, after (Lagat et al., 2014)

The bent samples were evaluated for their possible mechanical deterioration via tensile testing. Two tensile samples were cut out of each tube. One sample was cut away from the bent section. The other sample contained the bent section within its gauge length. The initial dimensions of the tubes were measured prior each tension test. Testing was carried out at ambient temperature.

Tension test results of fatigued and non-fatigued samples are shown in Table 4-2. Tension tests were performed in accordance to ASTM A370 (A370, 2010). The changes in elongation trends are minimal.

Table 4-2: Coiled tube test sections for tensile testing

Tube No.	Material	OD mm	t mm	Yield Strength, YS MPa (ksi)	UTS MPa	Elastic Modulus, E GPa	Elongation (%)	Comments (%)
Non-fatigued sections								
A1	HSLA Steel GT 100	50	5.69	757 (109.8)	772	206	9.5	Elongation not valid due to fracture occuring near the
B1	HSLA Steel GT100	50	4.45	700 (101.5)	869	205	15.0	
C1	HSLA Steel GT90	50	5.69	725 (105.1)	731	205	14.0	
D1	HSLA Steel GT90	50	4.45	701 (101.7)	745	204	14.0	
Fatigued sections								
A2	HSLA Steel GT 100	50	5.69	618 (89.6)	738	205	13.0	
B2	HSLA Steel GT100	50	4.45	775 (112.4)	848	207	13.0	
C2	HSLA Steel GT90	50	5.69	652 (94.6)	703	204	15.0	
D2	HSLA Steel GT90	50	4.45	638 (92.5)	717	202	15.0	

Stress-strain plots for the non-fatigued and fatigued steel tubes are presented in Figure 4-10 and Figure 4-11, respectively. Non Linearity of the stress-strain graphs are due to test errors, possible slipping of the sample from the grips.

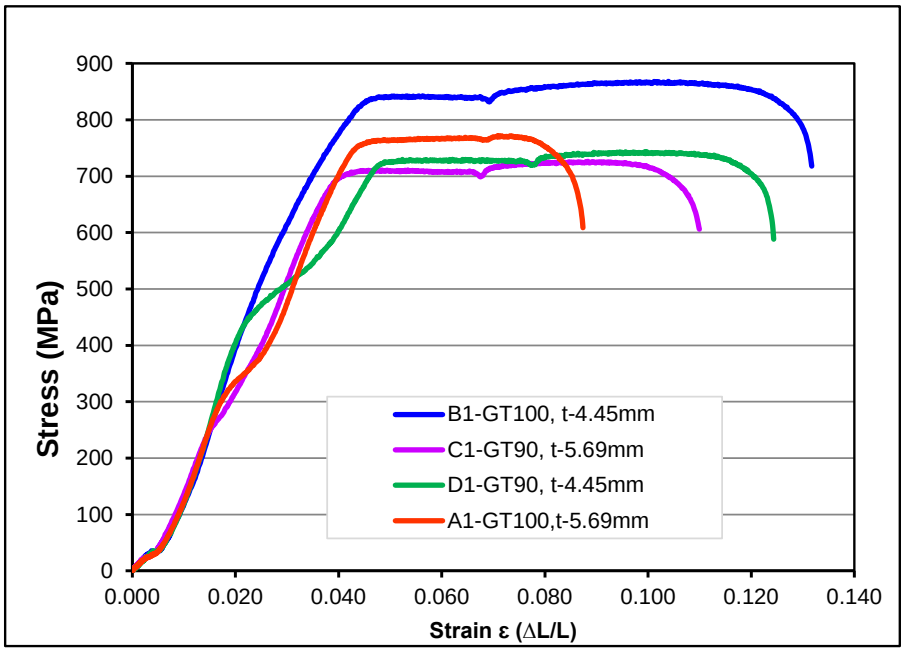

Figure 4-10: Stress-strain curves of non-fatigued sections, (Lagat et al., 2014)

Table 4-3 compares the strengths of fatigued and non-fatigued coiled tube samples. Tensile test results indicated that sample 1 (A1 vs. A2), a high grade and thick wall sample, had the highest reduction in yield strength after bending. The yield strength of fatigued sample A2 was reduced by about 18% compared to the non-fatigued sample A1. The low grade and thin wall sample had the lowest reduction in yield strength. Fatigued sample D2 yield strength decreased by only 9% compared to the non-fatigued sample D1. On the other hand, the high grade, thin wall fatigued sample, B2, yield strength increased by 10.7% compared to the non-fatigued sample, B1. It can be observed that the tube with increased yield stress after bending, tube B had the lowest rate of strain weakening as shown in Table 4-4. The Modulus of Elasticity of sample B slightly increased by approximately 0.98%, as presented in Table 4-2, compared to the other samples tested.

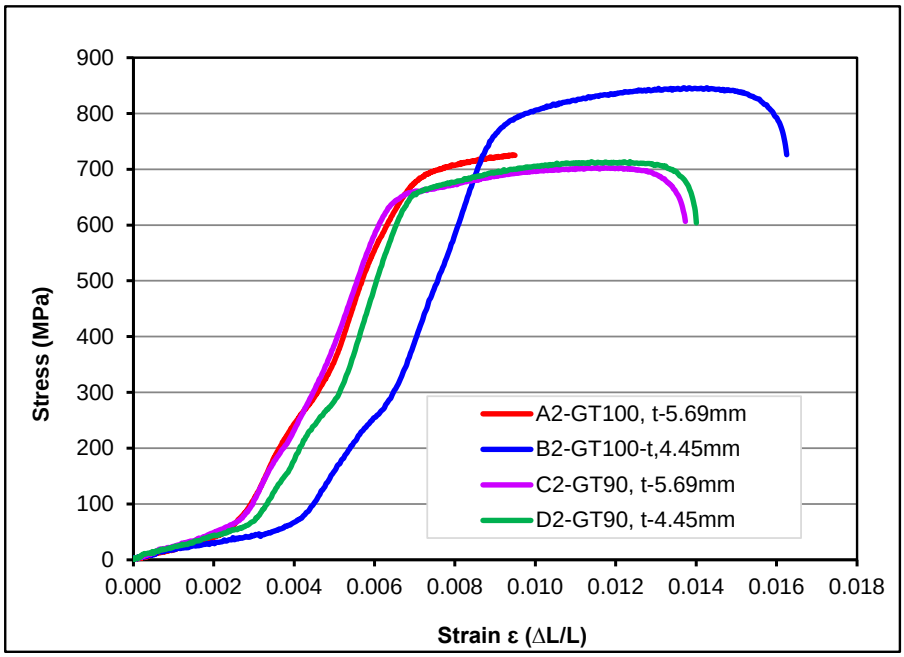

Figure 4-11 Stress-strain curves of fatigued sections, after (Lagat et al., 2014)

Table 4-3: Strength comparison of fatigued and non-fatigued tubes, after (Lagat et al., 2014)

	Non-fatigued sections		Fatigued sections		
Material	Tube number	Yield Strength, YS (MPa)	Tube number.	Yield Strength, YS (MPa)	Change (%)
HSLA Steel GT 10(	A1	757	A2	618	-18.36%
HSLA Steel GT100	B1	700	B2	775	10.71%
HSLA Steel GT90	C1	725	C2	652	-10.07%
HSLA Steel GT90	D1	701	D2	638	-8.99%

The increase in strength of tube B could be attributed to strain hardening of the material. Dislocations in the material crystal structure are generally moved by cold working or material deformation and would increase the strength of the material in subsequent bending loads (Wellman, May 2010). Figure 4-12 illustrates the effect of strain hardening (Wellman, May 2010).

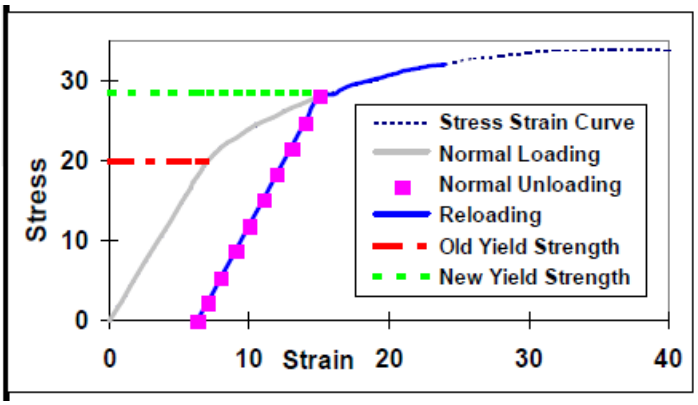

Figure 4-12: Stress-strain curve with strain hardening illustrated, after (Wellman, 2010)

Strain hardening of sample B is validated with the slight decrease of its ductility compared to the other listed samples, as shown in Table 4-4. As stated earlier, permanent deformation causes the dislocations to pile up, thus increasing the material strength. However, total elongation decreases as material strength increases (Wellman, May 2010). Elongation (ductility) decreases with strain hardening (Wellman, May 2010).The rate of weakening of the thin-walled tube B was lower compared to the thick-walled tube A. As anticipated, the lower strength (GT90), thin-wall sample (D2) had the highest rate of weakening.

Despite the fact that the tension test of sample A1 almost failed at the grip, the results trend appeared to be consistent from the strain hardening point of view and the mechanical test results. The test could not be repeated due to unavailability of pipe material.

Table 4-4: Change in geometric property of coiled tubes, (Lagat et al., 2014)

Item no	Material	OD	t	Final OD at fracture	Reduction in Area
		mm	mm	mm	(%)
Un-fatigued sections					
A1	HSLA Steel GT 100	50	5.69	43.40	24.66
B1	HSLA Steel GT100	50	4.45	43.90	22.91
C1	HSLA Steel GT90	50	5.69	43.60	23.96
D1	HSLA Steel GT90	50	4.45	43.70	23.61
Fatigued sections					
A2	HSLA Steel GT 100	50	5.69	42.80	26.73
B2	HSLA Steel GT100	50	4.45	44.05	22.38
C2	HSLA Steel GT90	50	5.69	42.90	26.38
D2	HSLA Steel GT90	50	4.45	42.60	27.41

4.5 Conclusions

When coiled tubing is subjected to multiple plastic deformation bending cycles, it accumulates damage and fails at a low cycle fatigue. The rate of weakening is faster for thin-walled coiled tubes with lower strength. It has been demonstrated experimentally that strain hardening due to cyclic bending took place for thin walled sample that was higher in strength (GT100 – 4.45mm thick). The strain hardening is noticed and confirmed by the increase of the yield strength, decrease of ductility and slight increase in its Modulus of Elasticity. However, this increase in strength and the corresponding reduction in ductility make fracture to more likely occur in the material. On the other hand, the weakest sample that handled the low cycle fatigue loading was the lower grade, thin wall sample, GT90-4.45 mm in wall thickness.

Cyclic bending of steel coil tube induces localized stresses and strains above the elastic limit (σy and εy), resulting in shorter fatigue life. Although, not part of PhD study, the bending machine was upgraded to undertake coiled tube bending tests with internal tube pressure. Four steel coiled tubes with 44.45mm (1.75 inches) OD and 3.4mm (0.134 inches) wall thickness obtained DET-CRC in Adelaide, South Australia, were tested with 0psi, 600 psi, 2200 psi and 3200 psi internal pressure, respectively. Tenaris^{TM} had performed simulation study on similar tube under various internal pressures. The experimental results were compared with Tenaris^{TM} simulation results, as shown in Table 6-2. Higher internal pressure greatly reduces the fatigue life of the steel coiled tube. Experimental results indicated that an increase of internal pressure from 600 psi to 3200 psi reduces the life of 44.45mm OD steel tube by approximately 87% (387 cycles to 50 cycles, respectively). Tube wall thinning, as a result of internal pressure, further reduces the fatigue life of steel tube.

Chapter 5 Composite Analysis

5.1 Introduction

Coiled tube in service will generally be subjected to flexural loading rather than pure axial loading. Hence fatigue is an important design consideration. The fatigue of fibre reinforced composites is primarily a function of fibre orientation angle (θ), stress ratio ($R = \sigma_{min}/\sigma_{max}$) and maximum stress (σ_{max}) applied (Hany El Kadi, 2002). Mechanical properties of composite materials largely depend on the fibre orientation distribution and fibre matrix shear strength (Forkes M.J., 1990).

Fibre orientation is an important parameter controlling the properties of a fibre reinforced composite material. It defines the orientation of fibres with respect to the loading directions. In uniaxial loading, fibres are most effective when the fibres are orientation angle is 0^o, that is, when they are oriented parallel to the loading direction. In pure shear loading, the fibres are most effective when they are oriented at -45^o and -45^o with respect to loading axis (Mallick.P.K., 1997). Fibre orientation is commonly defined using right handed coordinate system. By convention, orientation angle should lie between -90^o and $+90^o$ ($-90^o \leq 90^o$).

The matrix, which is the continuous phase in a composite material, plays several important roles: It holds the reinforcements in place, acts as a path for stress transfer between fibres and protects the reinforcements from adverse environmental effects. Matrix has a minor role in the longitudinal tensile properties of unidirectional composites. However, the selection of the matrix influences the transverse tensile modulus & transverse tensile strength, both longitudinal & transverse compressive properties, shear modulus and shear strength (Mallick.P.K., 1997).

Design calculations in this study were based on 3501 carbon – epoxy composite type AS4, which has a high strength, high strain, standard modulus (Department of Defense, 2002). Mechanical properties of the carbon/epoxy composite used in this study are shown in Table 5-1.

Table 5-1: Mechanical and thermal properties of carbon fibre composite (AS4/3501-6 epoxy) (Soden, Hinton, & Kaddour, 1998).

Property	Symbol	Unit	Value
Longitudinal modulus	E_1	GPa	126
Transverse modulus	E_2	GPa	11
In-plane shear	G_{12}	GPa	6.6
Major Poisson's ratio		fraction	0.28
Through Poisson's ratio		fraction	0.40
Longitudinal tensile strength	X_t	MPa	1950
Longitudinal compressive strength	X_c	MPa	1480
Transverse tensile strength	Y_t	MPa	48
Transverse compressive strength	Y_c	MPa	200
In-plane shear strength	S_{12}	MPa	79
Longitudinal Tensile failure strain	e_{1t}	%	1.38
Longitudinal compressive failure strain	e_{1c}	%	1.175
Transverse tensile failure strain	e_{2t}	%	0.436
Transverse compressive failure strain	e_{2c}	%	2.0
In-plane shear failure strain	e_{12}	%	2.0
Longitudinal thermal coefficient	α_1	$10^{-6}/^{o}C$	-1.0
Transverse thermal coefficient	α_2	$10^{-6}/^{o}C$	26.0
Stress free temperature		^{o}C	177
Fibre volume	V_f	fraction	0.6

The analysis involved the investigation of fibre orientation and stacking sequence of the fibre layers that constitute the composite tube laminate (J.H Park, 2001). 8-layer carbon/epoxy laminate, with varying fibre orientations was analysed. Design analysis was performed by comparing stresses (or strains) due to applied load with allowable strength (or strain capacity) of the composite material. Hypersizer uses orthotropic ply stress and strain allowables to calculate margins of safety. Margins of Safety (MS) are computed for each ply in the laminate structure and only the lowest value of MS is reported and considered for evaluating the whole laminate. Lowest value of MS indicates that such a layer will be the weakest to carry the load

and potential location of failure. Note that effective strengths are a function which failure mode is chosen.

5.2 Flat sheet laminate model

A rectangular 8-ply composite laminate was modelled using Hypersizer software. The software was utilized to find the optimum laminate design. In Hypersizer, a pool of candidate composite designs are sorted by unit weight and analysed sequentially. The first candidate material that passes all margin of safety checks is the optimum design. The sizing optimization is solidly based on detailed and accurate analyses that include the complete potential failure modes and margin of safety reporting. The failure analyses are efficient, thus optimization takes considerably shorter time.

The traditional formal optimization software, based on formal approaches such as gradient-based search algorithms, is rich in numerical sophistication. However, with the hundreds of dissimilar potential failure modes in composites, and the many different design variables, the formal optimization is unable to resolve the hundreds of local minimums that occur in the design evaluation process.

High strength carbon fibre Toray AS4 with 3501-6 epoxy resin was used for the model. The HyperSizer laminate material is defined by a sequence of ply materials, angles and thicknesses.

A layup was created, ply angles and thicknesses of each ply defined. Materials were assigned to the defined plies as shown in Figure 5-1.

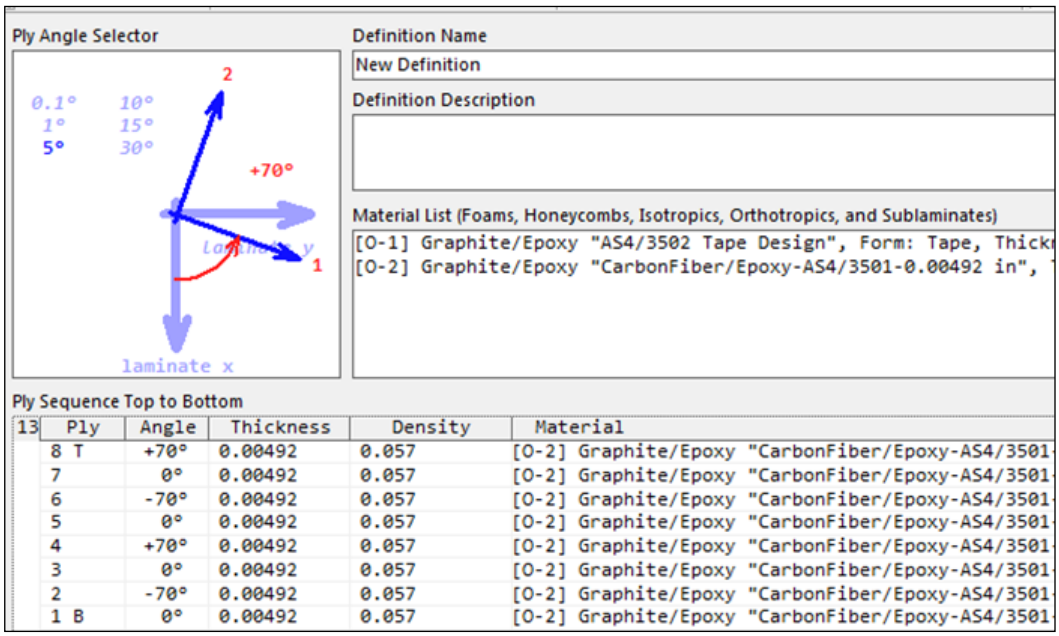

Figure 5-1: Laminate layup, ply angle and material definition

A number of simulation runs performed on carbon epoxy laminates, showed that laminates with low angle (0^o-10^o) and 70^o to 90^o angles have higher axial and flexural strength (Lagat C., 2014). The layup of the four modelled laminates shown in Table 5-2, were chosen based on earlier simulation runs. Material properties of the carbon epoxy composite with 60% fibre volume are given in Table 5-2.

Table 5-2: Stacking sequence and fibre orientation of 8-layer laminate

Case	**Laminate Layup**	**Ply thickness (mm)**	**Laminate thickness (mm)**
1	+70/0/-70/0/+70/0/-70/0	0.125 (0.00492 in)	1.0
2	+70/-70/0/0/+70/-70/0/0	0.125 (0.00492 in)	1.0
3	90/0/-90/0/90/0/-90/0	0.125 (0.00492 in)	1.0
4	+90/-90/0/0/+90/-90/0/0	0.125 (0.00492 in)	1.0

Each of the four carbon/epoxy laminates was subjected to uniaxial tension. The applied axial load in the X (N_x) direction was 2225 N (500 lb-f) in each of the four flat sheet laminates. The free body diagram is represented in Figure 5-2.

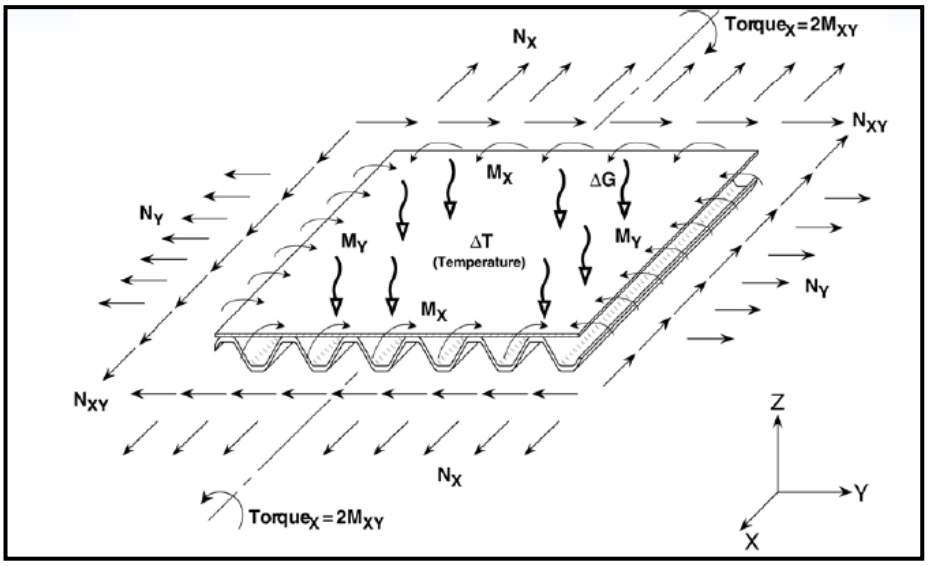

Figure 5-2: Free body diagram

Laminate stiffness properties, allowable stress and strain and a failure envelope are generated during the analysis. Ply-by-ply stresses and strains are computed relative to the material properties. Margins of safety (MS) are calculated for each ply in the laminate, based on Maximum stress theory. Only the lowest margin of safety was reported as shown in Figure 5-3.

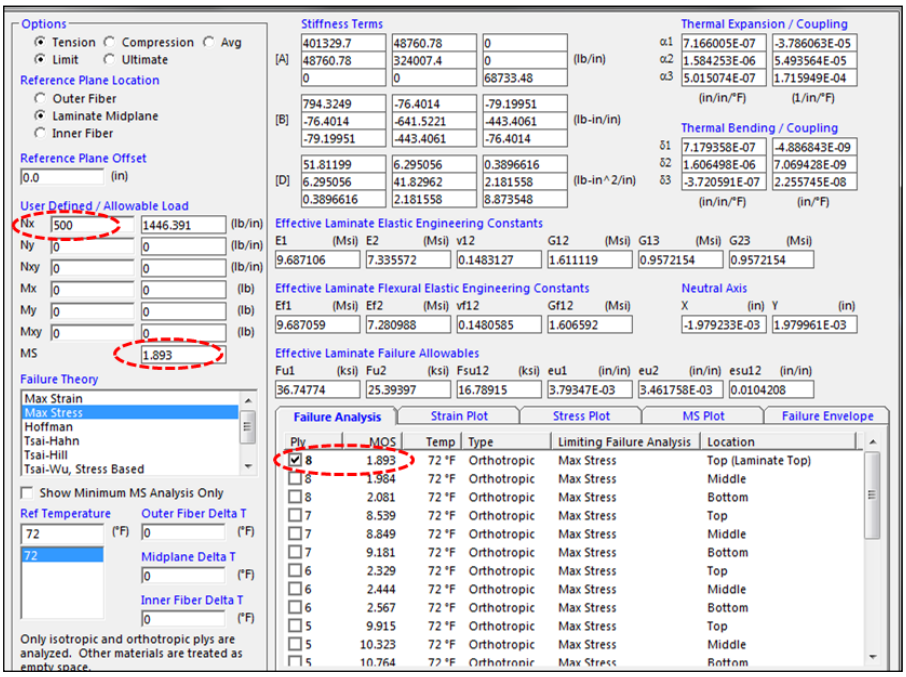

Figure 5-3: Flat sheet laminate analysis showing ply margin of safety

Stress analysis was repeated for four cases of laminates with various winding angles.

5.2.1 Simulation results of Flat sheet laminate model

The results obtained from the Hypersizer model are presented in this section. Figure 5-4 provides detailed results of margin of safety for corresponding winding angles in the 8-layer flat laminate sheets. Specimen 1, with fibre angles of +70/0/-70/0/+70/0/-70/0, exhibited highest margin of safety of 2.75 under applied axial load. A plot of ply-by-ply stress distribution in 1 (x) direction is shown in Figure 5-5. Specimen 3 with fibre orientation of had the least strength. It is evident from Figure 5-4 that winding angles of +70/0/-70/0/+70/0/-70/0 provide better material strength than the rest of the specimens.

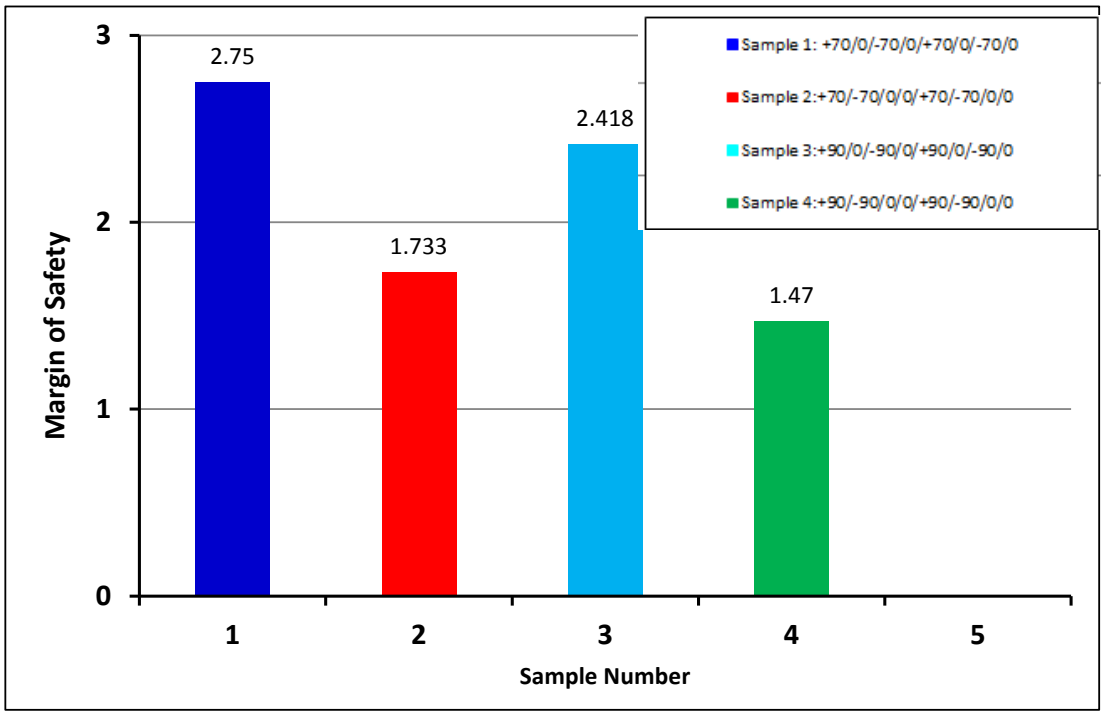

Figure 5-4: Case I - Effect of Fibre orientation on margin of safety in carbon fibre/epoxy laminate.

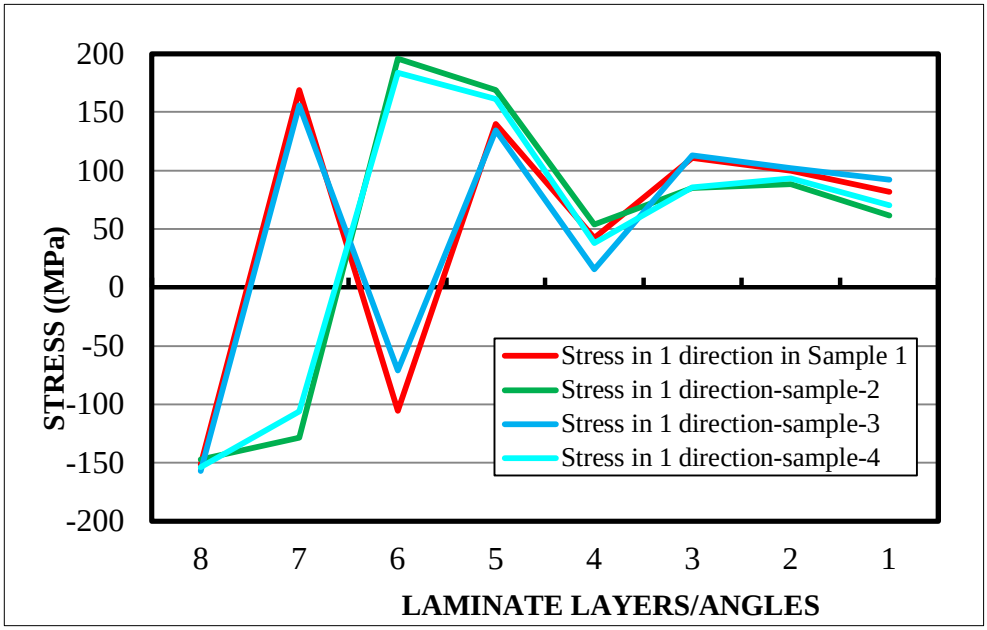

Figure 5-5: Ply-by-ply stress distribution of flat sheet samples under axial loading

Three tensile test specimens were cut from each of the four flat laminate sheets. The cuts were in the longitudinal direction.

5.3 Flat sheet laminate experimental study

Composite flat sheet samples used in this study were fabricated from Toray's T700S high strength, standard modulus carbon fibres (Toray Carbon Fibres America, 2008) and epoxy resin by hand lay-up. Each sample consisted of eight plies of carbon/epoxy. Carbon fibre properties were reported as shown in Table 5-3 (Toray Carbon Fibres America, 2008) and , respectively. Four laminate samples were made. The angle configurations of the specimens are shown in Table 5-4.

Table 5-3: Properties of Toray T700SC fibres used in experimental study, after (Toray Carbon Fibres America, 2008).

Fibre	Tensile strength (MPa)	Tensile modulus (GPa)	Tensile strain (%)	Compressive strength (MPa)	In-plane shear strength (MPa)	Transverse tensile strength (MPa)	Density (g/cm^3)	Filament diameter (µm)
Carbon type S	2450	125	1.7	1570	98	70	1.80	7.0

Table 5-4: Filament wound Laminate samples

Specimen No.	No. of layers	Material	Fibre Orientation
1	8	Carbon/epoxy	+70/0/-70/0/+70/0/-70/0
2	8	Carbon/epoxy	+70/0/-70/0/+70/0/-70/0
3	8	Carbon/epoxy	+90/-90/0/0/+90/-90/0/0
4	8	Carbon/epoxy	+90/-90/0/0/+90/-90/0/0

Figure 5-6 shows a ply lay-up cross section representation of sample no. 1. The angles chosen for the experimental samples were based on numerical simulation.

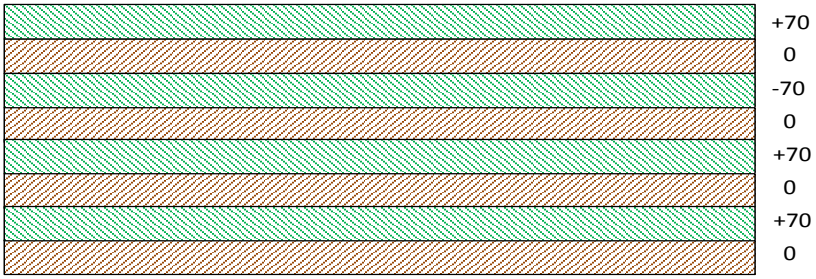

Figure 5-6: A typical cross section of a symmetric balanced angle-ply laminate in carbon/epoxy composite

5.3.1 Fabrication of composite flat laminate sheets

Vacuum bagging technique (Rachal & Krove, 1990) was utilized to fabricate the flat plate samples as shown in Figure 5-7. The samples were vacuumed at constant atmospheric pressure of 14.96 psi for 4 hours at room temperature. Figure 5-8 (a) shows sample no. 1 of carbon laid fibres prior to adding resin and vacuuming. A cured sample of carbon/epoxy flat plate composite is shown in Figure 5-8 (b).

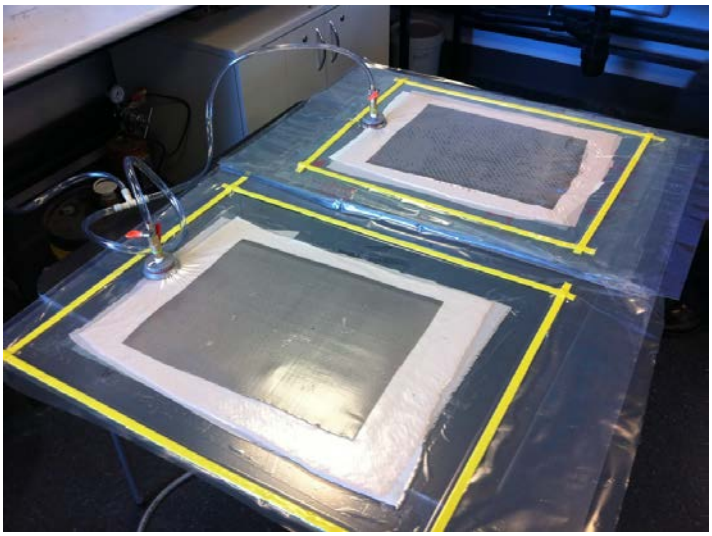

Figure 5-7: Vacuum bagging process

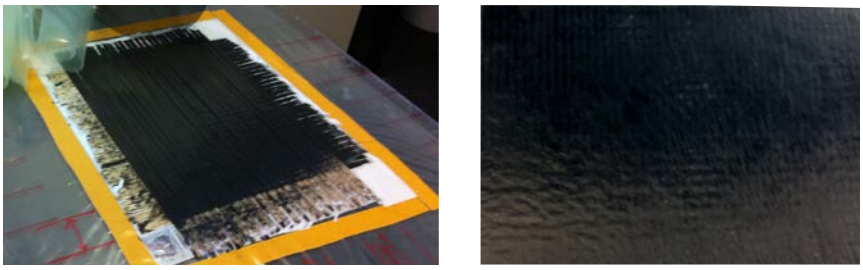

Figure 5-8: (a) Carbon fibre in ±90/0 direction (b) Cured carbon/epoxy composite

5.3.2 Testing

Mechanical tests and results

Tensile test specimens measuring nominally 50mm wide and 200mm long were cut from each of the cured flat plates. The specimens were tested in accordance with ASTM D3909 standard (ASTM, 2008). All mechanical testes were carried out at 50% relative humidity and 23^{o}C. The specimens were conditioned under similar circumstances for at least 24hrs. The cross sectional area of each specimen was measured with a calliper at three locations within the testing area prior to testing. Three duplicate tests were conducted for each specimen configuration. A wedge grip type was used. Aluminium tabs were applied at the grip section of the specimen to avoid grip damage and promote uniform stress within grip. To prevent slippage, the aluminium surfaces were serrated by a rough file and glued to the specimen by epoxy. Figure 5-9 shows a schematic cross section of configuration for tension testing. The central region or the gauge section gage section is the region in which a uniform state of stress is required and a suitable failure mode is desired (Daniel & Donald, 2002). Strain was recorded using an extensometer. Location of the extensometer on the specimen is shown in Figure 5-10.

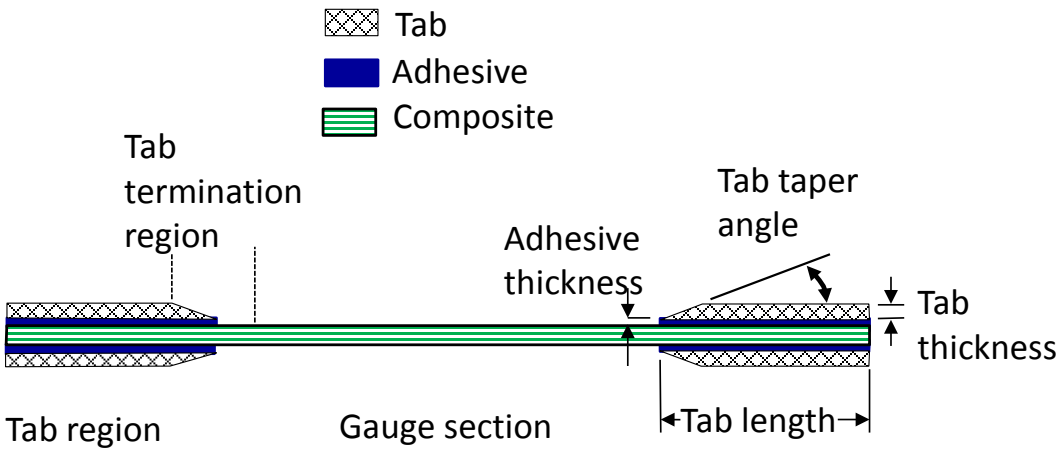

Figure 5-9: Typical tabbed composite tension specimen, after (Daniel & Donald, 2002)

Figure 5-11a and 1b show the experimental set up of the tensile tests.

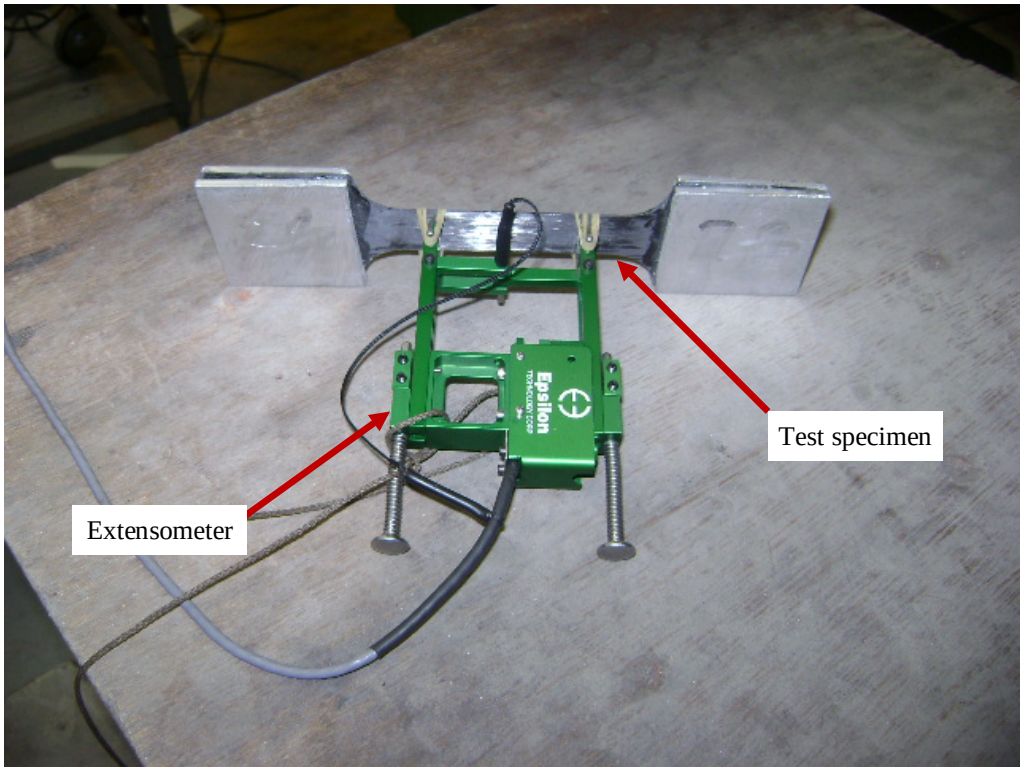

Figure 5-10: Location of extensometer on test specimen

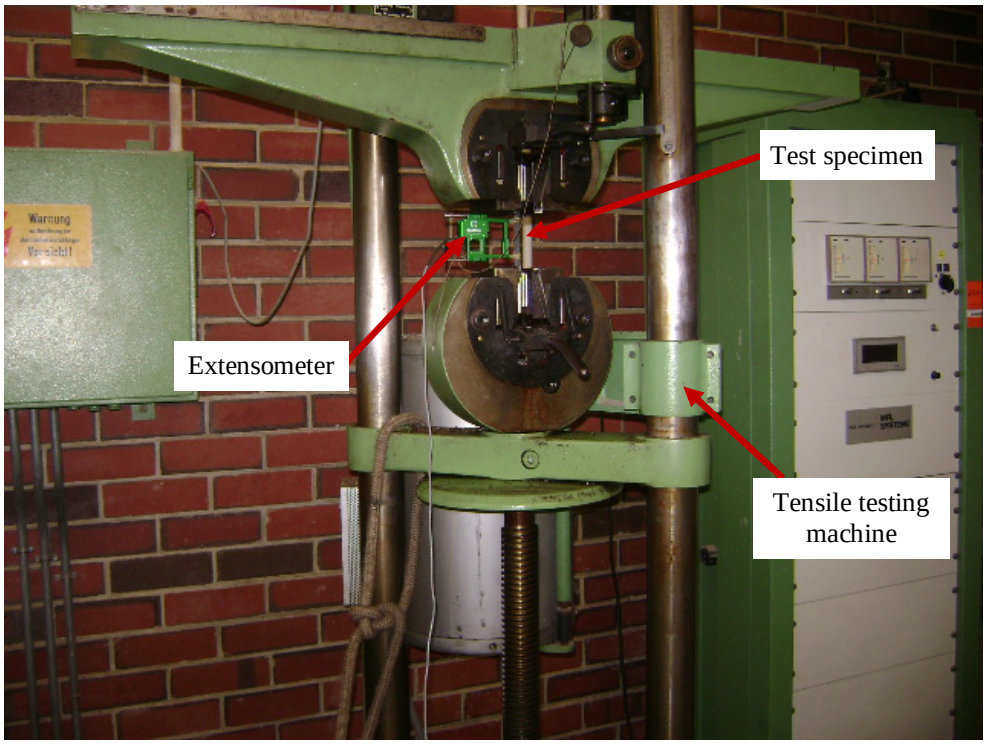

Figure 5-11a: Experimental set up of tensile test of composite flat sheet (zoomed view)

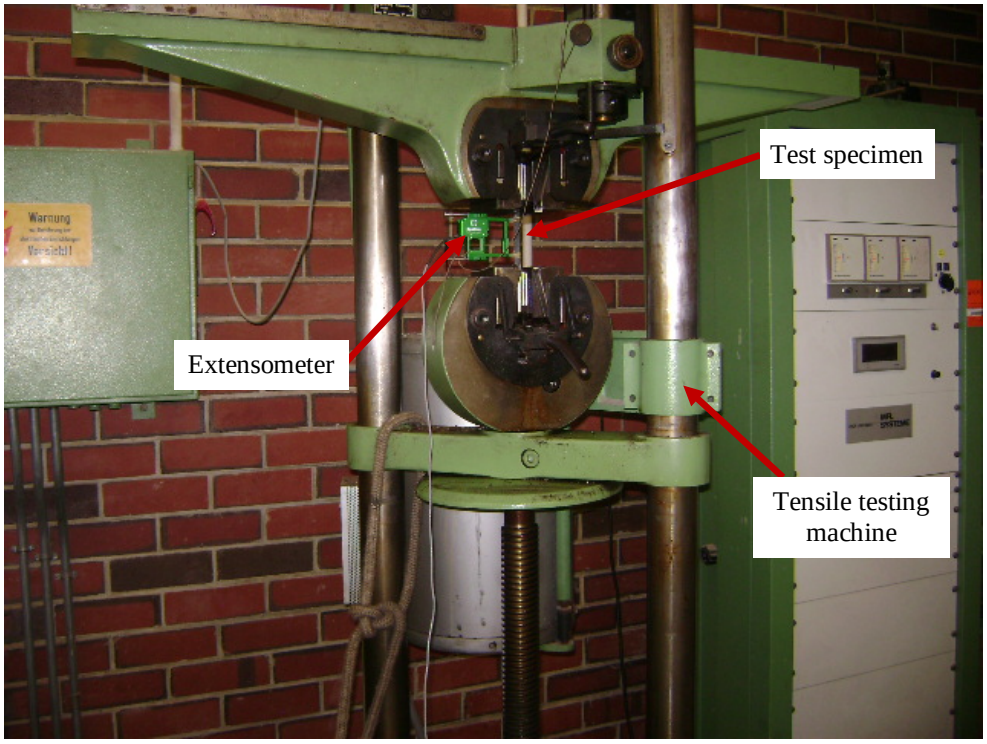

Figure 5-11b: Experimental set up of tensile test of composite flat sheet

Uniaxial tensile tests were carried out on flat specimens of four different fibre winding angles, as shown in Table 5-4. Three coupons were cut from each of the four different specimens and tests performed for each. Their stress-strain plots are shown in Figure 5-12 to Figure 5-15. These results were intended to give an indication of the extent to which fibre orientation is likely to influence the test results.

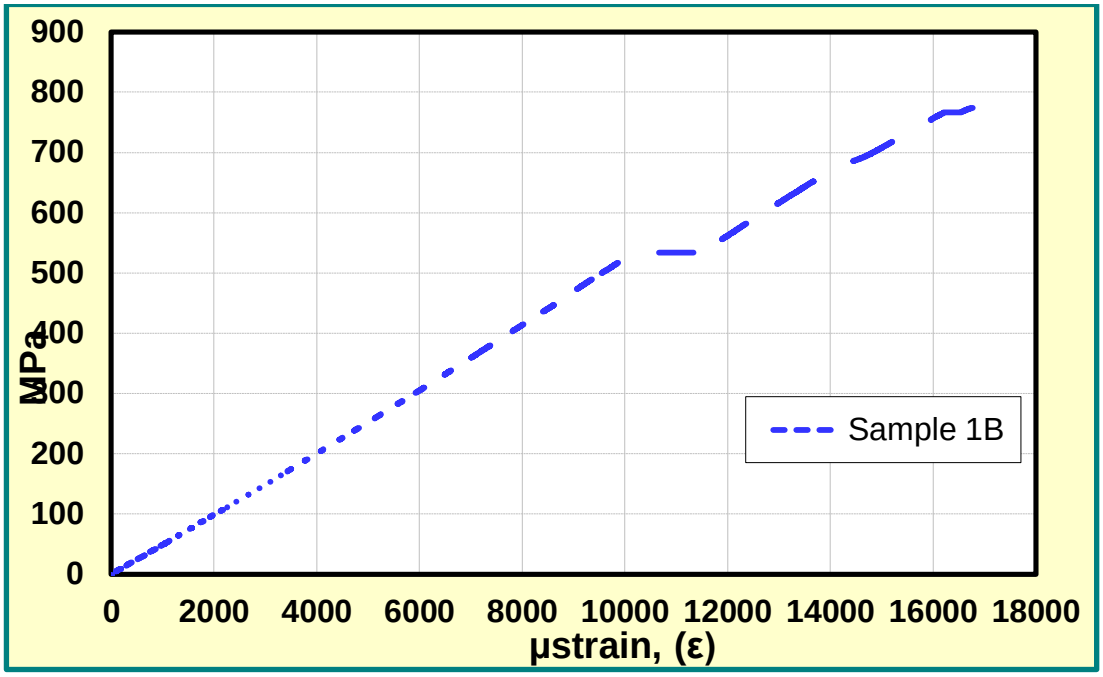

Figure 5-12: Stress-strain curve of sample 1 (winding angles of +70/0/-70/0+70/0/-70/0)

Samples 1A, 1C, 2B, 3A, 3C and 4C were not included as failure did not occur in the testing area, but in the area where they were fixed to the testing machine. Specimen 1B as indicated in Figure 5-12, showed fibre pull-outs prior to final fracture. The stress-strain curves for specimen 2A and 2C exhibit similar slope and fracture point.

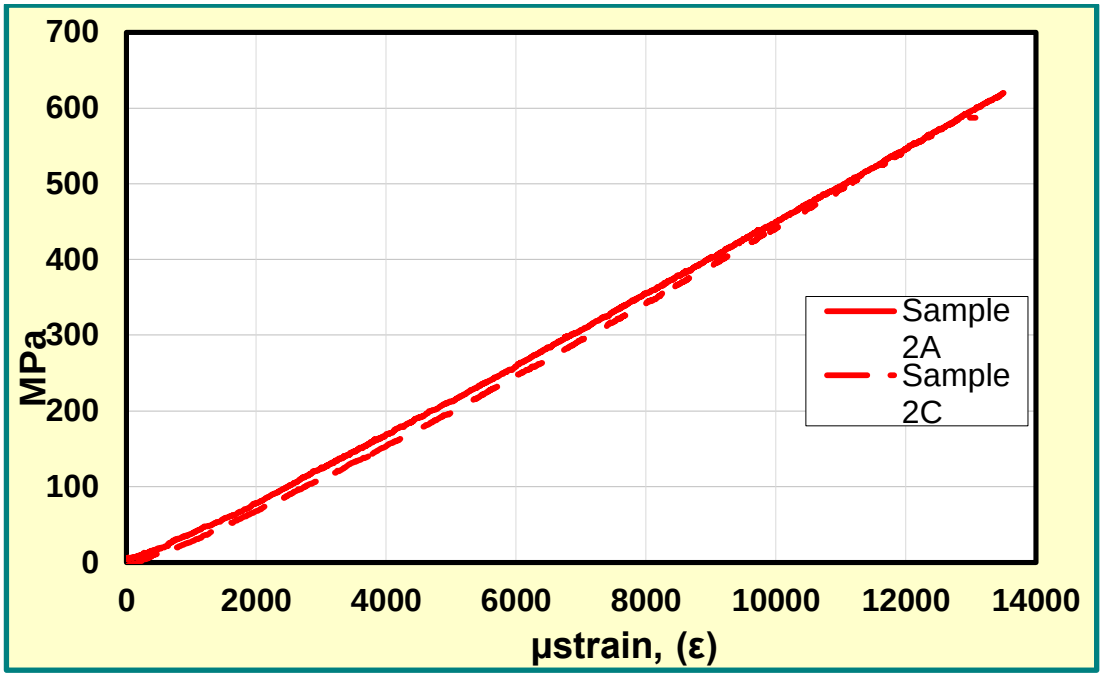

Figure 5-13: Stress-strain curves of sample 2 (winding angles of +70/-70/0/0+70/-70/0/0)

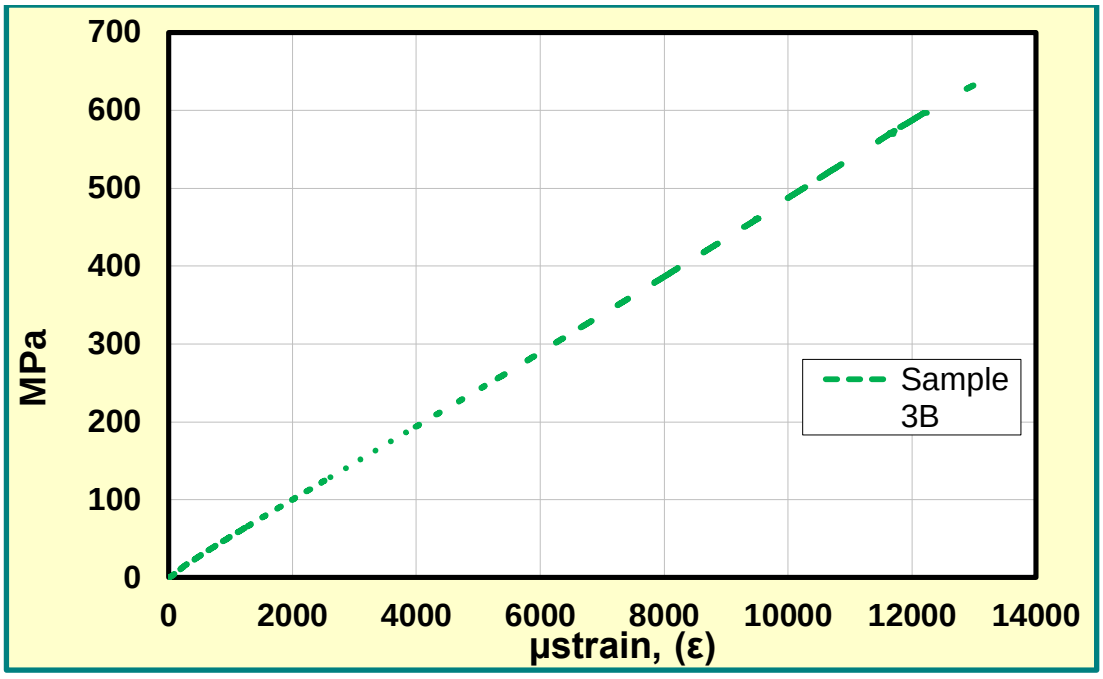

Figure 5-14: Stress-strain curve of sample 3 (winding angles of +90/0/-90/0+90/0/-90/0)

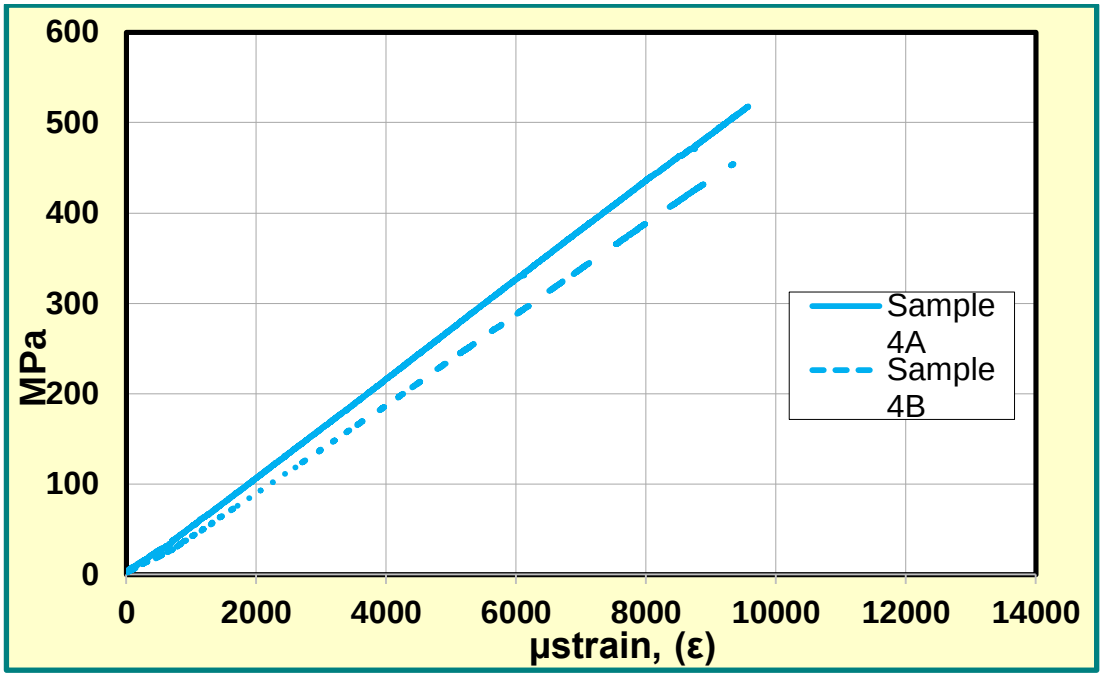

Figure 5-15: Stress-strain curves of sample 4 (winding angles of +90/-90/0/0+90/-90/0/0)

There was some variation in the failure stress results of specimen 4A and 4B, but the variation in the ultimate strength and the stress-strain slope was not large. This could be attributed to local fibre volume fluctuation in some parts of the samples due to non-uniform fibre placement during hand fibre lay-up.

Final failure was by fracture for all specimens. Exact sites of failure initiation were not always obvious because of the extensive damage of the specimens during test. Examples of all failures are given in Appendix 2.

Figure 5-16 and Table 5-5 compares the tensile properties of the flat specimens of four different fibre winding angles. The strengths of the composites varied with fibre orientations. Sample 1 (+70/0/-70/0/+70/0/+70/0) depicted the highest ultimate tensile strength and strain of 783.6 MPa and 1.71%, respectively, compared to other specimens. Specimen 4 (with fibre orientation of +90/-90/-0/0/+90/-90/0/0), showed the lowest strength, with ultimate tensile strength and strain of 487.5 MPa and 1.07%, respectively.

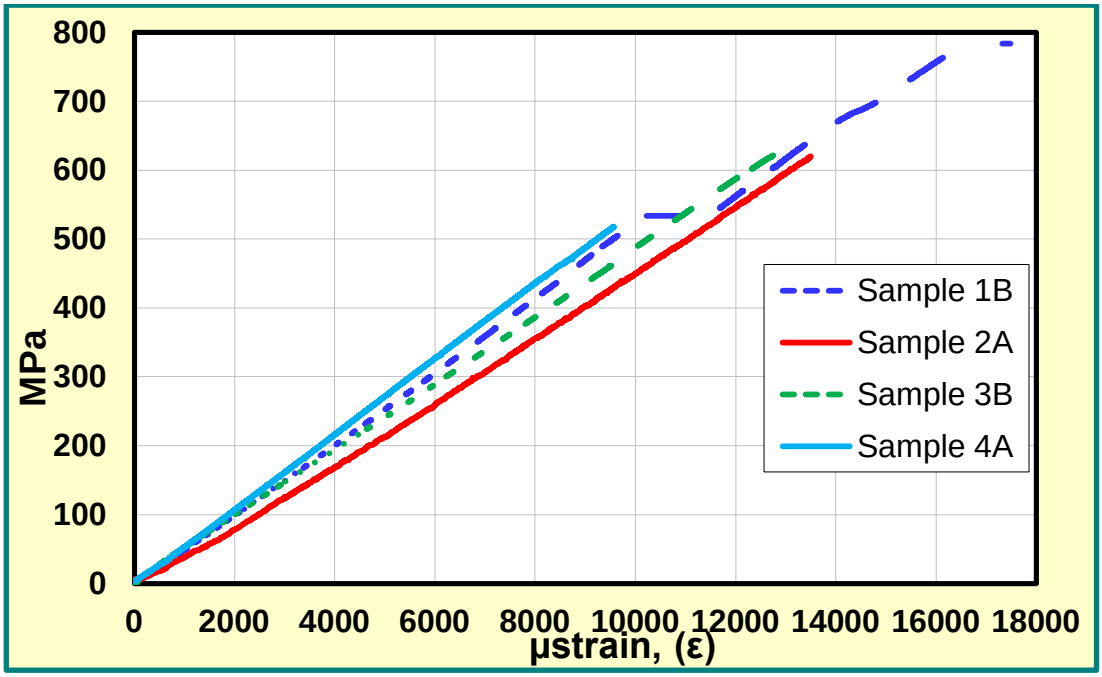

Figure 5-16: Stress-strain curves of carbon/epoxy flat sample sheets

Table 5-5: Strength comparison of carbon/epoxy flat sample sheets

Sample No.	Fibre Orientation (deg)	UTS (MPa)	Strain, ε (%)	Modulus, E (GPa)
1	+70/0/-70/0/+70/0/-70/0	783.6	1.71	53.2
2	+70/-70/0/0/+70/-70/0/0	620.0	1.35	46.8
3	+90/0/-90/0/+90/0/-90/0	682.9	1.46	47.7
4	+90/-90/0/0/+90/-90/0/0	487.5	1.07	55.1

Simulation tests and results

An eight layer composite flat sheet specimen was modelled in Abaqus simulation to emulate the experimental test specimen. During a tensile test, one end of the specimen is clamped in a loading frame while the other is subjected to a controlled displacement (Roylance, 2001). Figure 5-17 shows the boundary conditions and the applied force on the model. The lower end of the specimen is fixed and the upper section is free in the direction of applied force. The specimen is constrained in the transverse directions to avoid rotation or bending.

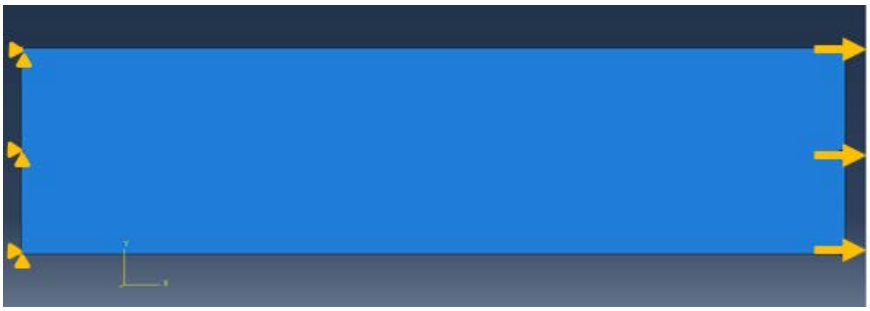

Figure 5-17: Boundary conditions and load applied on model

For this study, an eight-layer lamina of carbon/epoxy material was created. Mechanical properties of the orthotropic material are shown in

Table 5-1. A composite layup consisting of eight plies was created in Abaqus software. Carbon/epoxy material and orientation was then assigned to the plies. Layer thickness, number of section points required for numerical integration through each layer and associated orientation for each layer were specified during composite layup section definition as shown in Figure 5-18. Simpson integration rule and 3 integration points were used in the study.

Material	Thickness	Orientation Angle	Integration Points	Ply Name
Carbon/epoxy	0.125	70	3	Layer 8
Carbon/epoxy	0.125	0	3	Layer 7
Carbon/epoxy	0.125	-70	3	Layer 6
Carbon/epoxy	0.125	0	3	Layer 5
Carbon/epoxy	0.125	70	3	Layer 4
Carbon/epoxy	0.125	0	3	Layer 3
Carbon/epoxy	0.125	-70	3	Layer 2
Carbon/epoxy	0.125	0	3	Layer 1

Figure 5-18: Ply order, material used for each ply, thickness and fibre orientation of specimen 1

The layup of the four modelled laminates are shown in Table 5-2. Simulation runs were performed for the four cases of laminates with various winding angles.

5.3.3 Simulation and experimental results

Experimental results of the four carbon/epoxy specimens were validated via simulation study. The simulation results of stress-strain behaviour for the four specimens for each lamination arrangement are given in Figure 5-19a, 5.19b, 5.20a and 5.20b. Figure 5-21a and Figure 5-211b compares the simulation and experimental tensile test results of the four specimens. The fairly good agreement which can be noticed supports the validity of the margin of safety factors obtained in

Hypersizer simulation. The experimental stress-strain behaviour of the four specimens compare favourably with the simulation results.

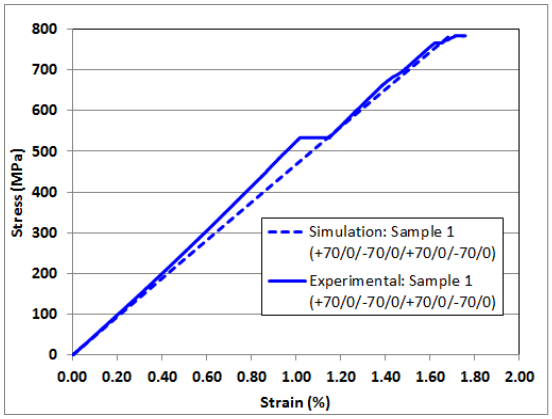

Figure 5-19a: Stress-strain behaviour of specimen 1

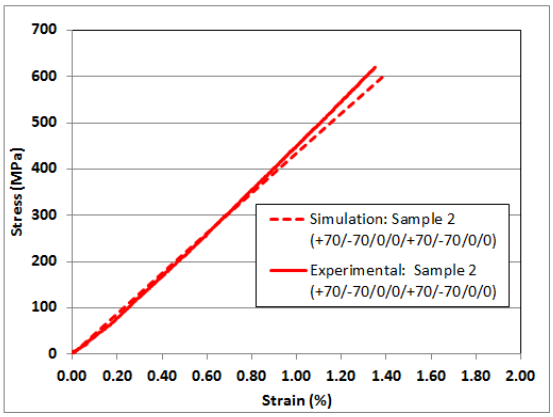

Figure 5.19b: Stress-strain behaviour of specimen 2

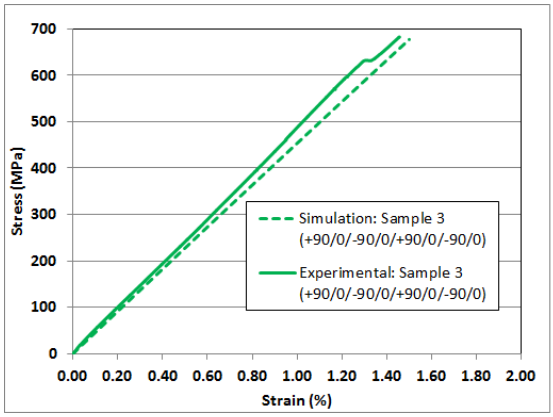

Figure 5-20a: Stress-strain behaviour of specimen 3

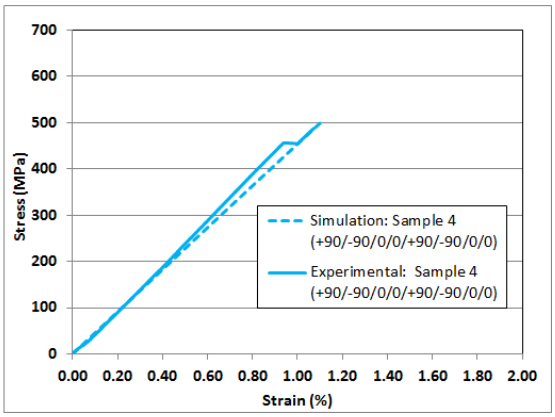

Figure 5.20b: Stress-strain behaviour of specimen 4

It can be noted from Table 5-6 that specimen 1, with fibre orientation of +70/0/-70/0/+70/0/-70/0, showed larger average ultimate tensile stress (UTS) and strain than specimen 2, 3 and 4. The experimental UTS and strain of the specimen was 783.6 MPa and 1.70%, respectively. The simulation results from HyperSizer also indicated that specimen 1 had the highest margin of safety (2.75) compared to specimen 2, 3 and 4.

Table 5-6: Experimental and simulation tensile test results

		Experimental		Simulation	
Sample No.	**Fibre Orientation (deg)**	**UTS (MPa)**	**Strain, ε (%)**	**UTS (MPa)**	**Strain, ε (%)**
1	+70/0/-70/0/+70/0/-70/0	783.6	1.71	781.7	1.70
2	+70/-70/0/0/+70/-70/0/0	620.0	1.35	605.9	1.40
3	+90/0/-90/0/+90/0/-90/0	682.9	1.46	677.6	1.50
4	+90/-90/0/0/+90/-90/0/0	487.5	1.07	498.6	1.10

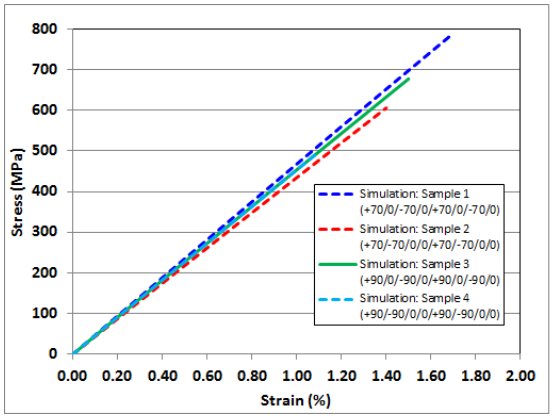

Figure 5-21a: Simulation stress-strain behaviour

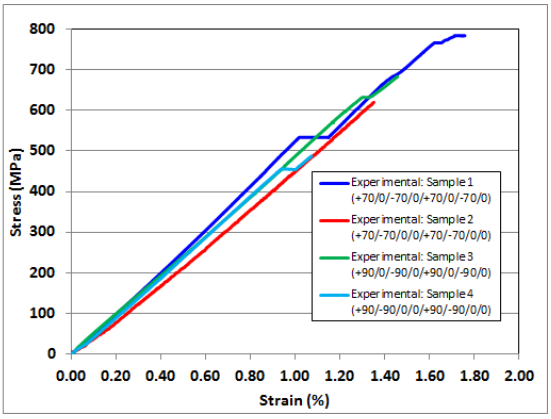

Figure 5.21b: Experimental stress-strain behaviour

5.4 Composite tube simulation study

Simulation study was carried out on an 8-layer carbon/epoxy tube subjected to axial, bending and internal pressure loads. The study was carried out to investigate the stress distribution across the layers of the composite tube when subjected to axial, pressure and bending loads.

5.4.1 Composite tube design

The design selection of composite tube was based the simulation and experimental test results of flat composite plates. The fibre orientation that gave better test results from the flat specimens was adopted. The fibre angle configurations of the specimen are shown in Table 5-7.

Table 5-7: Fibre orientation for tube sample

Sample No.	No. of layers	Material	Fibre Orientation
1	8	Carbon/epoxy	+70/0/-70/0/+70/0/-70/0

The physical properties of the carbon fibre tube are presented in Table 5-8.

Table 5-8: Physical properties of carbon fibre tube

Density, ρ (g/cm^3)	1.51
Matrix volume, V_m	0.39
Fibre volume, V_f	0.61

5.4.2 Composite tube model

Numerical study of a carbon/epoxy composite tube subjected axial, bending and internal pressure loads was also undertaken using Abaqus software. The simulation study was to evaluate the bendability of the tube and its structural strength. Composite tube fatigue simulation was not part of this research.

The desired outside diameter for the composite tube for the DET CRC mining application was 44.45mm (1.75 inches). Therefore, a composite tube with an outer diameter 44.45mm was modelled. The tube consisted of eight laminate layers, similar to the flat sheet model. Fibre orientation design selection of the composite tube was based on the test results of flat composite plates. The fibre orientation that gave better simulation results from the flat specimens was adopted.

High strength carbon fibres Toray AS4 with 3501-6 epoxy resin was used in tube model. Tube dimensions, layup and fibre orientation of the specimen is given in Table 5-7 . Figure 5-22 shows the coiled tube/reel model.

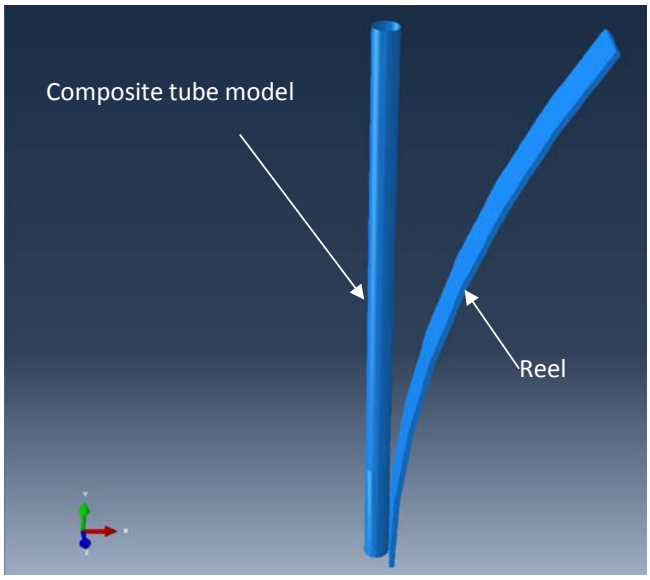

Figure 5-22: Composite tube model

Based on experimental studies performed on steel coiled tubes and the expected strain values on the composite tube, the reel diameter was selected to be 1778mm.

Table 5-9: Composite tube lay up

				Inner layer							
				layer 1	**layer 2**	**layer 3**	**layer 4**	**layer 5**	**layer 6**	**layer 7**	**layer 8**
Fibre Orienataion				0	-70	0	+70	0	-70	0	+70
Inside diameter	mm	33.75	min	33.75	35.09	36.43	37.76	39.10	40.44	41.78	43.11
Outside diameter	mm	44.45	max	35.09	36.43	37.76	39.10	40.44	41.78	43.11	44.45
Thickness	mm	5.35	sum	0.669	0.669	0.669	0.669	0.669	0.669	0.669	0.669

The stack-up of carbon fibre/epoxy layers in the composite tube is shown in Figure 5-23.

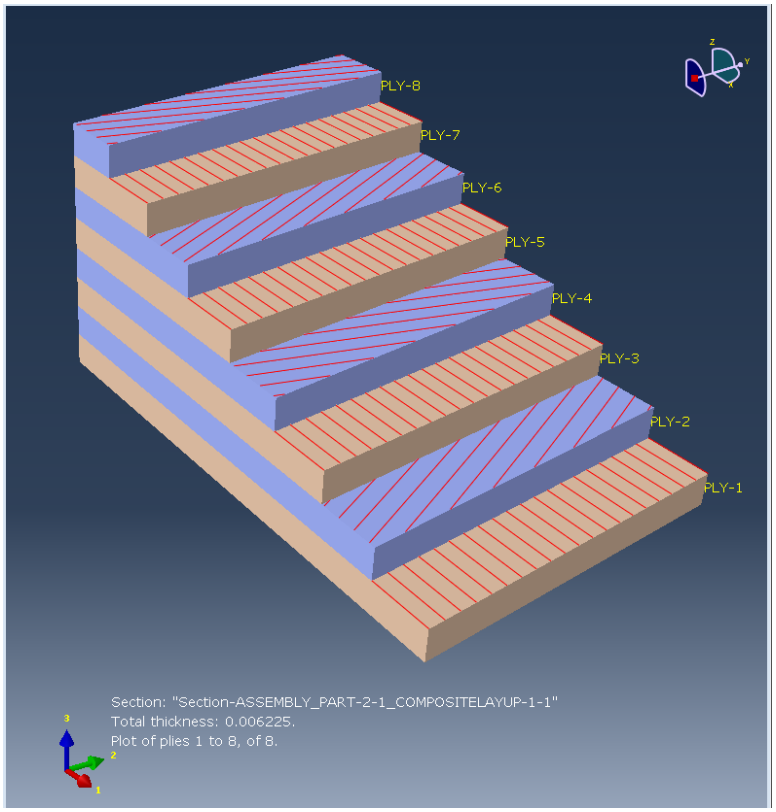

Figure 5-23: Composite tube stack-up plot

Numerical simulation procedure is outlined in Figure 5-24 below.

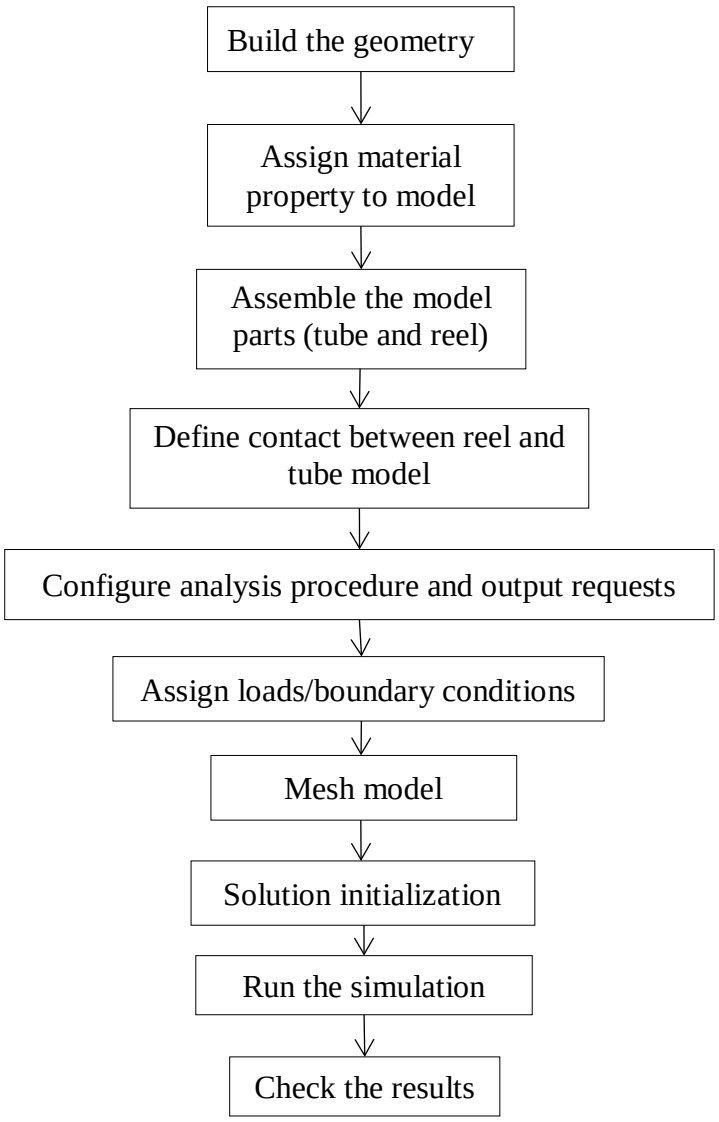

Figure 5-24: Simulation procedure for composite tube

As indicated, the first step is to sketch three-dimensional geometry and create parts representing coiled tube and reel. Material properties are then defined and assigned to the two model parts. The tube comprises of carbon/epoxy composite material while the reel is structural steel. The created tube and reel parts are oriented on their own coordinate systems and are independent of each other. The parts are assembled by positioning them relative to each other in a global coordinate system. Contact between regions of model, reel and tube, is then defined. This is followed by configuring the analysis procedure and output requests. Boundary conditions that constrains the bottom end of the tune in the x, y and z directions are applied. The entire reel is constrained in the x, y, and z directions. Axial, bending and internal pressure loads are applied to the tube. The model is then meshed using S8R shell

element in Abaqus. Eight-node (quadratic) quadrilateral elements were used. A job was created and submitted for analysis. The results of the analysis can be viewed in visualization window.

The expected axial force and internal pressure on the coiled tube during operation is approximately 39.86 kN (≈ 4 ton-f), and 3,000 psi, respectively. Hence design axial and pressure loads of 68.65kN (≈ 7 ton-f) and 6,000 psi, respectively, were applied to the tube. The tube wall thickness was 6.35mm.

Four cases of simulation runs were performed on the tube model as shown in Table 5-10. In case I, the tube wall thickness was set to 1mm, similar to the thickness of the flat sheet model. . Tube wall thickness in Case 2, 3 and 4 was 6.35mm.

Table 5-10: Coiled tube simulation run cases (Orientation lay-up: 0/-70/0/+70/0/-70/0/+70)

CASE I				
		LOADS		
Tube no.	Tube wall thickness (mm)	Bending	Internal pressure (6000 psi)	Axial load (68.65 kN)
1	1.0	√	-	-
2A	6.35	√	-	-
2B	6.35	√	√	-
2C	6.35	√	√	√

5.4.3 Simulation results of composite tube model

In this section results of four models of composite tube shown in Table 5-10 are presented. Figure 5-25 and Figure 5-26 show the longitudinal stress (S11) and strain (E11) distribution on the outer and inner layer of composite tube under combined bending, axial and pressure loads. The strain and stresses are highest on the outer layer (8^{th}) laminate layer of the tube. Similar trend of stress and stress distribution across the thickness of the tube was observed in all other the simulation cases.

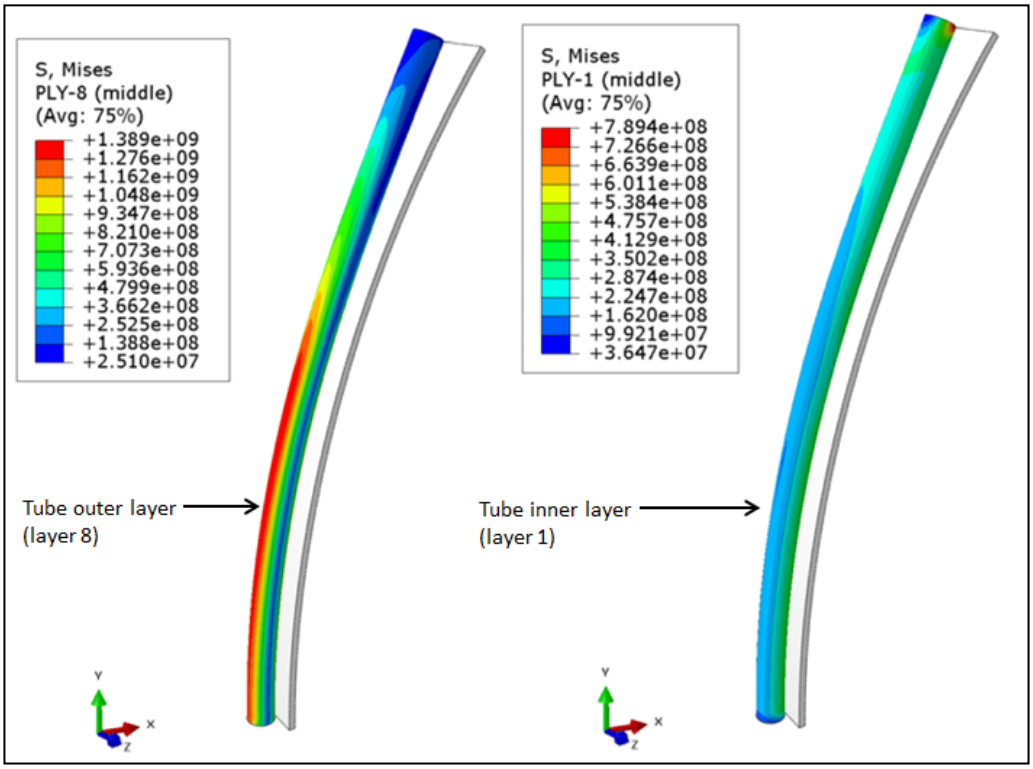

Figure 5-25: Longitudinal stress (S11) distribution on outer and inner layer of composite tube.

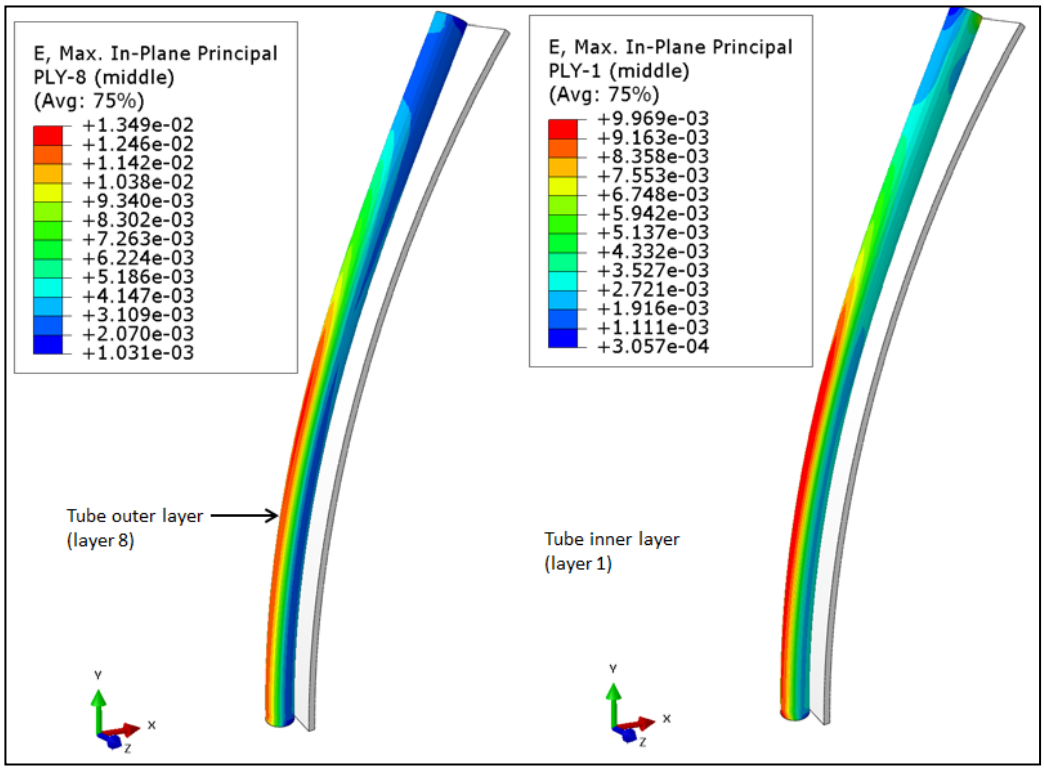

Figure 5-26: Longitudinal strain (S11) distribution on outer and inner layer of composite tube

The tension side stress (S11) and strain (E11) distribution across the thickness of composite tube is shown in Figure 5-27 and Figure 5-28, respectively.

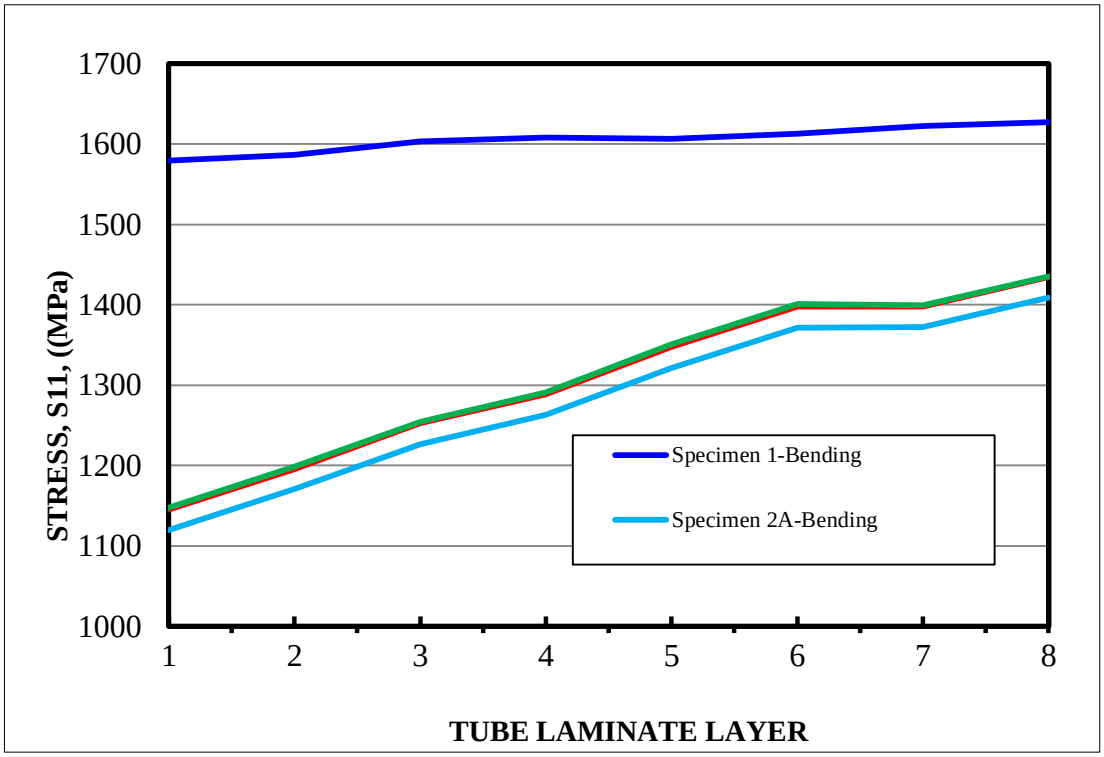

Figure 5-27: Tension side stress distribution in tube layers for simulation case 1, 2A, 2B & 2C

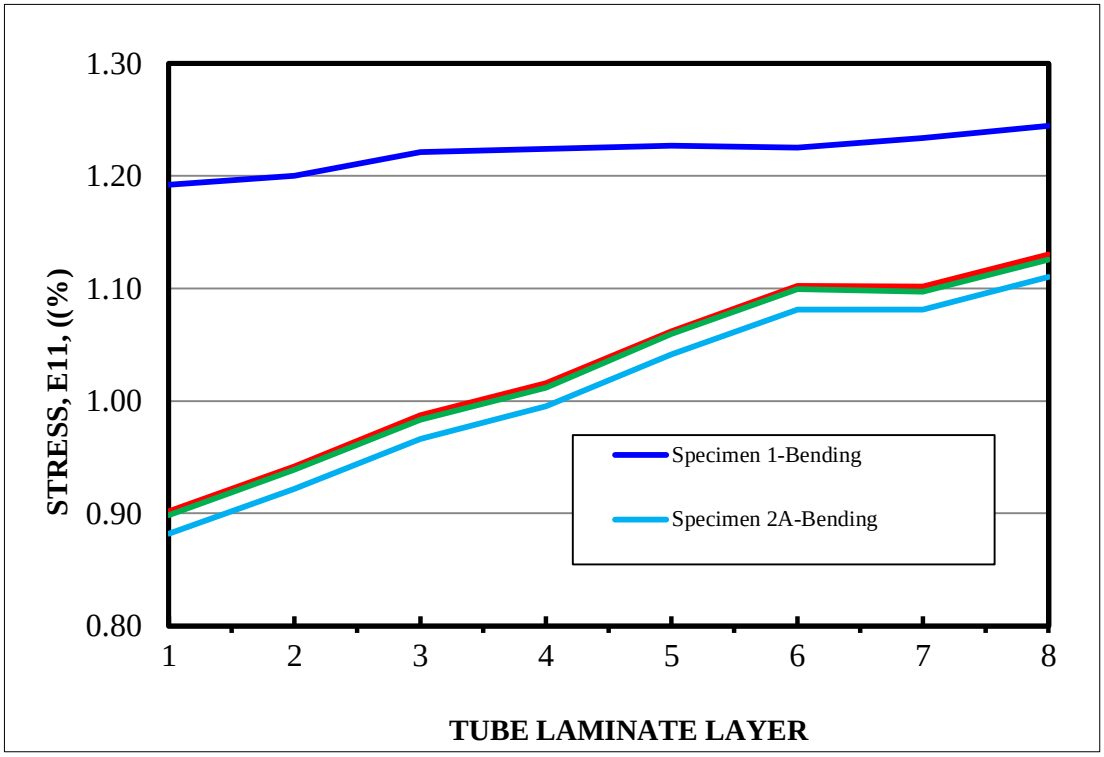

Figure 5-28: Tension side strain distribution in tube layers for simulation case 1, 2A, 2B & 2C

The outer layer of the tube carries the highest stress and strain, while the innermost layer carries the least. The inner layer is subjected to low stress, which is transmitted from the bend, axial and internal pressure loads. For bend loading, as shown in Figure 5-27, the thin-walled tube had higher stress on the laminate tube layers, compared to thick-walled tube. An increase in diameter-to-thickness ratio (D/t) from 7.0 (44.45/6.35) to 44.5 (44.45/1), i.e. reduction in tube wall thickness, increased the stress on outer-most layer of tube by 15.56%. A reduction in tube D/t ratio results in an increase in energy absorption, hence increase in the tube's strength (Farley, 1986).

As observed by others (Xia, Takayanagi, & Kemmochi, 2001), the variation of stresses in laminate layers was much lower in the thinner tube. The stress variation in thicker tube was more pronounced and non-linear. The thinner tube could not sustain additional tension loading, hence only one specimen for thin tube. Strain distribution across the thickness of the tubes, as shown in Figure 5-28, follow similar trend as the stress distribution. The variation in longitudinal stress between the inner and outer layer for the thin tube was approximately 3.0%. The thicker tube stress variation between the outer and inner layer was quite large for the thicker tube; it was approximately 25.1%.

Figure 5-27 shows that addition of tension loading on the thicker tube (specimen 2B), increases longitudinal stress on all the laminate layers of the tube by an average 2.02%. The increase was highest on the outer layer; with an increase of 2.25%. The effect of addition 4000 psi internal pressure (specimen 2C) on the tubing laminate layer stresses, as shown in Figure 5-27, was insignificant. The average stress increase on all the laminate layers of the tube was 0.17% with addition of pressure load to bending load.

The compression side stress (S11) distribution across the thickness of composite tube is shown in Figure 5-29. Bending results in higher layer stresses. Addition of tension load reduces the compression stresses by an average of 23.2%. The addition of 4000 psi internal pressure to the tube (specimen 2C) leads to a further slight reduction in compression stresses by about 3.0%.

The tube layers on the compression side of the tube experienced higher stresses than the tension side of the tube, as shown in Table 5-11 and Table 5-13.

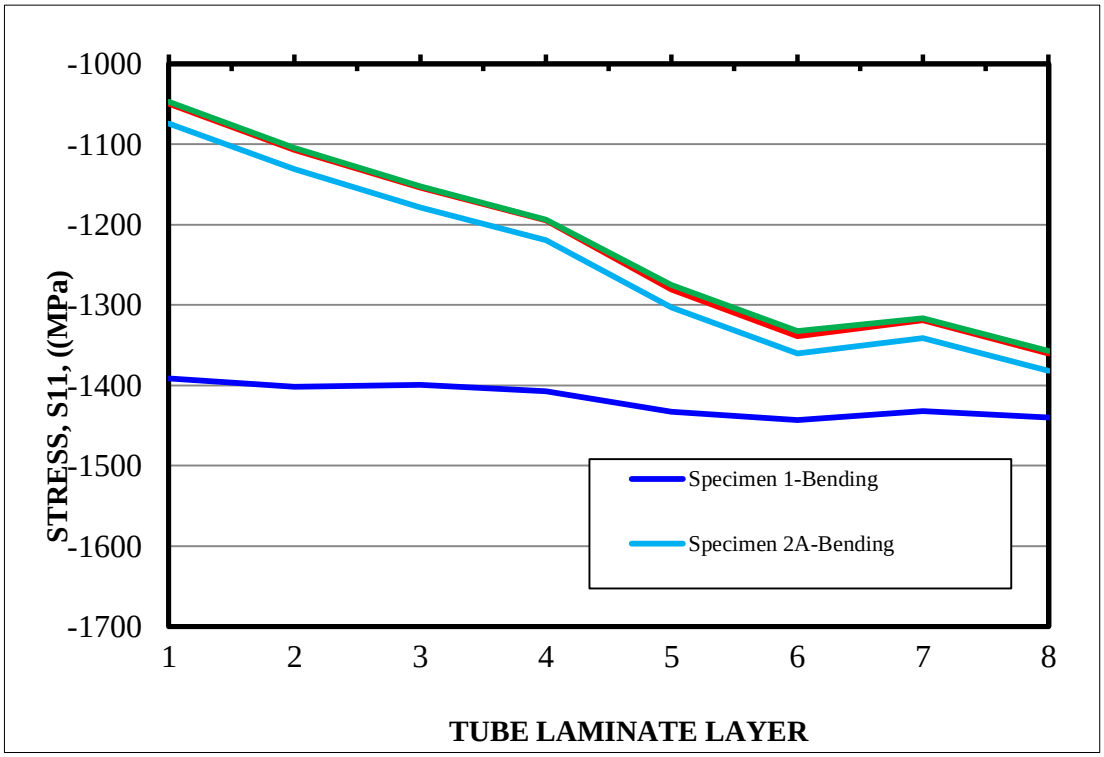

Figure 5-29: Compression side stress distribution in tube layers for simulation case 1, 2A, 2B & 2C

Table 5-11: Comparison of stresses on compression and tension side of tube

	COMPRESSION SIDE	TENSION SIDE
LAYER	SPECIMEN 2C S11 (MPa)	SPECIMEN 2C S11 (MPa)
1	-1047.7	1147.9
2	-1104.6	1198.5
3	-1152.7	1254.4
4	-1193.6	1290.6
5	-1275.4	1350.5
6	-1332.3	1401.2
7	-1316.3	1399.2
8	-1357.3	1435.4

Fibre failure modes in tension and compression are predicted by stress-based and strain-based failure model. The model measures the stress and strain in each ply component against the corresponding stress and strain limit. According to maximum stress theory, failure occurs when any stresses in the principal directions is equal or greater than the corresponding ultimate strength. The stress-based failure index is defined:

If $\sigma_{11} > 0$, set $X = X_t$, otherwise set $X = X_c$

If $\sigma_{22} > 0$, set $Y = Y_t$, otherwise set $Y = Y_c$

It requires that:

$$I_F = \left(\frac{\sigma_{11}}{X}, \frac{\sigma_{22}}{Y} \left| \frac{\sigma_{12}}{S} \right| \right) < 1.0 \qquad (5.1)$$

Fibre failure index in tension is computed using Equation (5.1). It requires that:

$FF = \frac{\sigma_{11}}{X} < 1.0$, FF is fibre failure.

The allowable tensile and compressive strength of the tube material is 1950 MPa and 1480 MPa, respectively. The applied stresses on the individual plies of the composite tube (specimen 2C) and their corresponding failure indices are tabulated in Table 5-12.

Table 5-12: Tension side layer stresses and failure indices

Layer/Ply	**Stress, σ_{11} (MPa)**	**Failure index**
1	1147.9	0.589
2	1198.5	0.615
3	1254.4	0.643
4	1290.6	0.662
5	1350.5	0.693
6	1401.2	0.719
7	1399.4	0.718
8	1435.4	0.736

For maximum strain failure theory, failure occurs when any ply strain in the principal directions is equal or greater than the corresponding ultimate strain. The strain-based failure index is defined:

If $\varepsilon_{11} > 0$, set $e_1 = e_{1t}$, otherwise set $e_1 = e_{1c}$

If $\varepsilon_{22} > 0$, set $e_2 = e_{2t}$, otherwise set $e_2 = e_{2c}$

Table 5-13: Compression side layer stresses and failure indices

Layer/Ply	Stress, σ_{11} (MPa)	Failure index
1	-1047.7	0.708
2	-1104.6	0.746
3	-1152.7	0.779
4	-1193.6	0.806
5	-1275.4	0.862
6	-1332.3	0.900
7	-1316.3	0.889
8	-1357.3	0.917

Maximum strain failure theory requires that:

$$I_F = \left(\frac{\varepsilon_{11}}{e_1}, \frac{\varepsilon_{22}}{e_2}, \left| \frac{\varepsilon_{12}}{e_{12}} \right| \right) < 1.0 \qquad (5.2)$$

Strain failure index is computed using Equation (5.2). It requires that:

$SF = \frac{\varepsilon_{11}}{e_1} < 1.0$, SF is strain failure.

The allowable tensile and compressive strain of the tube material is 1.38% and 1.175%, respectively. The longitudinal tension and compressive strains on the individual layers of the composite tube (specimen 2C) and their corresponding failure indices are tabulated in Table 5-14 and Table 5-15, respectively.

Table 5-14: Tension side layer strains and failure indices

Layer	Strain, ε_{11} (%)	Failure index
1	0.899	0.589
2	0.942	0.615
3	0.987	0.643
4	1.016	0.662
5	1.062	0.693
6	1.102	0.719
7	1.102	0.718
8	1.130	0.736

Table 5-15: Compression side layer strains and failure indices

Layer	Strain, ε_{11} (%)	Failure index
1	0.832	0.708
2	0.876	0.746
3	0.914	0.778
4	0.945	0.805
5	1.010	0.860
6	1.044	0.898
7	1.0403	0.885
8	1.072	0.912

The tube design is adequate as the failure indices for all the tube laminate layers are less than 1.0.

5.5 Composite tube experimental study

Composite tube sample used in this study was also fabricated from Toray's T700S high strength, standard modulus carbon fibres (Toray Carbon Fibres America, 2008) and epoxy resin by filament winding technique. The tube consisted of eight plies of carbon/epoxy. Carbon fibre properties were reported as shown in Table 5-3 above. One tube measuring 1200mm was fabricated. The tube was subjected to bending test and further evaluated for mechanical strength.

Composite tube with 44.45 mm (1.75 inches) outside diameter (OD) and 31.75 mm (1.25 inches) inside diameter (ID) 1200mm long was fabricated. The tube was thereafter subjected to bending test without internal pressure and further evaluated for mechanical its strength.

5.5.1 Fabrication of composite tubes

Filament winding technique was utilized to fabricate the carbon fibre tube samples. The specimens were manufactured at Teakle Cmposites company in Brisbane, Australia. Filament winding is one of the most common techniques for manufacture of composite tubes (Rousseau, Perreux, & Verdiere, 1999). The specimen was

produced using a numerical controlled winding machine. Eight tows of high strength-standard modulus carbon fibre material of 0.535g/m were dispensed. A winding tension of 28.8 N was applied to the individual fibres. The tows were guided through a dip-type resin bath and wetted with epoxy resin system, as shown in Figure 5-30.

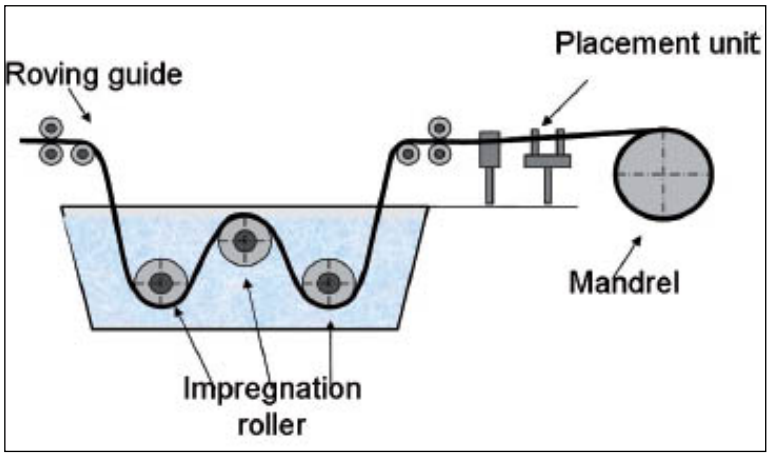

Figure 5-30: Schematic representation of a dip-type resin

Wet fibres were wound round a chrome-plated steel mandrel of 31.75mm diameter. A 1.5m tube specimen, consisting of eight plies with winding angle of +70/0/-70/0/+70/0/-70/0 was produced. A filament winding machine is shown in Figure 5-31.

Figure 5-31: Filament winding machine (Courtesy of Teakle Composites)

The tube was cured at 100 ^{o}C for 2 hrs; the temperature was slowly ramped up to 100 ^{o}C and held for 2 hrs. The specimens were extracted from the mandrel after curing. Figure 5-32 shows the cured sample tube.

Figure 5-32: Cured carbon/epoxy fibre tube

5.5.2 Experimental tests

Two tests were performed on the tube. Firstly the tube was subjecting cyclic bending to test its fatigue strength. The tube was then removed from the bending machine and cut into two pieces. The cut pieces were evaluated for their mechanical strength using the universal tensile testing machine.

Bending tests

The composite tube sample was tested for fatigue life using bending machine. Figure 5-33 shows the carbon/epoxy tube on bending machine during fatigue testing. Figure 5-34 is a screen capture of bending machine measurement outputs during testing.

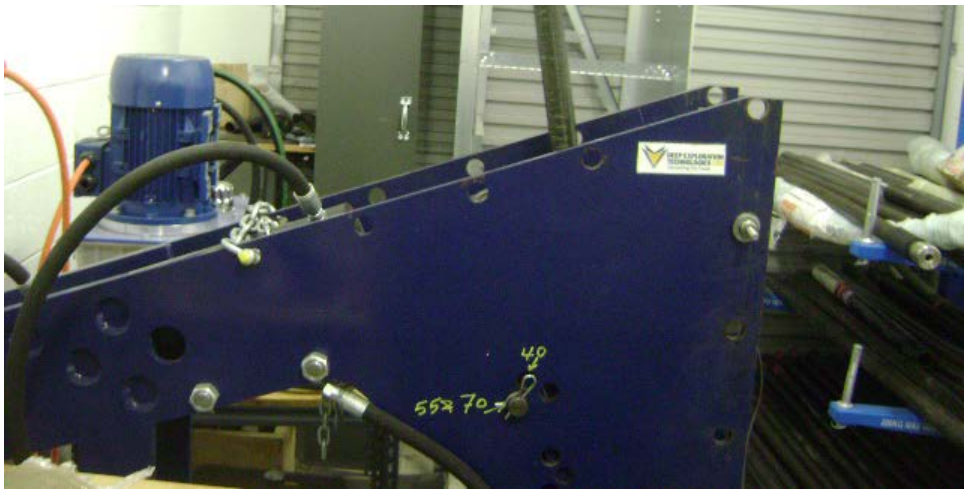

Figure 5-33: Fatigue testing of carbon/epoxy tube

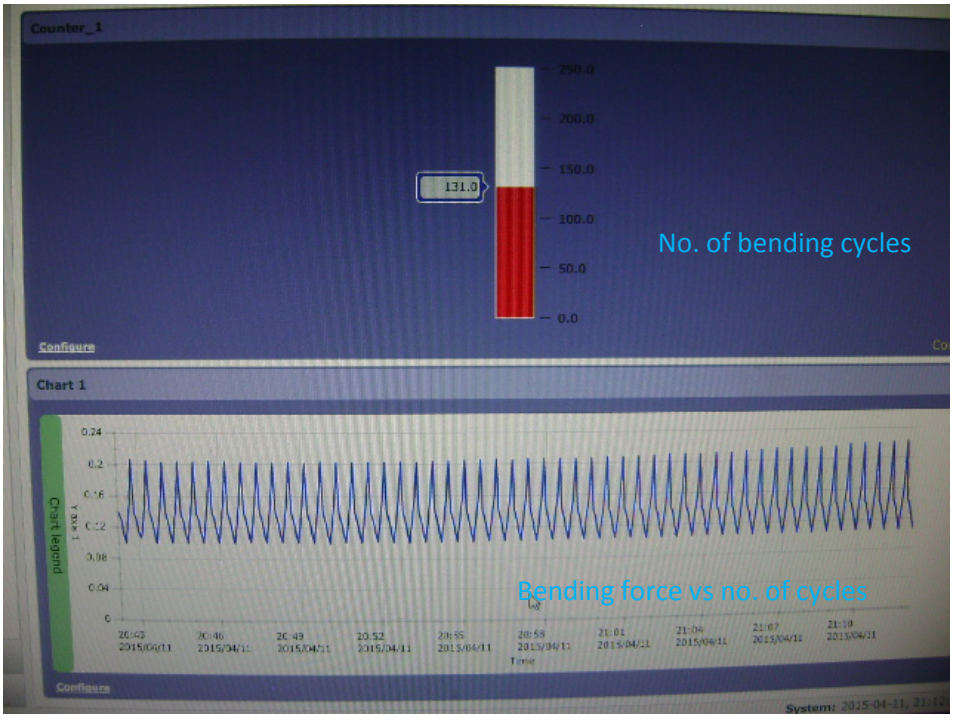

Figure 5-34: Screen capture of bending machine measurement outputs

Bending test results

The tube sample underwent 1712 bending cycles without failure. The tube sample was then removed from the bending machine.

Figure 5-35 shows the stress-cycle history for the [+70/0/-70/0/+70/0/-70/0] specimen, subjected to single-sided bending on a 70-inch (1778 mm diameter)

bending radius. The abscissa contains the number of cycles while the ordinate axis shows the corresponding maximum and minimum value of stress for each cycle.

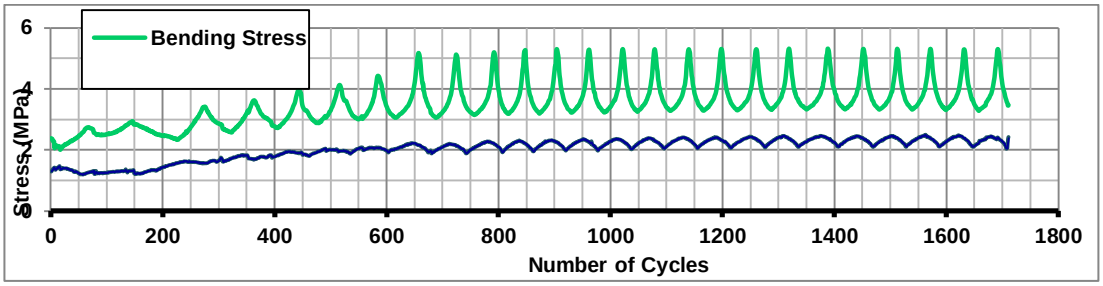

Figure 5-35: Stress-Cycles history for carbon fibre tube specimen on 1778mm bending radius

The bending/flattening force is initially lower in the first 200 cycles. The force gradually ramps up and stabilizes at approximately 650 cycles. This is attributed to the bending machine load cell mechanism. The load piston is inclined and is chained to avoid upward movement of the piston during bending. Hence, during the initial bending/flattening cycles, the piston's upward movement is constrained. This creates some extra load on the load cell, thus the higher bending force/stress values in the subsequent cycles. At 1712 cycles, no significant degradation in mechanical properties of the tube specimen can be observed; the stiffness of the specimen remains unchanged. No permanent deformation was observed after 1712 bending cycles. Figure 5-36 illustrates the constant stress amplitude response of the composite tube, which is computed using Equation (4.3). A review of one-dimensional fatigue model for single-sided bending is based on the phenomenological residual stiffness approach (Van Paepegem & Degrieck, 2003). In the continuum damage mechanics, stress and strain relationship can be written as:

$$\sigma' = \frac{\sigma}{1-D} = E_o \varepsilon \tag{5.3}$$

Where is σ' the effective stress, σ is the applied stress, ε is the nominal strain and E_o, is the undamaged Young's modulus and D is a measure for the fatigue. D is a measure of macroscopic measure for the fatigue damage and is defined as

$$D = 1 - \frac{E}{E_0} \tag{5.4}$$

The value of D lies between 0 (undamaged material) and 1 (final failure).

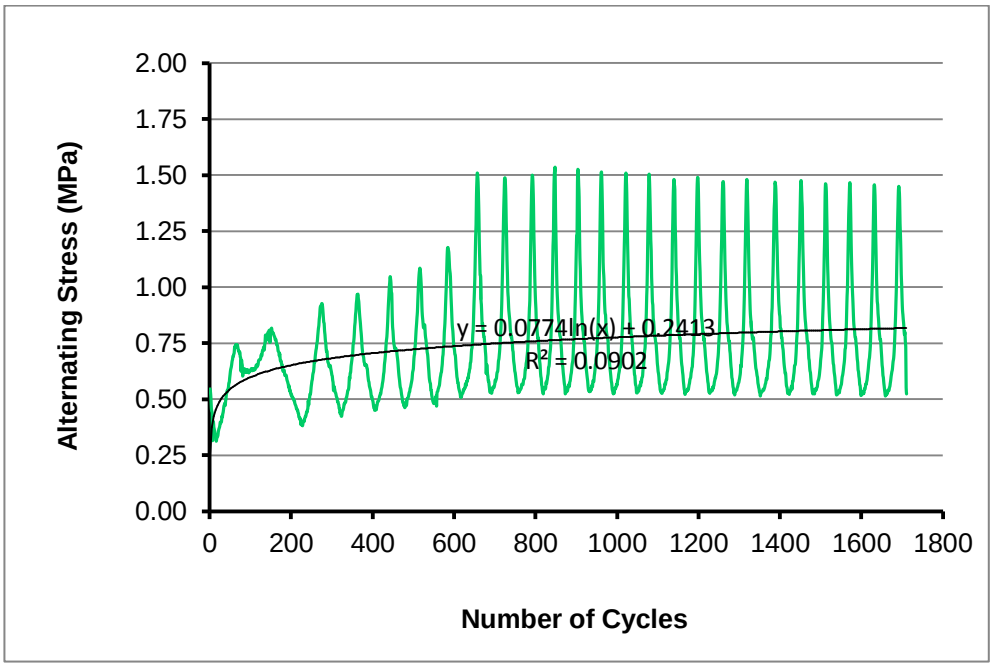

Figure 5-36: Alternating stress of carbon/epoxy tube

The damage evolution law, dD/dN, which predicts the damage increment per cycle, is a function of the stress amplitude (alternating stress). The larger the applied stress amplitude the faster the damage will initiate and propagate. As can be noted, the stress amplitude for the composite tube is significantly lower than that of steel coiled tubes. Consequently, crack propagation could be slower in composites compared to steel tubes.

Tensile tests

The bent tube was cut into two pieces. Mechanical properties of the tube two samples were evaluated via tensile testing. Show the arrangement of one of the samples during tensile testing. Thus two duplicate tests were conducted for the tube specimen. As with flat sheet samples, a wedge grip type was used. Polyvinyl chloride tabs were applied at the ends of the specimens to promote uniform stress within grip and prevent gripping damage. To prevent slippage, the Polyvinyl chloride surfaces were serrated by a sanding paper. The surfaces were cleaned before applying adhesive for attachment to the specimens.

Figure 5-37: Experimental set up of carbon/epoxy tube tensile test

Strains were recorded with an extensometer, located at the centre of the tube, as shown in Figure 5-37.

Tensile test results

Tension test results of the composite tube samples are shown in

Table 5-16. Tension tests were performed in accordance to ASTM D3039 (ASTM, 2008). Stress-strain plots of the composite tube samples are presented in Figure 5-38. Tensile test results indicated that the mechanical samples of both samples were relatively similar. The ultimate tensile strengths of sample 1A and 1B were 699.74MPa and 664.92 MPa, respectively – a difference of 0.05%. The low strain in both samples is attributed to failure of the samples at the gripping ends. Fibre breakage caused by grip damage was observed, as shown in Figure 5-39. After several attempts, the tabs applied at the ends of the specimens to promote uniform stress within grip and prevent gripping damage due to grips, could not sustain the tensile load applied to the tubes during testing. Hence the samples were finally tested without the end tabs.

Table 5-16: Mechanical properties of Carbon fibre tube

Tube no	Material	OD	t	UTS	UTS	Modulus of Elsticity, E	Strain	Comments
		mm	mm	kN.	MPa	GPa	(%)	
1A	Carbon fibre tube	44.45	6.35	531.84	699.74	70.73	0.95	Low strain due early fracture at grips
1B	Carbon fibre tube	44.45	6.35	505.05	664.92	70.49	0.94	Low strain due early fracture at grips

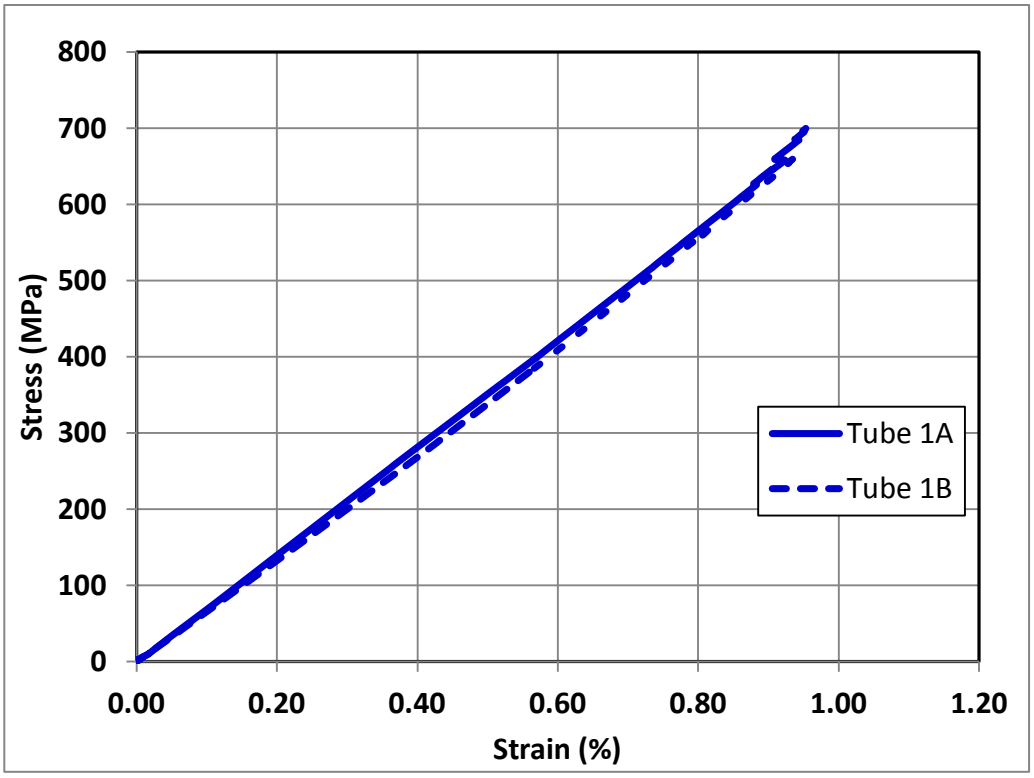

Figure 5-38: Stress-strain response for carbon/epoxy tube sample

The composites tube samples 1A and 1B sustained 54.2 tons and 51.5 tons, respectively, during tensile testing. This is more than 5 times the expected axial load (7 tons) during mineral exploration drilling operations.

Figure 5-39: Fibre breakage on carbon/epoxy tube during tensile testing (tube 1A)

The carbon/epoxy tube samples depicted fibre pull-outs at fracture, as shown in Figure 5-40.

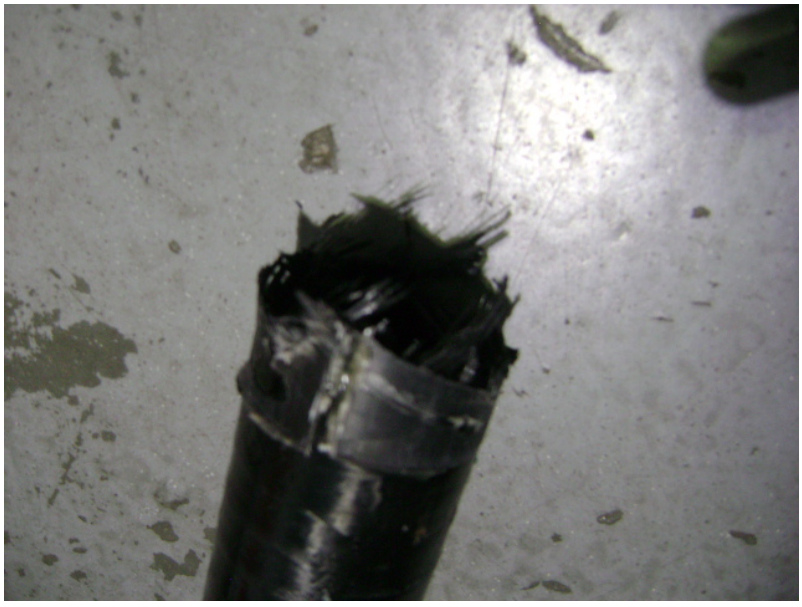

Figure 5-40: Carbon/epoxy failure during tensile testing

5.6 Conclusions

In composite tube design, fibre orientation and the sequence of fibre stacking impact on mechanical properties of the tube. Simulation study was undertaken to select a suitable fibre orientation and stacking sequence design for composite coiled tubing

material for mineral drilling application. A fibre orientation of +70/0/-70/0/+70/0/-70/0 was selected as it provided a higher material strength. Stress distribution on the designed composite tube layers when subjected to combined axial, bending and pressure loads was also analysed. Stresses in a composite generally vary in different layers. Simulation study showed that the tensile and compressive layer stresses on the thin-walled tube were higher compared to the layer stresses in thick-walled tube. An increase in diameter-to-thickness ratio (D/t), i.e. reduction in tube wall thickness, increased the stress on outer-most layer of tube. A reduction in tube D/t ratio results in an increase in energy absorption, and thus the increase in the tube's strength (Farley, 1986).

The variation of stresses in the tube's laminate layers was much lower in the thinner tube, as observed by Xia et al. (2001). The stress variation in the thicker tube was more pronounced and non-linear.

The composite tube layers on the compression side of the tube experienced higher stresses than the tension side of the tube. This agrees with Equation (2.5) which indicates that maximum stress on the tube occurs on the side where the bending stress is compressive.

The designed tube was bent over a bending form radius of 70 inches (1778mm) and it underwent 1724 bending cycles without any noticeable failure. This experimental result confirms the simulation study. The simulation study showed that the tube bent over the 70-inch reel, under axial and pressure loads, without failure. The tube's ultimate tensile strength was approximately 682 MPa (approximately 44 ton-force). This was approximately six (6) times more than the expected operational axial load on the DET CRC coiled tube rig.

Chapter 6 Conclusions and Recommendations

6.1 Conclusions

When steel coiled tubing is subjected to multiple plastic deformation bending cycles, it accumulates damage and fails at a low cycle fatigue. The rate of weakening is faster in thin-walled coiled tubes with lower yield strength. It was demonstrated experimentally that strain hardening due to cyclic bending took place in a thin walled sample with higher yield strength (GT100 – 4.45mm thick). The strain hardening was noticed and confirmed by the increase of the yield strength, decrease of ductility and slight a increase in its Modulus of Elasticity. However, this increase in strength and the corresponding reduction in ductility lead to likelihood of fracture occurrence in the material. On the other hand, the thin walled sample with lower yield strength (GT90 – 4.45mm thick) showed the lowest cycle fatigue loading.

Cyclic bending of steel coil tube induces localized stresses and strains above the elastic limit (σy and εy), resulting in shorter fatigue life. Coiled tube bending tests with internal tube pressure was not part of my PhD study. However, the bending machine was upgraded in order to be able to undertake coiled tube bending tests with internal pressure. Four steel coiled tubes with 44.45mm (1.75 inches) OD and 3.4mm (0.134 inches) wall thickness were tested with 0 psi, 600 psi, 2200 psi and 3200 psi internal pressure, respectively. Experimental results showed that higher internal pressure greatly reduces the fatigue life of the steel coiled tube. An increase of internal pressure from 600 psi to 3200 psi reduces the life of 44.45mm OD steel tube by approximately 87%. Tube wall thinning, as a result of internal pressure, reduces the fatigue life of steel tube.

It is worth noting that the internal pressure applied to the tube will vary significantly over its service life. Hence accurate prediction of the cycles-to-failure will most likely require the use of numerical models that will rely on detailed on site monitoring programs designed to evaluate all of the operating conditions of the CT during service.

Experiments and simulation studies were carried out and an optimal fibre orientation design of a composite coiled tube for mineral exploration drilling was determined. It was observed that the mechanical properties of composite tube are largely dependent on fibre orientation and the sequence of fibre stacking. Analyses were performed for pure axial and combined axial/bending loads. Optimum angle and coiled tubing material selected for mineral exploration drilling application is shown in Table 6-1.

Table 6-1: Coiled tubing design

Loading type	**Fibre orientation**	**Material selected**
Axial/bending	+70/0/-70/0/+70/0/-70/0	Carbon/epoxy

The selected coiled tubing design and material exhibited unique anisotropic characteristics that provided higher material strength, suitable for drilling.

It was shown that the stresses and strains on composite tubing are largely dependent on the fibre stacking sequence, orientation and wall thickness of the tube. This is in agreement with results by other researchers in literature. Stresses in a composite generally vary in different layers. The simulation study showed that the tensile and compressive layer stresses on the thin-walled tube were higher compared to the layer stresses in the thick-walled tube. An increase in diameter-to-thickness ratio (D/t), i.e. reduction in tube wall thickness, increased the stress on the outer-most layer of the tube. A reduction in tube D/t ratio results in an increase in energy absorption, and thus the increase in the tube's strength (Farley, 1986). The variation of stresses in the tube's laminate layers was much lower in the thinner tube, as observed by Xia et al. (2001). The stress variation in the thicker tube was more pronounced and non-linear. The composite tube layers on the compressional side of the tube experienced higher stresses than the tension side of the tube. This agrees with Equation (2.5) which indicates that maximum stress on the tube occurs on the side where the bending stress is compressive.

Tests undertaken on steel and composite coiled tubes indicate that the composite tubes have higher fatigue life compared to steel tube, in the order of three or more. Other advantages of composite CT include light weight, corrosion resistance and electrical conductors or optical fibres which could be embedded in the wall of the tube.

6.2 Recommendations

Literature studies show that pressure greatly impacts the performance of coiled tubing. The tubing design for pressure and experimental investigation were, however, not part of this study. A composite design could include an inner member/liner that serves as a pressure barrier especially while spooling the tube over the gooseneck and the reel. The layer could prevent leakage of internal drilling fluids from within the tubing. An outer protective layer could provide wear resistance and resistance against impacts and abrasion. These aspects of coiled design are recommended for future research.

The carbon/epoxy tube was tested on a 1778mm bending radius. This was the smallest achievable radius for the tube. To attain a smaller bending radius of 1400mm or less, for ease in rig transportation, the author of this thesis would suggest a hybrid composite tube material. The hybrid composite tube could consist of carbon/epoxy and glass/epoxy. Additionally, a fibre orientation of+80/-80/0/0/+80/-80//0/0 was recommended for any future design consideration.

The coiled tube experimental tests in this research were bench scale tests. A real field coiled tube test on a drilling rig is suggested to validate the bench scale tests.

6.3 Main Contributions of this research

- Proposed a composite CT material design to be used deep in hard rock drilling for mineral exploration, which will address tensile loads and high strains imposed by cyclic bending.
- Tests undertaken during research showed that composite coiled tubing require an inner member/liner that serves as a pressure barrier.
- Fatigue tests performed on steel and composite coiled tubes (with zero internal pressure) demonstrated that composite tube has the capability of exceeding HSLA steel tubing life by a factor of 3 or more.

References

A370, A. (2010). Standard Test Methods and Definitions for Mechanical Testing of Steel Products, A370. (14).

Abaqus. (2014). Abaqus data sheets. Retrieved 29-9, 2014, from http://www2.3ds.com/fileadmin/PRODUCTS/SIMULIA/PDF/datasheets/simulia-abaqus-standard-datasheet.pdf

Albright, J., Dreesen, D., Anderson, D., Blacic, J., Thomson, J., & Fairbanks, T. (2005). Road Map for a 5000 ft Microborehole. *Los Alamos National Laboratory*, P34.

ASM. (2008). Elements of Metallurgy and Engineering Alloys. *ASM International, 05224G*.

ASTM. (2008). ASTM D3039, Standard test method for tensile properties of polymer matrix composite materials. *ASTM D3039*.

Avakov, V., Foster, J., & Smith, E. (1993). *Coiled tubing life prediction.* Paper presented at the Offshore Technology Conference.

Bridge, C. (2011). *Combining Elastic and Plastic Fatigue Damage in Coiled Tubing.* Paper presented at the SPE/ICoTA Coiled Tubing & Well Intervention Conference and Exhibition.

Chung, D. (2012). *Carbon fiber composites*: Butterworth-Heinemann.

Corporation, C. R. (2012). Methods and Equations Composite Strength, Ply-Based. *HyperSizer*.

Crabtree, A., & Skrzypek, H. (1998). Investigation of coiled tubing failures over 2 years and corrosion prevention methods. *SPE/ICoTA Coiled Tubing Roundtable*.

Crabtree, A., Skrzypek, H., & Wilde, G. (1997). Determining the Mechanical Properties of Coiled Tubing. *SPE/ICoTA North American Coiled Tubing Roundtable*.

Crabtree, A., Skrzypek, H, and Wilde, G. (1997). Determining the Mechanical Properties of Coiled Tubing. *Society of Petroleum Engineers, 38412*, 3.

Crabtree, A. R., & Gavin, W. (2005). Coiled Tubing in Sour Environment-Theory and Practice. *SPE Drilling & Completion, 20*(01), 71-80.

CRC, D. (2014). Bending machine commissioned: Towards durable coiled tubing. Retrieved 12/3/2015, 2015, from https://www.youtube.com/watch?v=iqsDVSpMkwM

Crouse, P., & Lunan, W. (2000). Coiled tubing drilling-expanding application key to future. *SPE/ICoTA Coiled Tubing Roundtable*.

CTES, L. (2005). Coiled Tubing Manual. *CTES CT Manual*(21/7/2005), 2-9.

Daniel, A., & Donald, A. (2002). Testing Tech Tabbing composite test specimens: When and why. Page 9.

Department of Defense, U. S. A. (2002). Composite Materials Handbook. *Volume 2*(MIL-HDBK-17-2F).

Farag, M. M. (1997). *Materials selection for engineering design*: Prentice Hall London.

Farley, G. L. (1986). Effect of specimen geometry on the energy absorption capability of composite materials. *Journal of Composite Materials, 20*(4), 390-400.

Feechan, M., Quigley, P. A., & Wideman, T. W. (2009). Fiber reinforced spoolable pipe: Google Patents.

Forkes M.J., H. S. T. (1990). Mechanical Properties of Glass/Polypelyne Multilayer Laminates. *Journal of Material Science*.

Fowler, H. (1997a). *Update on Advance Composite Spoolable Pipe Developments.* Paper presented at the SPE/ICoTA North American Coiled Tubing Roundtable.

Fowler, H. (1997b). Update on Advanced Composite Spoolable Pipe Developments. *Society of Petroleum Engineers*.

Fowler, S., Feechan, M., & Berning, S. (1998). *Applications Update-Advanced Composite Coiled Tubing.* Paper presented at the SPE/ICoTA coiled tubing roundtable.

Glenn, A. (2004). Automating Structural Analysis of Spacecraft Vehicles

Technical Reports NASA Langley Research Centre, Hampton VA, USA.

Hancox, N., & Mayer, M. (1994). Design data for reinforced plastics: Chapman and Hall, London.

Hany El Kadi, Y. A.-A. (2002). Prediction of fatigue life of unidirectional glass fibbre/epoxy composite Laminae using different nueral network paradigms. *Composite Structures.*

ICoTA. (2005). An introduction to coiled tubing, History, applications, and benefits. *ICoTA.*

J.H Park, e. a. (2001). Stacking Sequence Design of Composite Laminates for Maximum Strength using Generaic Algorithms. *Composite Structures.*

Kamyab, M. (2014). *A Study of Cuttings Transport in Micro-Borehole Coiled Tubing for Mineral Exploration Drilling.* (PhD), Curtin University.

Lagat, C., Roufail, R., Rasouli, V., Evans, B., & Soe, S. (2014). *Experimental Investigation of Steel Coiled Tubes Performance Under Cyclic Bending.* Paper presented at the ASME 2014 33rd International Conference on Ocean, Offshore and Arctic Engineering.

Lagat C., R. R., Rasouli V., Brian E. (2014). *Design and Evaluation of Filament Wound Composite Coiled Tube For Hard Rock Drilling*. Paper presented at the Composites Australia, NewCastle, Australia.

Lane, P. (2005). Coiled tubing manual. *CTES*, 31-32.

Lee, Y.-L. (2005). *Fatigue testing and analysis: theory and practice* (Vol. 13): Butterworth-Heinemann.

Leising, L. J., & Newman, K. R. (1993). Coiled-Tubing Drilling. doi: 10.2118/24594-PA

Majoribanks, R. (2010). *Geological methods in mineral exploration and mining* (Vol. Second Edition). Berlin, Germany: Springer.

Malik, M., CHOUDHARY, V., & Varma, I. (2000). Current status of unsaturated polyester resins. *Journal of Macromolecular Science, Part C: Polymer Reviews, 40*(2-3), 139-165.

Mallick, P. K. (1993). *Fiber-reinforced composites: materials, manufacturing, and design*: CRC press.

Mallick.P.K. (1997). Composite Engineering Handbook.

McClachie, D. W., Reynolds, T. J. (1999). Applications Engineering For Composite Coiled Tubing. *Society of Petroleum Engineers*(SPE 54507).

McClatchie, D., Reynolds, H., Walsh, T., & Lundberg, C. (1999). Applications engineering for composite coiled tubing. *SPE/ICoTA Coiled Tubing Roundtable*.

Mechanictips. (2011). Universal testing machine. Retrieved 24/05/2015, from http://nees.berkeley.edu/Facilities/images/clip_image004.jpg
Miracle, D. B., Donaldson, S. L., Henry, S. D., Moosbrugger, C., Anton, G. J., Sanders, B. R., . . . Muldoon, K. (2001). *ASM handbook*: ASM international Materials Park, OH, USA.
Nestles, A. T. (1994). Basic mechanics of laminated composite plates. *National Aeronautics and Space administration, Marshal Space Flight Centre, 1351*.
Nettles, A. T. (1994). *Basic mechanics of laminated composite plates*: Marshall Space Flight Center, National Aeronautics and Space Administration.
Newman, K., Newburn, D., & Schlumberger, D. (1991). SPE 22820 Coiled-Tubing-Life Modeling.
Perry, K. (2007). Microhole coiled tubing drilling concept applied to mature Niobrara gas play in Kansas, Colorado. *Drilling contractor, 63*(2), 88-90.
. Policy for the transport of oversize and overmass indivisible loads and vehicles. (2006) (Vol. MR 434 06/06): Government of Australia

Rachal, D. M., & Krove, J. R. (1990). Vacuum bagging process for fiber reinforced thermoplastics: Google Patents.
Ratna, D. (2009). Handbook of Thermoset Resins: Smithers Rapra Technology.
Research, C. (2011). Methods and Equations-thermoelastic stiffness formulation.
Research, C. (2012). Methods and equations, composite strength, ply based.
Research_Corporation, C. (2012). Material Strength, Composite, Ply-based. *HyperSizer Methods and Equations*.
Roufail, R., & Rasouli, V. (2012). Material substitution of coil tubes in CT drilling technology for hard rocks. *Petroleum and Mineral Resources, 81*, 133.
Rousseau, J., Perreux, D., & Verdiere, N. (1999). The influence of winding patterns on the damage behaviour of filament-wound pipes. *Composites Science and Technology, 59*(9), 1439-1449.
Roylance, D. (2001). Stress-strain curves. *Massachusetts Institute of Technology study, Cambridge*.
Sas-Jaworsky, A., & Williams, J. G. (1993). *Development of Composite Coiled Tubing for Oilfield Services.* Paper presented at the SPE Annual Technical Conference and Exhibition.
Schodde, R., & Guj, P. (2012). Where are Australia's mines of tomorrow: Centre for Exploration Targeting, University of Western Australia, September.
Soden, P., Hinton, M., & Kaddour, A. (1998). Lamina properties, lay-up configurations and loading conditions for a range of fibre-reinforced composite laminates. *Composites Science and Technology, 58*(7), 1011-1022.
Staab, G. (1999). *Laminar composites*: Butterworth-Heinemann.
Tipton, S. M., & Newburn, D. A. (1996). Plasticity and Fatigue Damage Modeling of Severly Loaded Tubing. *Advances in Fatigue Lifetime Predictive Techniques*, 369-382.
Toray Carbon Fibres America, I. (2008). Torayca T700S Datasheet. (CFA-005).
tubing, G. (2012). Coiled tubing technical data.
Urayama, T., Yonezawa, T., Hamada, M., Sugino, M., Takabe, H., & Ikeda, A. (2000). *Research and Development of Advanced Coiled Tubing.* Paper presented at the IADC/SPE Drilling Conference.
Van Paepegem, W., & Degrieck, J. (2003). Modelling damage and permanent strain in fibre-reinforced composites under in-plane fatigue loading. *Composites Science and Technology, 63*(5), 677-694.

Vargo. (2002). Coiled tubing handbook.
Wellman, B. (2010). Strain Hardening & Strength. (No. 17).
Wellman, B. (May 2010). Strain Hardening and Strength. *A publication of Brush Wellman Alloy Products*(Issue No. 17).
Xia, M., Takayanagi, H., & Kemmochi, K. (2001). Analysis of multi-layered filament-wound composite pipes under internal pressure. *Composite structures, 53*(4), 483-491.
Yang, Y. (1999). Understanding Factors Affecting Coiled-Tubing Engineering Limits.
Yung-Li Lee, J. P., Richard Hathaway, Mark Barkey. (2005). Fatigue Testing and Analysis - Theory and practice.

Appendix 1 Alternating Stress

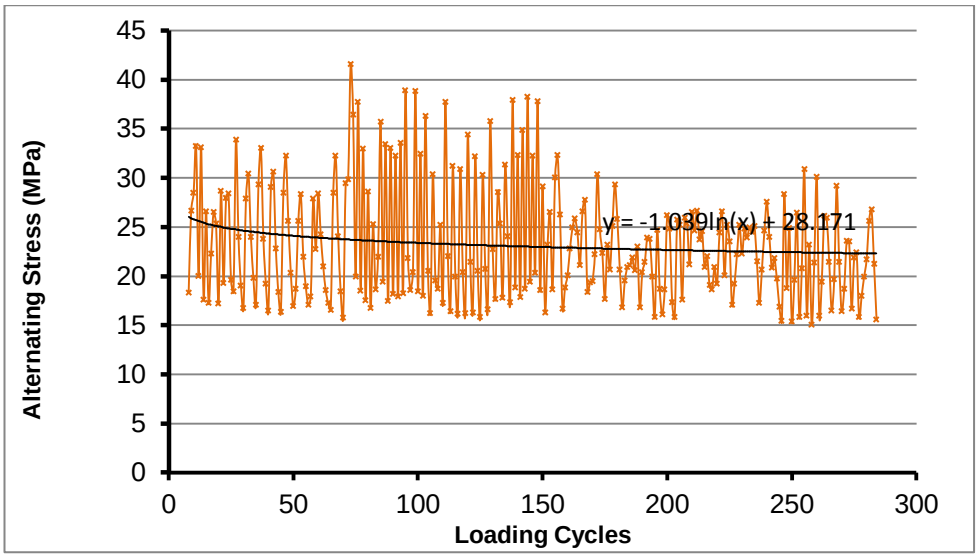

1. Appendix 1-1: Alternating stress (tube B), after (Lagat et al., 2014)

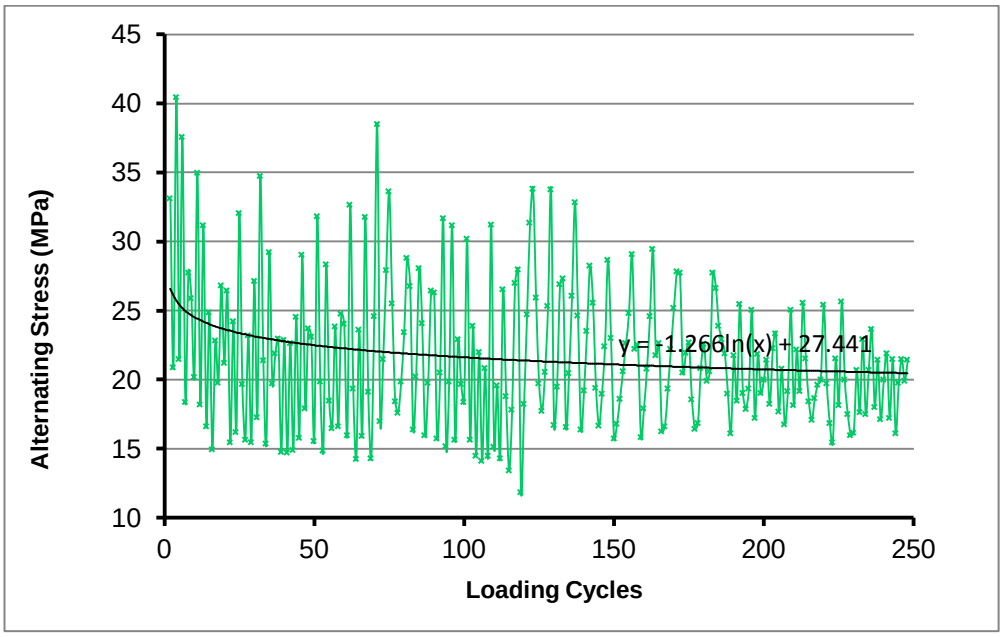

Appendix 1-2: Alternating stress (tube C), after (Lagat et al., 2014)

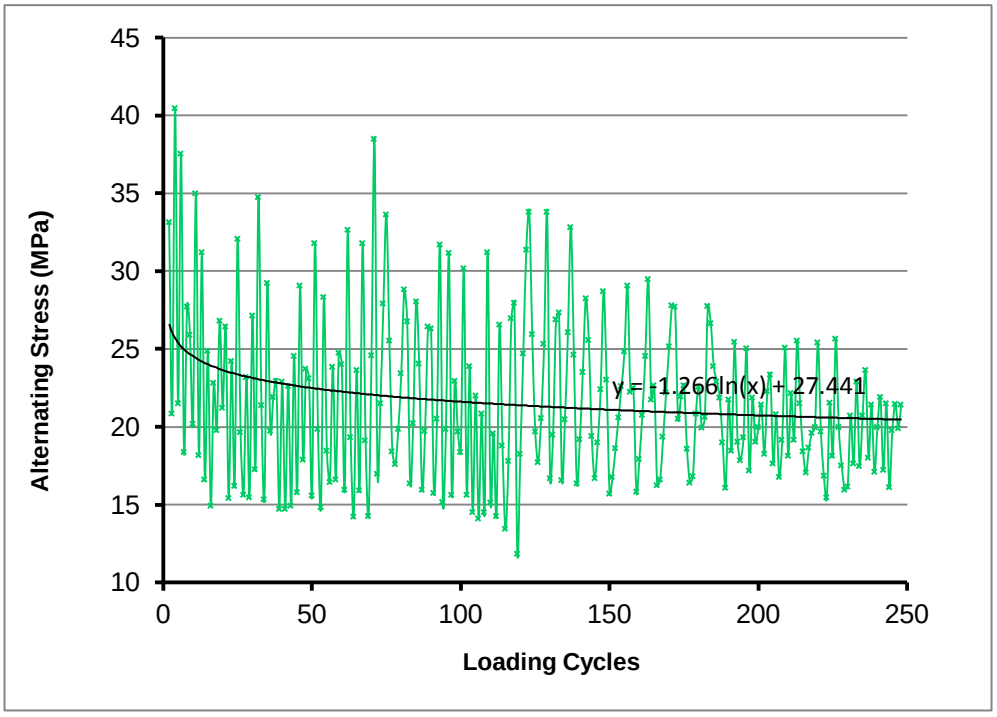

Appendix 1-3: Alternating stress (tube D), after (Lagat et al., 2014)

Appendix 2 Flat sheets Tensile test specimens

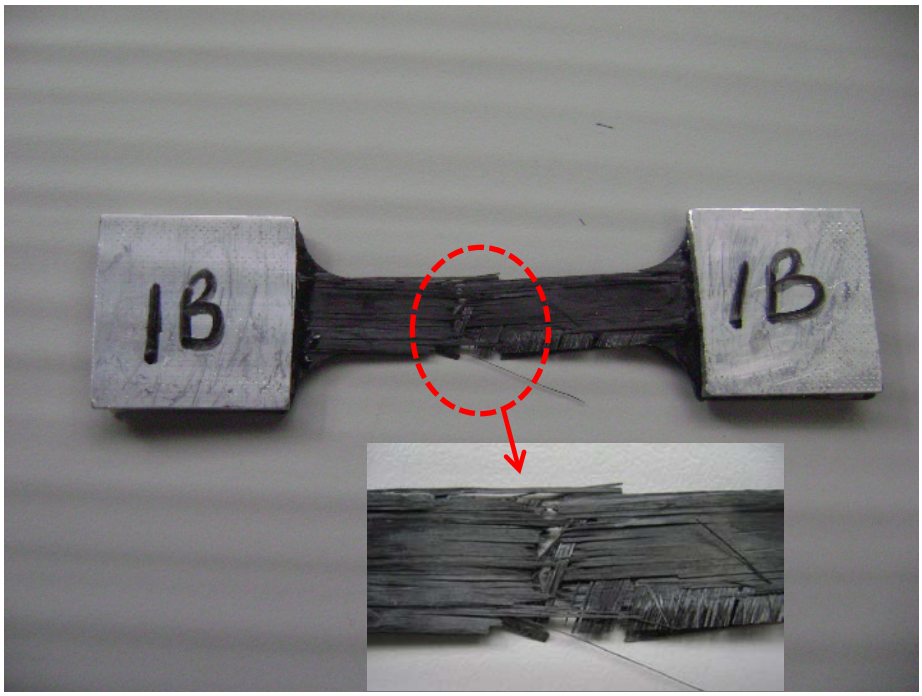

Appendix 2-1: Specimen 1B

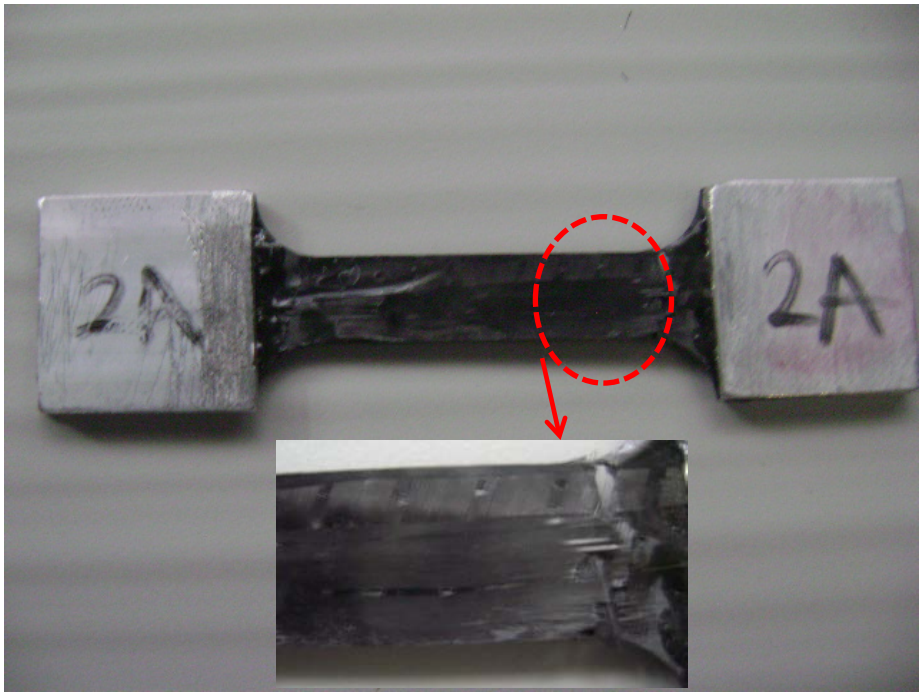

Appendix 2-2: Specimen 2A

Appendix 6-4: Specimen 3B

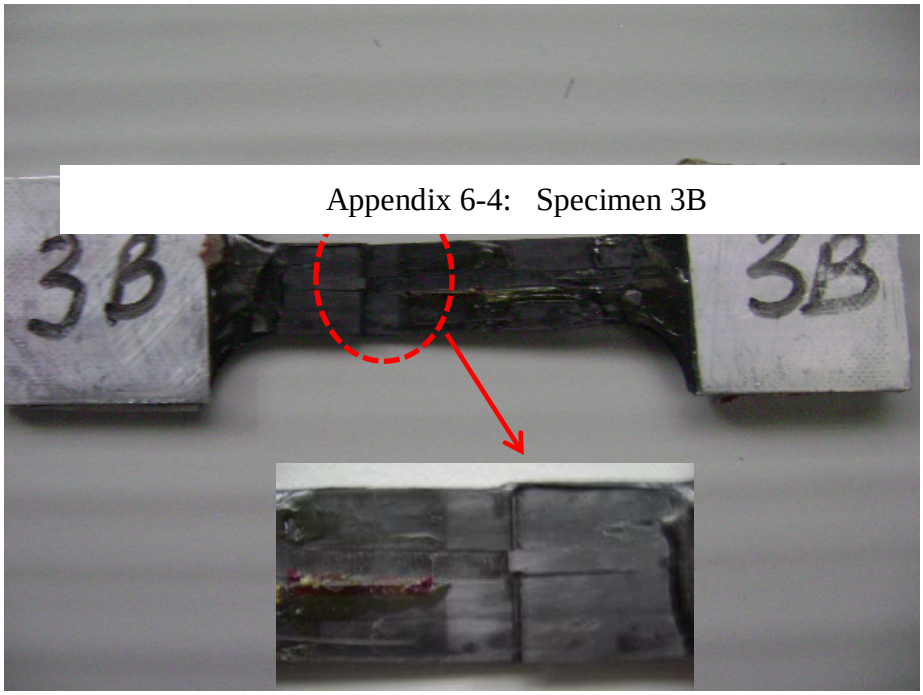

Appendix 2-3: Specimen 3B

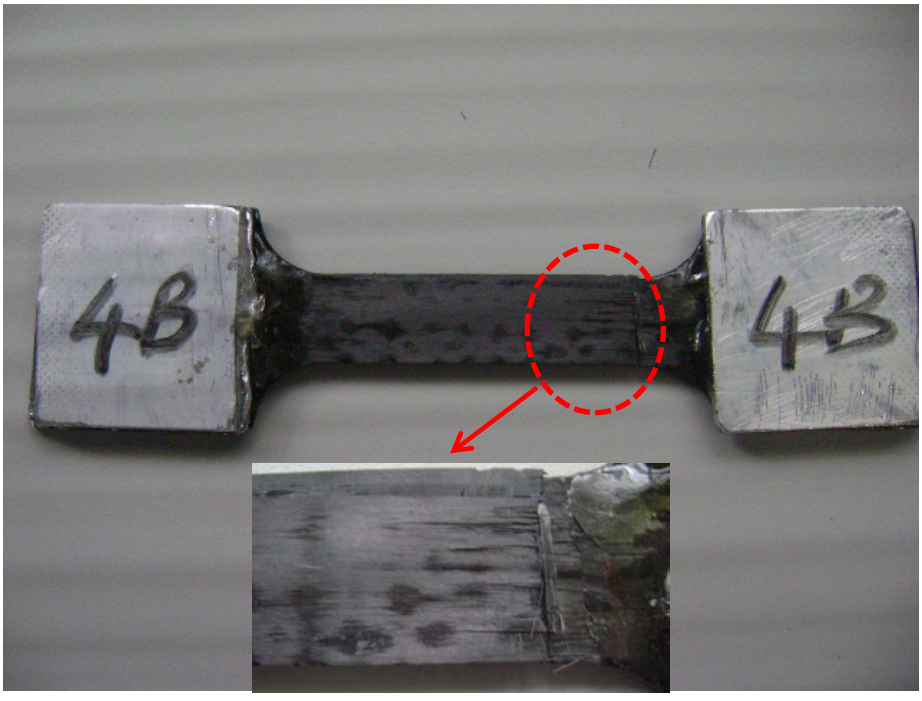

Appendix 2-4: Specimen 4B

Appendix 3 Steel coiled tubes fatigue tests

Though not part of my PhD study, the bending machine was upgraded to undertake coiled tube bending tests with internal tube pressure. Four steel coiled tubes with 44.45mm (1.75 inches) OD and 3.4mm (0.134 inches) wall thickness obtained DET-CRC in Adelaide, South Australia, were tested with 0psi, 600 psi, 2200 psi and 3200 psi internal pressure, respectively. Tenaris^{TM} had performed simulation study on similar tube under various internal pressures. The experimental results were compared with Tenaris^{TM} simulation results, as shown in Table 6-2.

The large variation between the experimental and simulation results for Tube 1 was attributed to the fact that, due to lack of internal tube pressure, pinhole crack initiation could not be easily detected. The tube was tested to fracture as shown in Appendix 5.1. Only one sample per test was available for the tests. It was evident that higher internal pressure greatly reduces the fatigue life of the steel coiled tube. Experimental results showed that an increase of internal pressure from 600 psi to 3200 psi reduces the life of the tube by approximately 87% (387 cycles to 50 cycles, respectively).

Table 6-2: Comparison of experimental and simulation cycles to failure of steel coiled tube

	Internal Pressure (psi)	**Experimental Estimates**		**Tenaris^{TM} Simulation estimate**	
		Cycles to failure	**Trips to failure**	**Cycles to failure**	**Trips to failure**
Tube 1	0	1549	516	600	200
Tube 2	600	387	129	561	187
Tube 3	2200	77	25	381	127
Tube 4	3200	50	17	77	25

Appendix 4 Composite coiled tubes fatigue failure

Appendix 4.1: Coiled tube Specimen 1A

Appendix 4.2: Coiled tube Specimen 1B

Appendix 5 Steel coiled tubes fatigue failure

The pictures below show failure modes of steel tube (OD 1.75 in and 0.134 in wall thickness) under cyclic bending with varying internal pressure.

Appendix 5.1: Tube 1 Fracture failure

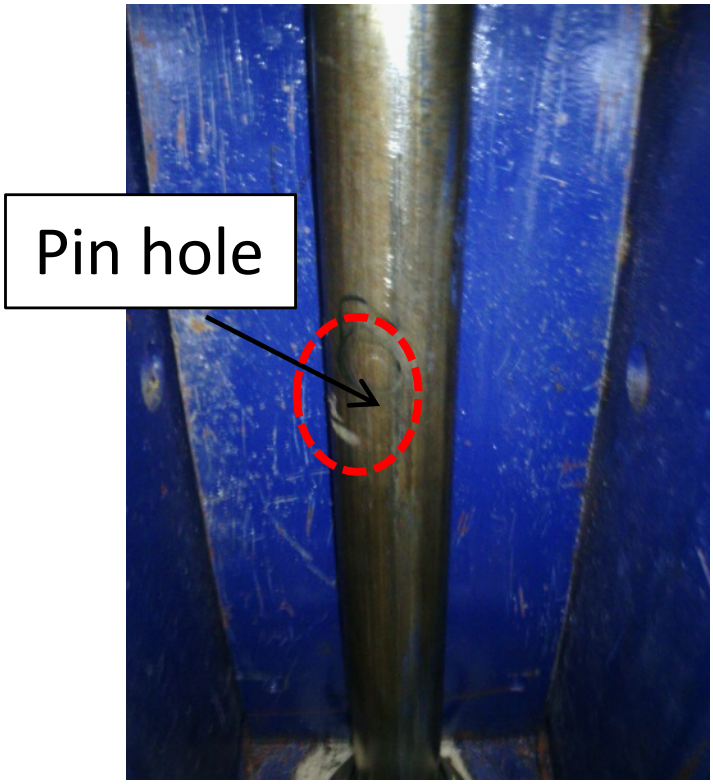

Appendix 5.2: Tube 2 pinhole failure

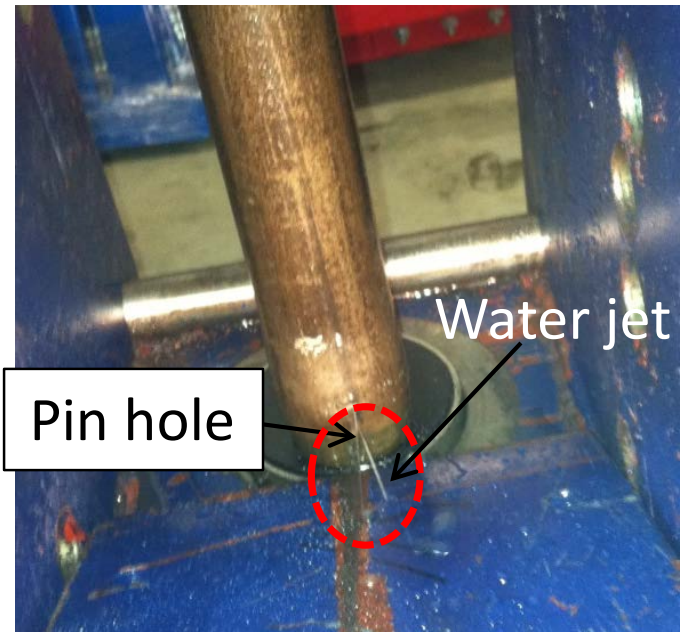

Appendix 5.2: Tube 3 pinhole failure

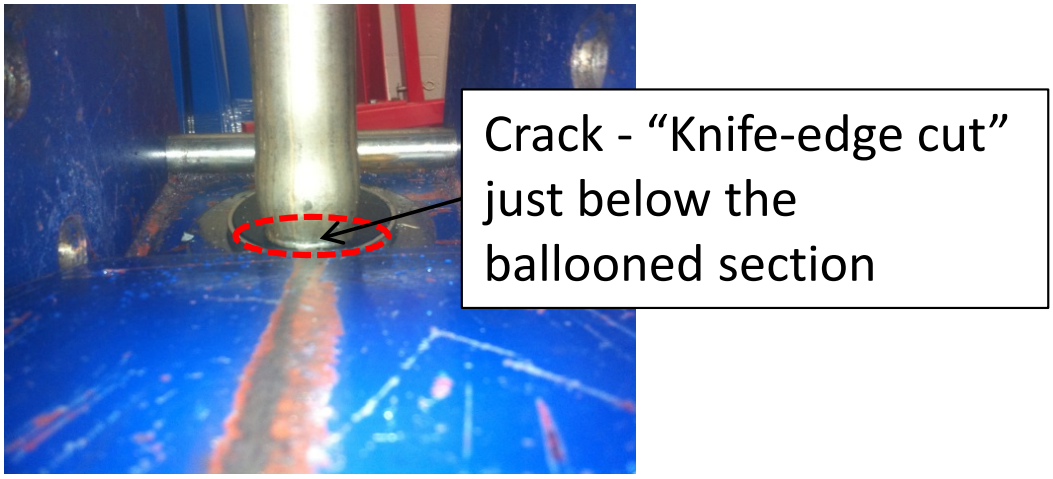

Appendix 5.3: Tube 4 fracture failure